CONDUCTANCE STATES OF MOLECULAR JUNCTIONS FOR ENCODING BINARY INFORMATION: A COMPUTATIONAL APPROACH

A Dissertation

by

LUIS ALBERTO AGAPITO

Submitted to the Office of Graduate Studies of
Texas A&M University
in partial fulfillment of the requirements for the degree of

DOCTOR OF PHILOSOPHY

May 2006

Major Subject: Electrical Engineering

CONDUCTANCE STATES OF MOLECULAR JUNCTIONS FOR ENCODING BINARY INFORMATION: A COMPUTATIONAL APPROACH

A Dissertation

by

LUIS ALBERTO AGAPITO

Submitted to the Office of Graduate Studies of
Texas A&M University
in partial fulfillment of the requirements for the degree of

DOCTOR OF PHILOSOPHY

Approved by:

Chair of Committee,	Jorge M. Seminario
Committee Members,	Yue Kuo
	Jun Kameoka
	Garng M. Huang
Head of Department,	Costas N. Georghiades

May 2006

Major Subject: Electrical Engineering

ABSTRACT

Conductance States of Molecular Junctions for
Encoding Binary Information: A Computational Approach. (May 2006)
Luis Alberto Agapito, B.S., Universidad Nacional de Ingeniería;
M.E., University of South Carolina
Chair of Advisory Committee: Dr. Jorge M. Seminario

Electronic devices, for logical and memory applications, are constructed based on bistable electronic units that can store binary information. Molecular electronics proposes the use of single molecules—with two distinctive states of conductance—as bistable units that can be used to create more complex electronic devices. The conductance of a molecule is strongly influenced by the contacts used to address it. The purpose of this work is to determine the electrical characteristics of several candidate molecular junctions, which are composed of a molecule and contacts. Specifically, we are interested in determining whether binary information, "0" or "1," can be encoded in the low- and high-conductance states of the molecular junctions.

First, we calculate quantum-mechanically the electronic structure of the molecular junction. Second, the continuous electronic states of the contacts, originated from their infinite nature, are obtained by solving the Schrödinger equation with periodic boundary conditions. Last, the electron transport through the molecular junctions is calculated based on a chemical interpretation of the Landauer formalism for coherent transport, which involves the information obtained from the molecule and the contacts. Metal-molecule-metal and metal-molecule-semiconductor junctions are considered. The molecule used is an olygo(phenylene ethynylene) composed of three benzene rings and a nitro group in the middle ring; this molecule is referred hereafter as the nitroOPE molecule. Gold, silicon, and metallic carbon nanotubes are used as contacts to the molecule.

Results from the calculations show that the molecular junctions have distinctive states of conductance for different conformational and charge states. High conductance is found in the conformation in which all the benzene rings of the nitroOPE are coplanar. If the middle benzene ring is made perpendicular to the others, low conductance is found. Also, the negatively charged junctions (anion, dianion) show low conductance. Whenever a semiconducting contact is used, a flat region of zero current is found at low bias voltages. The results indicate that the use of Si contacts is possible; however, because of the flat region, the operating point of the devices needs to be moved to higher voltages.

DEDICATION

To my parents

ACKNOWLEDGMENTS

I want, first, to thank Dr. Jorge M. Seminario for introducing me to the fascinating field of molecular electronics and for the four and a half years that he has had me in his research group. I am grateful to him for his support and continuous advice during my years as a graduate student.

I want to thank to Dr. Yue Kuo, Dr. Jun Kameoka, and Dr. Garng M. Huang for their time and effort in being members of my committee.

I also want to thank members of Dr. Seminario's research group who contributed to my understanding of the nanoscopic phenomena through useful discussions and their countless explanations about the theoretical (Dr. Liuming Yan, Dr. Pedro Derosa, Dr. Juan Sotelo, and Dr. Agustín Zúñiga) and experimental (Dr. Francisco Zuno and Dr. Gloria Sánchez) aspects of this interesting field of science.

I would like to thank all the members of my family for standing by me through all my years of school. I could not have gotten this far without their support.

NOMENCLATURE

CMOS	Complementary MOS
CNT	Carbon nanotubes
DFT	Density Functional Theory
DFT-GF	Combined Density Functional and Green Function approach
DOS	Density of states
ECP	Electronic chemical potential = μ
EECP	Effective ECP = μ^*
EM	Extended molecule
ESP	Electrostatic potential
FCC	Face centered cubic
FPGA	Field-programmable gate array
GF	Green function
HOMO	Highest occupied molecular orbital
ITRS	International technology roadmap for semiconductors
I-V	Current-voltage
MOS	Metal-oxide-semiconductor
MOSFET	MOS field effect transistor
NDR	Negative differential resistance
OPE	Oligo(phenylene ethynylene)
SRAM	Static random-access memory
SRC	Semiconductor Research Corporation
SiNW	Silicon nanowire
STM	Scanning tunneling microscope
SWCNT	Single-wall CNT

TABLE OF CONTENTS

Page

CHAPTER Page

CHAPTER Page

LIST OF FIGURES

Page

Page

Page

Page

Page

Page

LIST OF TABLES

Page

CHAPTER I

INTRODUCTION

1.1 Historical background

The use of computers has become ubiquitous in our daily life. The overwhelming increase of computational power has been possible mainly due to the use of solid-state transistors, invented in 1947.

A transistor is a device made of a semiconducting material that can work either as a signal amplifier or as an electronic switch. All digital circuits, including the microprocessor, which powers a computer, are based on these electronic switches. An electronic switch allows turning a circuit on and off by the application of a controlling voltage. A circuit with two stable and well-differentiated states, a bistable circuit, allows the physical implementation of the two logic states used in Boolean logic, generally referred as “0” and “1”. More complex circuits that are able to solve Boolean functions can be designed based on the bistable units. Moreover, general-purpose circuits such as the microprocessors are capable of solving any Boolean–type function.

The most commonly used transistor in digital circuits is the MOSFET. Two complementary types of MOSFETs, one n- and one p-type, are normally used in pairs to implement a digital circuit, which is the basis principle in the CMOS technology. One type is in its ON state whenever the other is in its OFF state and vice versa.

The decrease of the time that a transistor takes to switch between its ON and its OFF state is associated with the speed at which a computer can perform a logical operation. The decrease of the switching time is accomplished by reducing the physical length of the channel of the transistor.

This dissertation follows the style of *Science*.

Therefore, the advancement of computers and any digital-logic circuit is intimately related the scaling-down of the MOSFETs.

1.1.1 Moore's law

The size of the transistor has been steadily scaled-down for the last 41 years, following the prediction given by Intel's Dr. Gordon Moore in 1965. As early as the year 2000, the semiconductor industry entered the nanotechnology era with commercially available transistors featuring sub-100 nm sizes.

Off-state leakage current is the main problem in scaling the transistor below gate lengths of 10 nm, as shown in Fig. 1. The off-state leakage current depends exponentially on the threshold voltage; high threshold voltage reduces the leakage current. On the other hand, the bias voltage (V_{dd}) needs to be reduced, along with the scaling of the transistor, to avoid high electric fields in the drain-source channel and to keep the power manageable (*1*). However, the threshold voltage cannot be increased arbitrarily since it has to be lower than the bias voltage. This is the conundrum of achieving low leakage current in transistors with short gate lengths.

Doyle *et al*. have shown that MOSFETs with physical gate lengths of 30, 20, and 15 nm still behave as controllable switches; however, at gate length of 10 nm, they reported poor short-channel control and high off-state leakage current (*2*). The increase of off-state leakage current at gate lengths less than 10 nm is intimately related to the predominance of dopant discontinuities, interfacial states, and quantum-mechanical effect. Considering the transistor channel to be a Si-crystal cube of 10 nm per side, a doping level of 10^{18} cm^{-3} represents an average of only one dopant inside the channel. The effect of a discrete number of dopants needs to be addressed from the atomistic point of view.

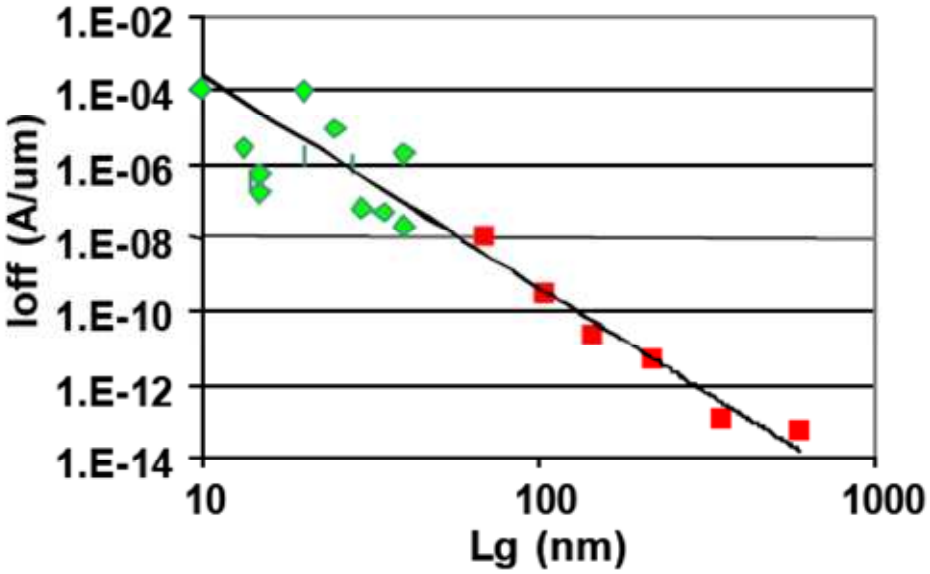

Fig. 1. Off-state leakage current for MOSFET transistors with different physical gate lengths. The red squares represent commercially available transistors and the green diamonds indicates research devices, from data published in the year 2002. From reference (*2*).

Interfacial states are discontinuities of the crystal structure at the interfaces between two different materials. Those states are created by the formation and breakage of chemical bonds, which are driven by the thermodynamics of the system looking to minimize its energy. The high interfacial-area-to-volume ratio in structures of atomistic sizes makes the effect of the interfacial states to prevail over the properties of the bulk material. A high density of interfacial states can distort or destroy (i.e. filling partially or totally the bandgap) the semiconducting electronic property of the material. A satisfactory study of the nature of formation of chemical bonds requires the use of quantum-mechanical tools.

1.1.2 Approaching the quantum realm

The Semiconductor Research Corporation predicts that the scaling down in the CMOS technology will face fundamental limitations at or beyond the 22 nm

technology node (*3*). This technology node corresponds to a physical gate length of 9 nm (~50 atomic layers of Si) and is predicted to be in production by 2016 (*4*).

The Semiconductor Industry Association in their 2005 estimation (*5*) states that "channel lengths of silicon films of a few nanometers cannot be accurately represented without (partially) ballistic transport models, which also include quantum effect." Since at atomistic dimension quantum-mechanical effects are prevailing, the design of future electronic devices, whether they are CMOS-compatible or not, requires the use of quantum-mechanical tools describe in this work.

Quantum-mechanical effects can change drastically the electronic properties of the bulk material. For instance, the bandgap of semiconductors increases with the decrease in the size of the structure (*6-8*). Silicon, which is considered a poor light emitter because of its small and indirect bandgap, has been shown to exhibit visible luminescence (red, orange, yellow, and green) at room temperature in structures of ~5 nm in diameter (*9*).

It is difficult to set a sharp and well-defined boundary between a classical system and a quantum-mechanical system. In principle, a classical system is a special case of a quantum-mechanical system in the limit when the wave-nature of a particle is neglected; therefore, it can be explained under the quantum-mechanical framework too, yet it could be unnecessarily tedious. However, there are physical phenomena than cannot be explained by classical physics; these systems will be referred to, hereafter, as pure quantum-mechanical systems. If concepts beyond the classical picture need to be introduced in order to explain or extend the explanation of a system, that system will also be referred as quantum-mechanical. For instance, an electronic system which requires the adoption of a wave picture for the electron (in order to understand the phenomena going on in that specific system) will be referred to as quantum-mechanical. In the case when the particle picture for the electron suffices, the system will be called classical.

1.1.2.1 Classical vs. quantum systems

A pure quantum-mechanical system is characterized by the fact that the system can be found only on discrete states. For instance, a classical harmonic oscillator (mass-spring system) could be found oscillating at any real value of angular frequency. However, a quantum-mechanical harmonic oscillator can oscillate only on predefined discrete values of angular frequency; all continuous values of frequency between two consecutive allowed frequencies are physically forbidden. Since each state of the system is associated with a particular energy value, we can say that such quantum-mechanical system has only quantized (discrete) values of energy. The molecular junctions analyzed in this work are examples of quantum-mechanical systems, as isolated molecules.

1.1.2.2 Why quantum-mechanical systems now?

Light presents dual behavior, sometimes acting like a particle, other times more like a wave. Any shade in between particle and wave is also possible, depending on the conditions of the experiment. Similarly, we say that a system presents dual character, a classical and a quantum-mechanical. The strength of each character depends on the conditions of the system, i.e. size, shape, temperature, etc. Some characteristic lengths help to set qualitatively the prevailing regimen of the system. One characteristic length is the *elastic mean free path length* (L_m), which is the average distance on which the electron is collision-free. Another is the *phase-coherence length* (L_ϕ), this refers to the length over which the electron retains memory of its phase. It is also defined as the length over which the phase of the electron varies linearly with time. For lengths larger than L_ϕ, two electrons that started traveling with the same wavelength will end-up with different wavelengths due to inelastic scattering. The current in a system is composed mainly of the electrons with energies closed to the Fermi energy, which are the ones that contribute to conduction. The associated wavelength of an electron with energy equal to the Fermi energy is called *electron Fermi wavelength* (λ_f). Conversely, electrons with

kinetic energy less that the Fermi energy have wavelengths larger than λ_f and do not contribute to conduction.

The larger the size of the system with respect to L_m and L_ϕ, the stronger the classical character of the system. On the other hand, the closer the size of the system to the λ_f, the stronger its quantum-mechanical character. Electron transport in classical (macroscopic) systems is described by the assumption of the electrons being tiny particles, incorporated in the Boltzmann equation of transport. Because of modern fabrication capabilities and the ability to control low temperatures, the assumptions made in the Boltzmann equation* are no longer valid. The phenomena taking place on mesoscopic, and smaller structures cannot be fully explained by classical models, requiring more or less the inclusion of quantum-mechanical concepts.

1.1.2.2.1 Ballistic transport

When the length of the channel is smaller than the elastic mean free path length, the electrons travel without being scattered; such regime of transport is known as ballistic transport. Although this has nothing to do with quantum mechanics, it shows a regime where the traditional theories of electron transport fails. For instance, GaAs/GaAlAs heterostructures at low temperatures can reach mobilities of 10^6 cm^2/Vs, yielding an elastic mean free path of ~10 μm and an inelastic (phase-coherent) mean free path length even longer (*10*). Since the fabrication of structures of ~1 μm is within reach, we can have a structure where the electrons can travel ballistically. A single-moded ballistic channel has a tunneling probability of crossing the channel equal to 1

* Assumptions in the Boltzmann equation of transport:
a) Scattering processes are local and assumed to take place on a single point in space
b) The scattering is instantaneous in time
c) The scattering is weak
d) Only events slower that the mean free time are of interest.

and a characteristic resistance G_0^{-1}. Consequently, the conductance of a multi-moded ballistic channel is not a continuous but a discrete property. It has been found experimentally that the conductance varies in integer multiples of the quantum conductance $G_0 = \frac{2e^2}{h}$.

1.1.2.2.2 Tunneling

A classical particle cannot exist in a region of space where the potential energy is higher than the energy of the particle Those regions are considered potential barriers for the particle; for example, a ball cannot penetrate a brick wall without having enough energy to break through it. However, this is no longer true for quantum systems where there is a non-zero probability of finding the electron in regions with potential energy higher than the energy of the electron. The conducting channels in nanostructures are considered potential barriers; therefore, the current of electrons through those channels are a consequence of the quantum-mechanical phenomenon of tunneling. Tunneling diodes are commercial applications of this quantum effect.

1.2 Description of the problem to study

As pointed out by the Semiconductor Industry Association in 2005 (*5*), modeling and simulation at the quantum-mechanical level is necessary to examine and enable new solutions for electronic devices of atomistic sizes.

Early in 1959, Richard P. Feynman envisioned the manipulation of matter at the scale of individual atoms and molecules in his lecture “There’s plenty of room at the bottom.” The specific use of a single molecule as electronic device was first proposed by Aviram and Ratner in 1974 (*11*). Since then, the field of molecular electronics has experienced a rapid growth and represents an alternative to go beyond the 22 nm technology node. The design of molecular electronic circuits requires the conception of

new architectures and new simulation methods that can cope with the quantum-mechanical nature of the system.

Mainly, two different architectures for molecular electronics have been proposed: the NanoCell (*12-14*) and the crossbar (*15-28*) approach. The two types of architectures can be used for both memory and logic applications.

1.2.1 The crossbar approach to molecular electronics

A crossbar architecture is comprised of two parallel planes containing conducting wires lying on each plane. The wires contained in the same plane are parallel to each other but perpendicular to the wires contained in the other plane. Electronic storage cells are placed between the parallel planes connecting two perpendicular wires at the projected intersection, as seen in Fig. 2.

Each storage cell, which can be addressed only by a unique combination of two wires lying on different planes, is used to storage 1-bit of information. The main requirement for a hardware implementation of a storage cell is the two distinctive and stable states, i.e. “0” and “1,” that it should possess. Since a storage cell has to switch between two different states, it will also be referred to as an electronic switch.

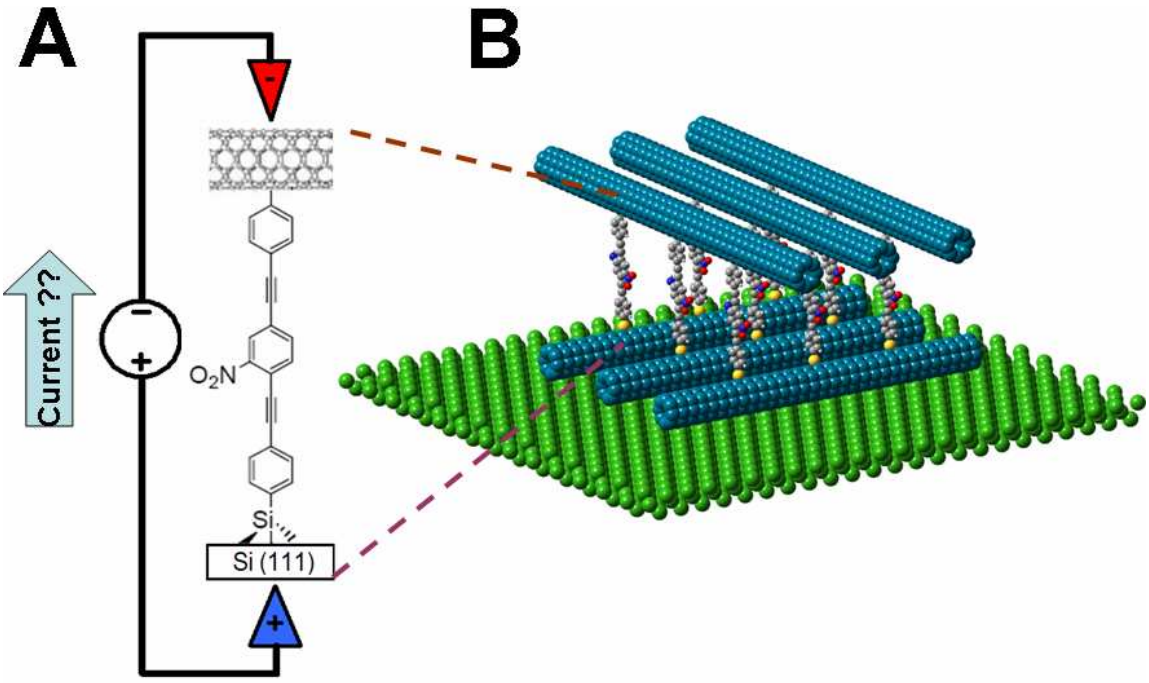

Fig. 2. (A) Pictorial representation of a molecular crossbar array. At each crossing, the data is encoded by using two definite states of the nitroOPE molecule. (B) Amplification of a single data-storage cell; the electrical properties of this (4,4) CNT-nitroOPE-Si junction will be assessed to determine the viability of this molecule for memory and/or logic applications.

A schematic of a standard 4 × 4-bit SRAM memory is shown in Fig. 3. Each electronic switch (storage cell) is addressed by a unique combination of two wires (one W and one B wire). In standard electronics, a MOSFET-based circuit is used to implement the storage cell. In this particular case, a combination of six (two n-type and four p-type) MOSFETs are used to implement the storage cell, i.e., to store 1-bit of information. The physical implementation of six transistors per bit of information is a constraint in the reduction of the physical area needed per bit of information. Moreover, the use of complementary types of MOSFETs in the same cell (an n- and a p-type) increases the area needed. The increase in the performance (speed and density) of devices for memory applications depends on how small the MOSFET can be made; the case is the same for logic devices.

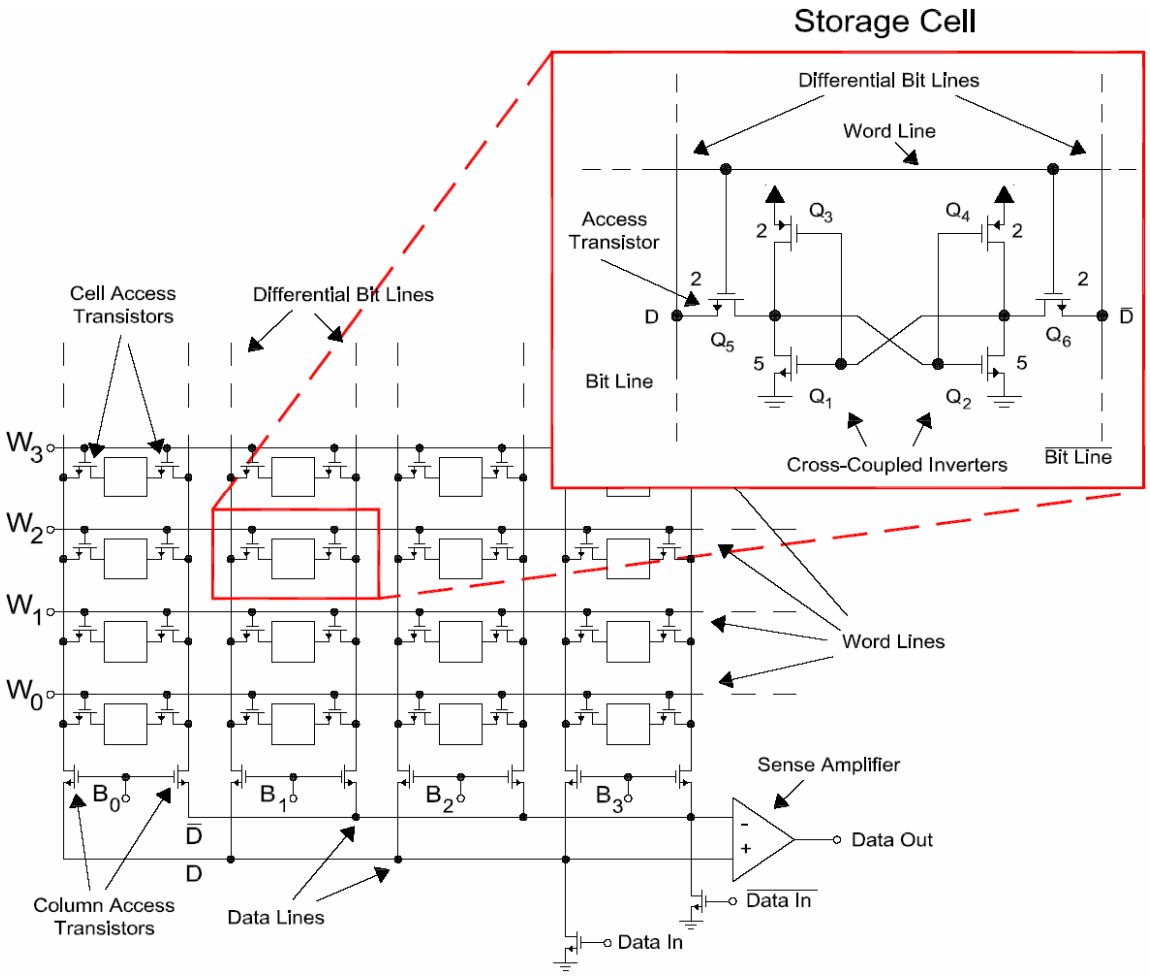

Fig. 3. Schematic of a 4 × 4-bit SRAM memory. The circuitry is based on a 4 × 4 crossbar array, at each crossing a storage cell, able to keep 1 bit of information, is present. Adapted from reference (*29*).

The idea of molecular electronics is to find suitable molecules to be used as electronic switches (storage cells) in the design of digital-logic circuits (logic and memory applications). The use of molecules in molecular-crossbar memories has already been tested at the research level, yielding densities as high as 6.4 Gbits/cm^2 (*20, 25*). Moreover, the fabrication of crossbar arrays of metallic and semiconducting

nanowires with density of ~10^{11} crossings/cm^2 has been reported (*30*). Fig. 2 shows a pictorial representation of a molecular crossbar array.

Crossbar arrays can be used for memory and logic applications. Both types of applications are based on saving 1-bit of information in the storage cell, which for the case of a molecular crossbar array is implemented as a molecule. Information is kept in the molecule by setting it to one of two well-defined molecular states. Any kind of molecular state could be used to store information; however, molecular states showing distinctive conductance are preferred since conductance can be "easily" read by performing an electrical measurement. We will refer to those states as high- and low-conductance states, which are arbitrarily associated with logic "1" and "0".

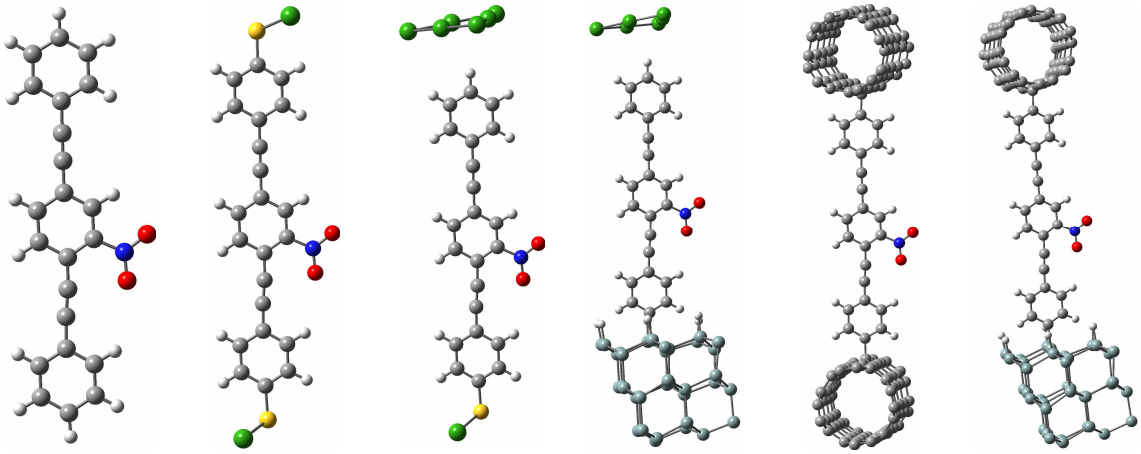

Fig. 4. (A) nitroOPE molecule. (B) nitroOPE under two gold contacts (green), sulfur atoms (yellow) are used to attach the molecule to the gold atoms. (C) Six gold atoms are used to model the top contact. The nitroOPE is attached to the top gold contact through a physical bond. (D) Gold and Si (light blue) contacts. (F) The metallic (4,4) CNT is used for both contacts. (F) The metallic (4,4) CNT and Si (111) is used for the top and the bottom contact respectively.

1.2.2 The nitroOPE molecule

A molecule that exhibits two strong conducting states is needed to encode binary information. Several organic molecules, ranging from the commercially available to specially synthesized, have been tried as bistable electronic devices. OPE-type

organic molecules have been consistently reported to be able to switch between a high- and a low-conductance state upon the application of external stimuli (*31*). We will focus our study in a particular OPE molecule, the "nitroOPE," which is shown in Fig. 4A.

1.2.3 Metal-molecule-semiconductor junctions

As discussed previously, the design of future electronic devices based on molecular crossbar arrays (and in general based in any type of architecture) will gravitate around our ability to simulate changes in molecular properties, such as conductance, when the molecule switches between two predefined states.

For our target of using conductance states to encode binary information in molecular crossbar-based circuits (Fig. 2B), the problem is reduced to calculate the current through a single molecule that is attached to the two cross wires, a "molecular junction" (Fig. 2A). Formally, a molecular junction is composed of two contacts and an organic molecule sandwiched between them (Fig. 2A).

The electron transport through a molecular junction is expected to greatly depend on the type of attachment between the molecule and the contacts (*32*). Therefore, we have to consider in our study not only the molecule but also the crossbar wires to which the molecule is connected. That is, the conductance of the whole molecular junction, including the semi-infinite nature of the contacts.

NitroOPE-based junctions with metallic and semiconducting contacts are studied in this work; several molecular junctions are shown in Fig. 4, B to D. Traditionally, metals have been used as contacts in experimental and theoretical determinations of electron transport through molecular junctions (*33-36*). Moreover, recently, it has been possible to bind covalently organic molecules to CNTs (*37-39*), opening the way to use metallic CNTs as contacts to organic molecules. Because of the technological expertise and infrastructure, molecule-based devices are most likely to be constructed around silicon-based nanostructures. In addition, reliable synthetic procedures to bind covalently organic molecules to hydride-passivated Si surfaces have

been developed (*40, 41*). Si-C bonds are characterized for their high bond strength and low polarity (*42*) that provide two very desirable effects: a stronger contact-molecule coupling and a more electronically continuous interface.

Ohmic I-V characteristic at low bias voltage has been reported for an OPE-type molecule, containing both an amino and a nitro group, under metallic contacts (*31*). Metallic contacts follow ohmic behavior, and we can assume that they do not detriment totally the desired bistability of the molecule; however, the I-V of nitroOPE-based junctions that contains both a metallic and a semiconducting contact is yet to be determined, which is one of the aims of this work. The combination of both types of material introduces an extra unknown, the Schottky barrier. Schottky barriers, which are innate in metal-semiconductor interfaces, hinder the injection of carriers from a metallic to a semiconducting material. In experimental I-V measurements of semiconductor-molecule-metal, where the metal contact is an STM tip, zero-current is observed at low bias voltages (*43-46*), which can be attributed to a Schottky barrier. For the design of devices based on metal-molecule-semiconductor junctions, we have to focus not only in the electrical properties of the molecule but also in the effects of having a metal-semiconductor interface. Would the switching properties of the nitroOPE persist when using the technologically important silicon as a contact?

1.3 Summary and outline of this dissertation

The aim for this work is to assess the viability of using the nitroOPE molecules to store binary information when the molecule is embedded in a crossbar array, as depicted in Fig. 2. Any logic and memory device can be implemented based on crossbar architectures. The information is encoded in the conductance of the molecule, which is read by performing an electrical measurement of the molecular junction (Fig. 2A). The present work focuses on the conductance of a molecule that is attached to two semi-infinite contacts, and not just on the isolated molecule. Some technologically important materials such as silicon and CNTs are tested as contacts; these materials have

been made available as contacts due to recent advances in synthetic chemistry, such as the direct covalent attachment of organic molecules to CNT and silicon.

A molecular junction is defined as a single molecule attached to two semi-infinite contacts. Because of the computationally expensive nature of full-quantum-mechanical calculations, we cannot include an infinite number of atoms to represent the molecule and the semi-infinite contacts. In practice, the number of atoms is limited to a few hundred, which includes the molecule and a few atoms representing each contact; this reduced molecular junction will be named hereafter as the extended molecule.

In Chapter II, we begin to undertake the problem of calculating the electronic states of a molecule that is attached to two semi-infinite contacts. The contacts are modeled as crystal lattices whose continuous distribution of electronic states is obtained through quantum-mechanical calculations with periodic boundary conditions. Then, we describe the mathematical formalism needed to incorporate the effect of the semi-infinite contacts on the discrete electronic states of the extended molecule. The chapter closes with an application example based on our published work (*47*), where these techniques are applied to study the adsorption of molecular oxygen on a metallic substrate, a problem sensitive for the design of catalysts for fuel cells.

In Chapter III, we explain our quantum-mechanical implementation of the Landauer formalism for coherent transport to calculate the current through metal-molecule-metal junctions. The changes in conductance of the nitroOPE molecule due to conformational and charge-state changes are analyzed; gold and the (4,4) CNT are tested as prospective metallic contacts. A combined experimental-theoretical application example shows the use of the technique outlined in this chapter to explain the leakage current observed in discontinuous gold films. This application example is based on another published work (*48*).

In Chapter IV, we discuss the electron transport in several metal-molecule-semiconductor junctions. Silicon is used for the semiconducting contact and either gold or the (4,4) CNT is used for the metallic contact. We study the feasibility of having the desirable high- and low-conductance states from the metal-nitroOPE-Si junctions by

producing changes in the molecular geometry and charge. The changes in conductance are explained based on the analysis of the molecular orbitals and the electrostatic-potential spatial distribution.

Finally, in Chapter V, we state our conclusions and provide suggestions for future work. The output files for most of the quantum-mechanical calculations are available in the digital attachment of this dissertation. See Appendix 5 for a list of the available files.

CHAPTER II

THE INTERFACE PROBLEM: MOLECULAR ADSORPTION ON A SURFACE*

2.1 Introduction

From the computational viewpoint, primarily two types of molecular systems are involved in the work presented in this dissertation: Finite and infinite systems. Finite systems refer to molecules with a finite number of atoms whereas an infinite system refers to crystalline material. The tools to study both types of systems, which are presented at the beginning of this chapter, are well established in computational chemistry. However, systems that combine both a finite and a infinite character represent a new and challenging area of research; this is the case for the study of a single molecule (finite) adsorbed to one contact tip (modeled as a infinite crystal material).

The discrete electronic states of an isolate molecule are obtained by solving the Schrödinger equation; we solve that equation following the DFT methodology.

When the molecule is adsorbed on a contact tip, the continuous electronic states of bulk material modify the discrete electronic states of the molecule. In other words, electrons from the contacts leak into the molecule, modifying its electronic properties. A mathematical formalism based on the Green function (GF) is used to account for the effect of the bulk contacts.

surface, which is a relevant problem for engineering new catalyst materials used in fuel-cell devices.

---

* Reproduced in part with permission from P. B. Balbuena, D. Altomare, L. Agapito, J. M. Seminario, *J. Phys. Chem. B* **107**, 13671 (2003). Copyright 2003 American Chemical Society.

Early in this chapter, we present the general DFT-GF formalism to evaluate the density of states of a single molecule attached to two infinite contacts. Later on, the DFT-GF formalism is applied to study the adsorption of the O_2 molecule on a platinum

2.2 Electronic properties of molecules and clusters

The electronic properties of a molecular system can be calculated from its associated wavefunction, which is built as a determinant of molecular orbitals (MO). MOs are linear combinations of all the atoms composing the system. In other words, the atomic orbitals are the basis functions, χ, used to expand the MOs.

2.2.1 Basis functions

Gaussian-type functions (GTFs), which form a complete set of functions, are defined in their Cartesian form as:

$$g_{ijk} = K x_b^i y_b^j z_b^k e^{-\alpha r_b^2} \tag{1}$$

where i, j, k are nonnegative integers, α is a positive orbital exponent, x_b, y_b, z_b, are Cartesian coordinates and r_b is the radial coordinate. The subscript b indicates that the origin of the coordinates is at the nucleus b. K is a normalization constant.

The sum $l = x + y + z$ is analogous of the angular momentum of an atomic orbital. Depending on if l equals 0, 1, or 2; the GTF is called s-, p-, or d-type respectively. There is no analogy for the principal quantum number n.

A basis function χ_r, also referred to as contracted Gaussian-type orbitals (GTOs), is defined as a normalized linear combinations of GTFs (g_u)

$$\chi_r = \sum_u d_{ur} g_u \tag{2}$$

where d_{ur} are called contraction coefficients. Basis sets published in the literature provide the values of α (Eq. 1) and d_{ur} (Eq. 2). A basis function is constructed to resemble a given atomic orbital. Throughout this work, two basis sets are used: the LANL2DZ and the 6-31G(d).

For instance, in the 6-31G(d) basis set, the inner shell 1*s* atomic orbital of carbon is formed by contracting six GTFs, as follows

$$\chi_{1s} = \sum_{u=1}^{6} d_u g_{1s}(\alpha_u) \tag{3}$$

where the contraction coefficients d_u and the Gaussian exponents α_u are given in Table 1. For an s-type function, the GTF given in Eq. 1 simplifies to

$$g_{1s}(\alpha) = e^{-\alpha(x^2+y^2+z^2)} \tag{4}$$

where the normalization constant *K*, defined in Eq. 1, has been included in the contraction coefficients.

Table 1. Contraction coefficients and Gaussian exponents for the inner 1*s* atomic orbital of the carbon atom, which is given in Eq. 3. The values correspond to the 6-31G(d) basis set.

u	contraction coefficients d_u	Gaussian exponents α_u
1	0.001834700	3047.52490
2	0.014037300	457.369510
3	0.068842600	103.948690
4	0.232184400	29.2101550
5	0.467941300	9.28666300
6	0.362312000	3.16392700

2.2.2 Density functional theory

For a polyatomic molecular system, the electronic non-relativistic Hamiltonian can be written as

$$\hat{H}_{el} = -\frac{1}{2}\sum_i \nabla_i^2 + \sum_i \sum_b \frac{Z_b}{r_{ib}} + \sum_i \sum_{j>i} \frac{1}{r_{ij}} \tag{5}$$

where *i* and *j* count over all electrons and *b* over all nuclei, Z_b is the atomic number of the atom *b*. If the system contains *n* electrons then the wavefunction of the molecular system is a function of 3*n* spatial coordinates and *n* spin coordinates. Therefore, calculating the complete electronic wavefunction is computationally expensive; in practice, only very small systems could be calculated. The wavefunction is a mathematical entity that contains more information of the system than needed for specific applications.

The first Hohenberg-Kohn theorem (*49*) established that all the properties of a molecular system in the ground state are determined by ground-state electron probability density $\rho_0(x, y, z)$, which is a function of only 3 variables. This theorem circumvents the strict use of the wavefunction; instead, the electron probability density function is used to calculate the properties of a molecular system. This theorem finally set Density Functional Theory (DFT) on a formal basis and allows studying larger molecular systems.

In 1965 Kohn and Sham (*50*) published a method to find the electron probability density without having to find first the wavefunction. They demonstrated that the electron density of a molecular system of interacting electrons can be represented with the electron density of an equivalent system of non-interactive electrons subjected to an effective potential v_s. Therefore, the interacting many-electron problem is split into several non-interacting one-electron problems, which are governed by the following one-electron Kohn-Sham (KS) equation

$$\hat{h}^{KS}(r)\theta_i^{KS}(r) = \varepsilon_i^{KS}\theta_i^{KS}(r) \tag{6}$$

where the one-electron KS Hamiltonian $\hat{h}^{KS}$ is defined as:

$$\hat{h}^{KS}(r) = -\frac{1}{2}\nabla_r^2 + v_s(r) \tag{7}$$

and the fictitious external potential is defined as:

$$v_s(r) = -\sum_b \frac{Z_b}{|r - r_b|} + \int \frac{\rho(r')}{|r - r'|} dr' + v_{xc}(r) \tag{8}$$

where v_{xc} is the exchange-correlation potential

$$v_{xc}(r) \equiv \frac{\delta E_{xc}[\rho(r)]}{\delta\rho(r)} \tag{9}$$

The external potential (v_s) is found by solving Eq. 6 self-consistently. The KS molecular orbitals (θ_i^{KS}), shown in Eq. 6, are expanded in terms of the GTOs defined in Eq. 2.

$$\theta_i^{KS} = \sum_{r=1}^{B} c_{ri}\chi_r \tag{10}$$

where *B* is the number of basis functions of the molecular system. By inserting Eq. 10 in Eq. 6 and applying the variational principle, a Roothaan-type matricial equation is obtained. For example, the matricial equation for a molecular system that has only five basis functions is

$$\begin{pmatrix} h_{11}^{KS} & h_{12}^{KS} & h_{13}^{KS} & h_{14}^{KS} & h_{15}^{KS} \\ h_{21}^{KS} & h_{22}^{KS} & h_{23}^{KS} & h_{24}^{KS} & h_{25}^{KS} \\ h_{31}^{KS} & h_{32}^{KS} & h_{33}^{KS} & h_{34}^{KS} & h_{35}^{KS} \\ h_{41}^{KS} & h_{42}^{KS} & h_{43}^{KS} & h_{44}^{KS} & h_{45}^{KS} \\ h_{51}^{KS} & h_{52}^{KS} & h_{53}^{KS} & h_{54}^{KS} & h_{55}^{KS} \end{pmatrix} C = \begin{pmatrix} S_{11} & S_{12} & S_{13} & S_{14} & S_{15} \\ S_{21} & S_{22} & S_{23} & S_{24} & S_{25} \\ S_{31} & S_{32} & S_{33} & S_{34} & S_{35} \\ S_{41} & S_{42} & S_{43} & S_{44} & S_{45} \\ S_{51} & S_{52} & S_{53} & S_{54} & S_{55} \end{pmatrix} E^{KS} C \tag{11}$$

where h_{rs}^{KS} are matrix elements of the one-electron KS Hamiltonian operator $\hat{h}^{KS}$. These matrix elements are defined as

$$h_{rs}^{KS} = \langle \chi_r | \hat{h}^{KS} | \chi_s \rangle \tag{12}$$

S_{jk} is the overlap integral between two basis functions

$$S_{jk} = \langle \chi_j | \chi_k \rangle \tag{13}$$

C is a matrix composed of the expansion coefficients c_{ri}, which are defined in Eq. 10. E^{KS} is a diagonal matrix composed of all the eigenvalues (energies) of the one-electron K-S equation defined in Eq. 6.

$$E^{KS} = \begin{pmatrix} \varepsilon_1^{KS} & 0 & 0 & 0 & 0 \\ 0 & \varepsilon_2^{KS} & 0 & 0 & 0 \\ 0 & 0 & \varepsilon_3^{KS} & 0 & 0 \\ 0 & 0 & 0 & \varepsilon_4^{KS} & 0 \\ 0 & 0 & 0 & 0 & \varepsilon_5^{KS} \end{pmatrix} \tag{14}$$

The expansion coefficients, c_{ri}, of the molecular orbitals are found by solving iteratively Eq. 11 (*51*).

$$\rho = \sum_{i=1}^{n} \left| \theta_i^{KS} \right|^2 \tag{15}$$

At all steps of the iteration, the expansion coefficients are updated. Consequently, new KS molecular orbitals (Eq. 10) and electron probability densities (Eq. 15) are obtained during the iterative process. When self-consistency is reached, the ground-state electron probability density and KS molecular orbitals can be evaluated. All properties for the molecular system can be extracted from the ground-state probability density, according to the Hohenberg-Kohn theorem.

2.2.3 Molecular Electrostatic Potential

A molecular system can be modeled as an electronic device, encapsulating all the chemistry of the system behind the electron probability density ρ. The equivalent electrostatic potential (ϕ) for such electronic device, measured at point of space *r = (x, y, z)*, can be calculated as:

$$\phi(x,y,z) = \sum_{\alpha} \frac{Z_\alpha}{|r - R_\alpha|} - e \iiint \frac{\rho(x',y',z')}{|r - r'|} dx'dy'dz' \tag{16}$$

where the electron probability density, ρ, is defined in Eq. 15.

2.3 Electronic properties of crystalline materials

In the case of finite systems, atomic orbitals (Eq. 2) are used to build up the molecular orbitals. For infinite systems, Bloch functions, $\phi_\mu(\vec{r};\vec{k})$, are used to build up crystalline orbitals $\psi_i(\vec{r};\vec{k})$

$$\psi_i(\vec{r};\vec{k}) = \sum_{\mu} c_{\mu i}(\vec{k})\,\phi_\mu(\vec{r};\vec{k}) \tag{17}$$

where $\vec{r}$ and $\vec{k}$ represent vectors in the direct and reciprocal space, respectively. Bloch functions are defined as follows

$$\phi_\mu(\vec{r};\vec{k}) = \sum_{\vec{T}} \chi_\mu(\vec{r} - \vec{A}_\mu - \vec{T})\, e^{i\vec{k}.\vec{T}} \tag{18}$$

where $\vec{T}$ represents all direct lattice vectors. χ_μ represents contracted GTOs as defined in Eq. 2. The subscript μ counts over all the basis functions used to expand the unit cell, $\vec{A}_\mu$ indicates the coordinates of the atom on which χ_μ is centered. The Bloch functions (Eq. 18) are constructed to satisfy the Bloch theorem:

$$\phi_\mu(\vec{r} + \vec{T};\vec{k}) = \phi_\mu(\vec{r};\vec{k}) e^{i\vec{k}.\vec{T}} \tag{19}$$

Bloch functions with different wavevectors, *k*, do not interact each other; therefore, a periodic system can be solved independently for each value of *k*.

It is seen that a crystalline orbital (Eq. 17) resembles the definition of a molecular orbital (Eq. 10) in finite systems. The expansion coefficients for the crystalline orbitals $c_{\mu i}$, Eq. 17, are found analogously to the case of finite systems. The matrix *C*(*k*), which contains the coefficients $c_{\mu i}$, is found by solving self-consistently Eq. 20 for each *k* point.

$$H^{KS}(k)C(k) = S(k)C(k)E(k) \tag{20}$$

where $H^{KS}(k)$ is the Kohn-Sham Hamiltonian matrix in reciprocal space

$$H_{\mu\nu}^{KS}(k) = \left\langle \phi_\mu(\vec{r};\vec{k}) \middle| \hat{h}^{KS} \middle| \phi_\nu(\vec{r};\vec{k}) \right\rangle = \sum_{\vec{T}} \left\langle \chi_\mu(\vec{r} - \vec{A}_\mu - \vec{0}) \middle| \hat{h}^{KS} \middle| \chi_\nu(\vec{r} - \vec{A}_\nu - \vec{T}) \right\rangle e^{i\vec{k}.\vec{T}}$$

$S(k)$ is the overlap matrix over the Bloch functions

$$S_{\mu\nu}(k) = \left\langle \phi_\mu(\vec{r};\vec{k}) \middle| \phi_\nu(\vec{r};\vec{k}) \right\rangle = \sum_{\vec{T}} \left\langle \chi_\mu(\vec{r} - \vec{A}_\mu - \vec{0}) \middle| \chi_\nu(\vec{r} - \vec{A}_\nu - \vec{T}) \right\rangle e^{i\vec{k}.\vec{T}}$$

$E(k)$ is a diagonal matrix that contains the eigenvalues ε_i^k for a given point k. The number of eigenvalues per k point is equal to the number of basis functions of the unit cell, and $C(k)$ contains columnwise the coefficients of the crystalline orbitals.

The density of states (DOS) of the infinite system is found according to

$$DOS(\varepsilon) = 2\sum_{i,k} \delta(\varepsilon - \varepsilon_i^k) = \frac{2}{V_{BZ}} \sum_i \int_{BZ} \delta(\varepsilon - \varepsilon_i^k) d^3k \qquad (21)$$

where V_{BZ} is the volume of the first Brillouin zone. The commercial software Crystal 03 (*52*) is used to calculated the density of states for the different crystalline materials that are use throughout his dissertation.

2.3.1 DOS of Au and Pd crystals

The Au and the Pd crystals are modeled as FCC lattices with space group number 225. The lattice parameter for the conventional cells are a = 4.078 Å for gold and a = 3.891 Å for palladium. The primitive cell for both crystals contains one atom and is defined by the following primitive vectors

$$A_1 = \frac{1}{2}a\hat{y} + \frac{1}{2}a\hat{z}$$
$$A_2 = \frac{1}{2}a\hat{x} + \frac{1}{2}a\hat{z}$$
$$A_3 = \frac{1}{2}a\hat{x} + \frac{1}{2}a\hat{y}$$

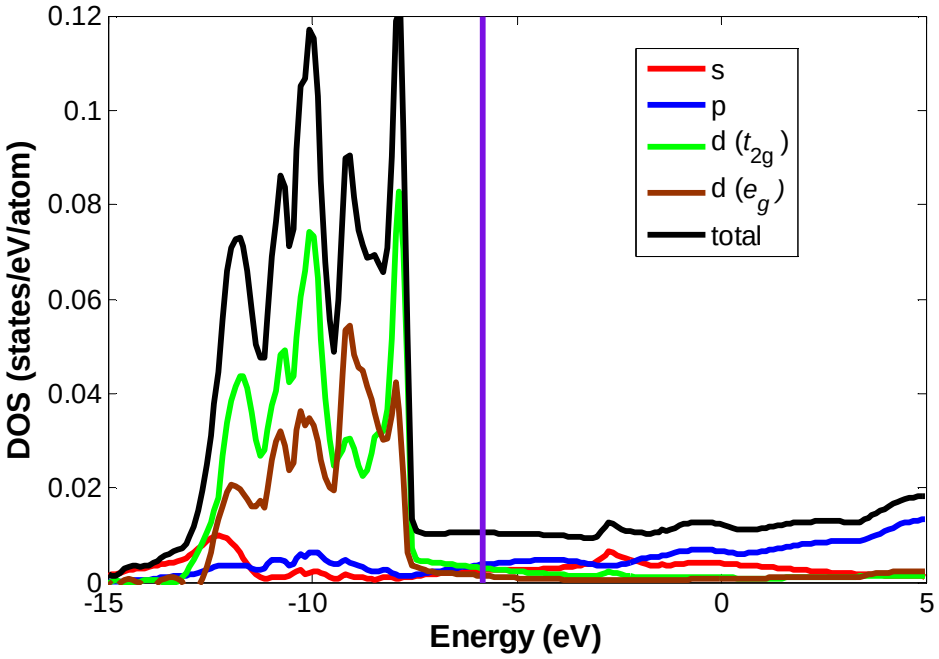

Fig. 5. DOS for the Au crystal, ECP is at -5.83 eV. It is obtained using the B3PW91 functional and LANL2DZ basis set. The necessary input files are given in Appendix 1.

The calculation of the electronic structure is performed at the B3PW91 level of theory combined with the LANL2DZ basis set. The total DOS for gold (black curve) is reported in Fig. 5. We also compute the contribution of each type of basis function (s-, p-, or d-type) to the total DOS. For consideration to the symmetry of the d-type functions, their contribution are split into two groups: the contribution of the d_{xz}, d_{yz}, d_{xy}

basis functions, which present t_{2g} symmetry and the contribution of the d_{z^2} *, $d_{x^2-y^2}$ basis functions, which present e_g symmetry. The DOS for the Pd crystal is reported in Fig. 6. For Au and Pd, most of the electrons available for conduction (at their ECP) have a d-character.

The necessary input files to calculate the Au DOS using the Crystal 98 code are given in Appendix 1.

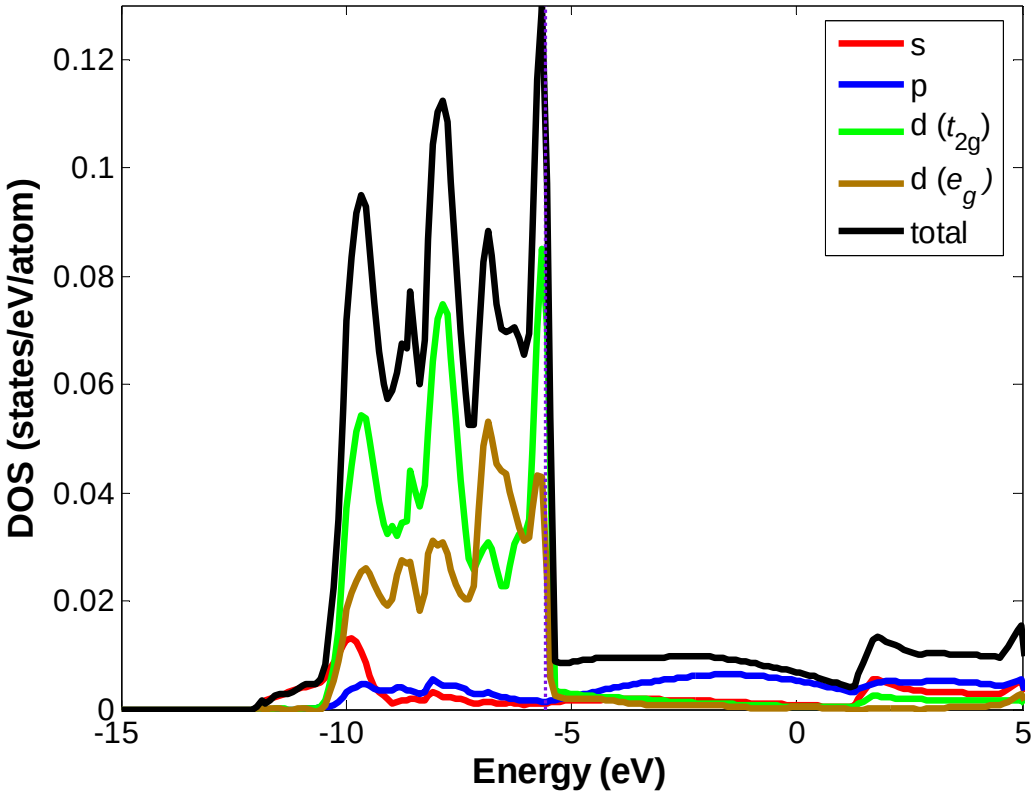

Fig. 6. DOS for the Pd crystal obtained using the B3PW91 functional and LANL2DZ basis set. The ECP is marked by the vertical dotted line at -5.59 eV.

* The orbital d_{z^2} is more properly referred as $d_{2z^2-x^2-y^2}$

2.3.2 DOS of silicon crystal

Silicon presents a crystal structure of the diamond (point group number 227). The conventional cell has a lattice parameter a = 5.42 Å. The primitive cell is defined by the following primitive vectors

$$A_1 = \frac{1}{2}a\hat{y} + \frac{1}{2}a\hat{z}$$
$$A_2 = \frac{1}{2}a\hat{x} + \frac{1}{2}a\hat{z}$$
$$A_3 = \frac{1}{2}a\hat{x} + \frac{1}{2}a\hat{y}$$

with two atoms per each primitive cell, the basis vectors for these atoms are

$$B_1 = -\frac{1}{8}A_1 - \frac{1}{8}A_2 - \frac{1}{8}A_3 = -\frac{1}{8}a\hat{x} - \frac{1}{8}a\hat{y} - \frac{1}{8}a\hat{z}$$
$$B_2 = +\frac{1}{8}A_1 + \frac{1}{8}A_2 + \frac{1}{8}A_3 = +\frac{1}{8}a\hat{x} + \frac{1}{8}a\hat{y} + \frac{1}{8}a\hat{z}$$

The crystal is calculated using the B3PW91 level of theory. Two sets of calculations, using different basis sets, are carried out.

The full-electron 6-31G(d) basis set uses one s- and two sp-type basis functions for the Si atom. The total DOS and the s, p, and d projections obtained using that basis set are shown in Fig. 7. The states around the ECP have mostly a p character and a bandgap of 0.72 eV; the midgap is at -2.22 eV. The two input files required for the Crystal 03 software are shown in Appendix 2.

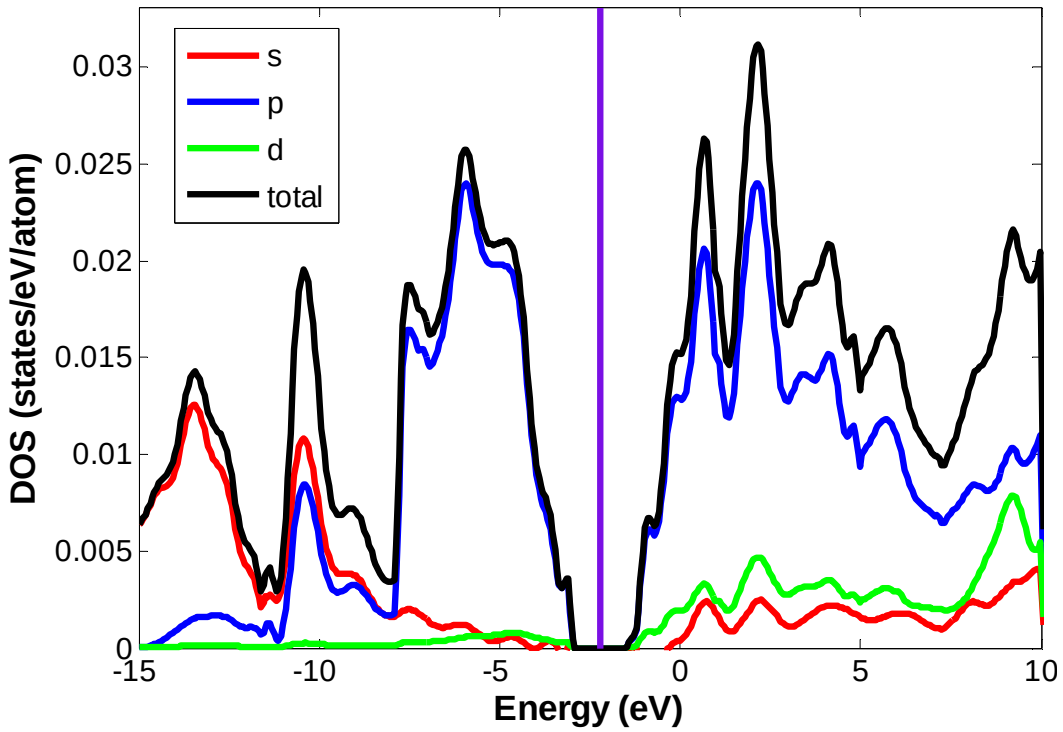

Fig. 7. DOS for a silicon crystal calculated using the B3PW91 method and the 6-31G(d) basis set. The necessary input files to the Crystal 03 software are given in the Appendix 2.

The LANL2DZ basis set supports elements with high atomic numbers, such as gold. Whenever the molecule under study contains gold atoms, the system is calculated using the LANL2DZ basis set. Therefore, for compatibility purposes, the DOS of Si using the LANL2DZ basis set is also obtained. LANL2DZ is not a full-electron basis set for Si; only the four valence electrons are represented by basis functions; the remaining ten core-electrons are modeled by an effective core potential (ECP). The Si DOS using this basis set is reported in Fig. 8; notice that there is not d projection of the total DOS since no d-type basis functions are associated to Si in the LANL2DZ basis set.

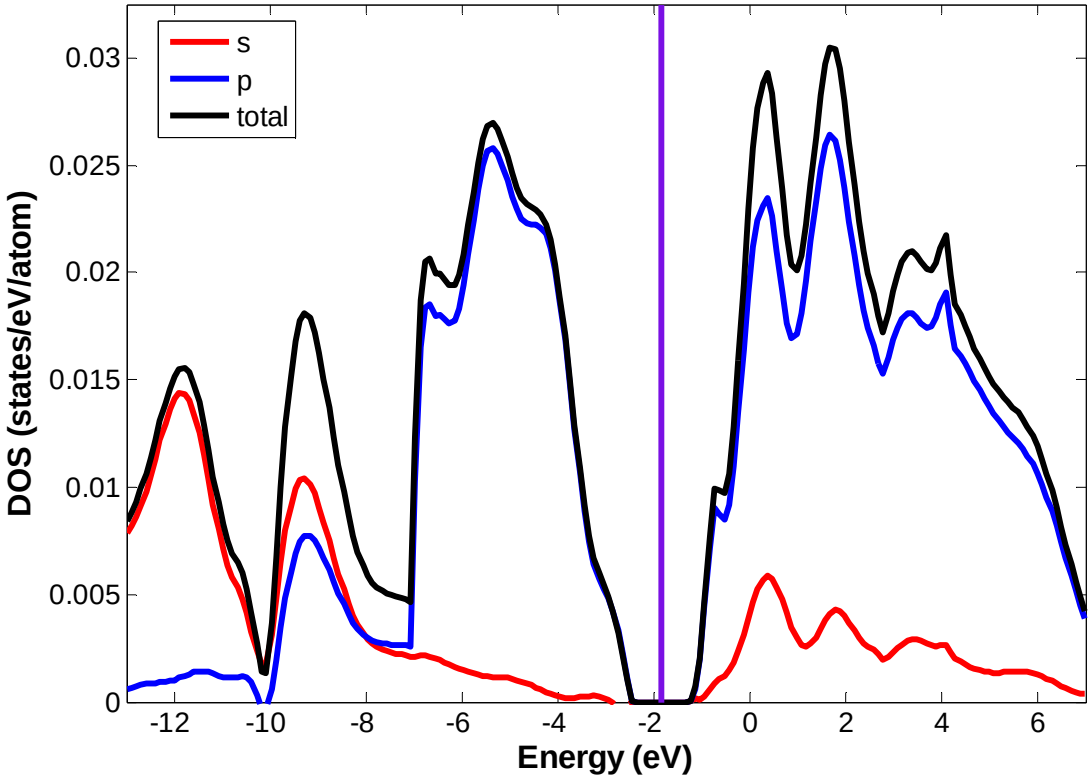

Fig. 8. DOS for a silicon crystal calculated using the B3PW91 DFT method and the LANL2DZ basis set. The ECP for the material (purple line) is at -1.85 eV. The calculated bandgap is 1.11 eV.

2.3.3 DOS of the (4,4) CNT

SWCNTs are one-dimensional crystals with interesting mechanical and electrical properties. The geometry and the electrical behavior of a SWCNT are defined by two integer numbers (*m*,*n*). It is known (*53*) that

$$if\begin{cases} n-m=3q \\ n-m=0 \\ n-m\neq 3q \end{cases} then\begin{cases} semimetallic \\ metallic \\ semiconductors \end{cases} ;bandgap\begin{cases} \sim meV \\ 0\,eV \\ 0.5-1eV \end{cases} \quad (22)$$

where q is a non-zero integer. Recent breakthroughs in synthetic chemistry (*54*) have opened the possibility of using metallic CNTs as contacts to organic molecules. We use the (4,4) CNT, which is a metal according to Eq. 22, to explore the electrical characteristic of CNT-nitroOPE-CNT molecular junctions. The DOS of the (4,4) CNT, , Fig. 9, is calculated using the B3PW91 DFT functional and the 6-31G basis set. Despite the presence of a gap in the CNT DOS at ~3.50 eV, the absence of gaps at the ECP confirms the metallic character of this material. The calculated DOS is in agreement with previous experimental (*55*, *56*) and theoretical (*57-60*) findings.

A unit cell of the (4,4) CNT is modeled by sixteen carbon atoms. The geometry and other input files for the Crystal 03 software are given in the Appendix 3.

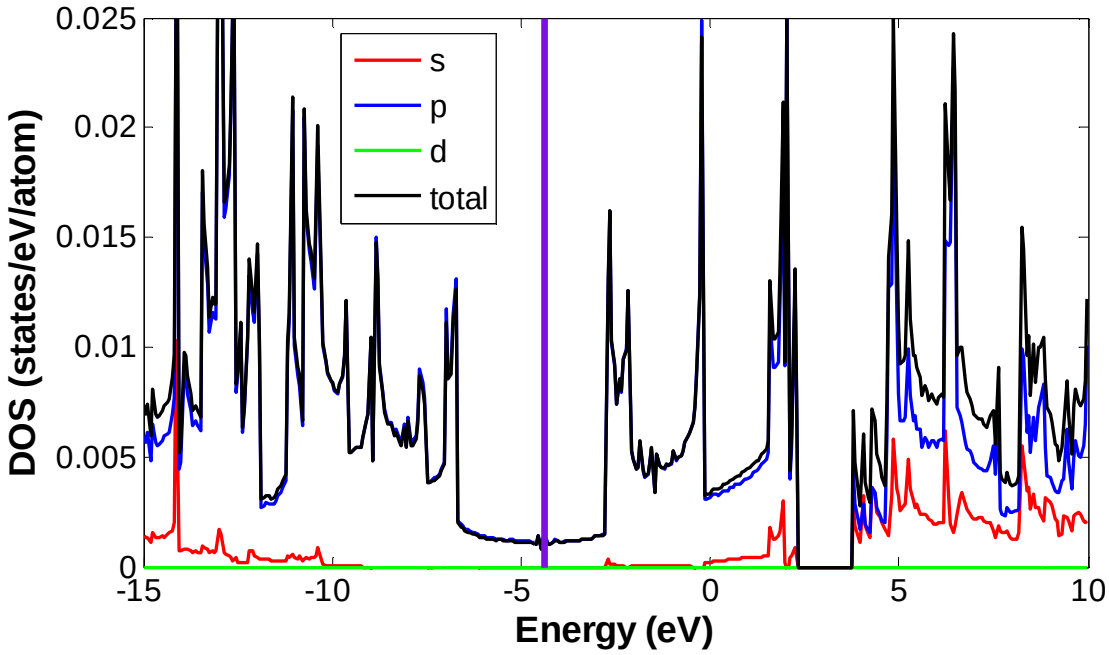

Fig. 9. DOS for the metallic (4,4) CNT, which is calculated using the B3PW91/6-31G method and basis set. The ECP (purple vertical line) is at -4.39 eV. The input files for Crystal 03 are given in Appendix 3.

2.4 Combined DFT-GF approach to calculate the DOS of a molecule adsorbed on macroscopic contacts

An isolated molecule has discrete electronic states, which are precisely calculated from the Schrödinger equation. When the molecule is attached to macroscopic contacts, the continuous electronic states of the contacts modify the electronic properties of the molecule. A technique that combines the Density Functional Theory and the Green function (DFT-GF) (*61, 62*) is used to account for the effect of the contacts on the electronic states of adsorbed molecule.

In a real system, molecules are chemically attached to real contacts, made of atoms, and not to ideal surfaces. Therefore, information about the interface, obtained at the molecular level, needs to be provided. This is accomplished through coupling matrices obtained from quantum-mechanical calculations of the extended molecule (i.e., the molecule attached to a few atoms from the contacts). The Gaussian 03 (*63*) commercial software is used for the quantum-mechanical calculations of all the finite systems throughout this work. Thus, our calculations consider explicitly the chemistry of the attachment of the molecule to the contacts instead of unrealistic simulations of a molecule attached to perfect or ideal surfaces.

For a hypothetical molecular system that has only five basis functions (χ), the elements of the Kohn-Sham Hamiltonian matrix (H^{KS}) are given by

$$H^{KS} = \begin{pmatrix} \langle \chi_1 | \hat{h}^{KS} | \chi_1 \rangle & \langle \chi_1 | \hat{h}^{KS} | \chi_2 \rangle & \langle \chi_1 | \hat{h}^{KS} | \chi_3 \rangle & \langle \chi_1 | \hat{h}^{KS} | \chi_4 \rangle & \langle \chi_1 | \hat{h}^{KS} | \chi_5 \rangle \\ \langle \chi_2 | \hat{h}^{KS} | \chi_1 \rangle & \langle \chi_2 | \hat{h}^{KS} | \chi_2 \rangle & \langle \chi_2 | \hat{h}^{KS} | \chi_3 \rangle & \langle \chi_2 | \hat{h}^{KS} | \chi_4 \rangle & \langle \chi_2 | \hat{h}^{KS} | \chi_5 \rangle \\ \langle \chi_3 | \hat{h}^{KS} | \chi_1 \rangle & \langle \chi_3 | \hat{h}^{KS} | \chi_2 \rangle & \langle \chi_3 | \hat{h}^{KS} | \chi_3 \rangle & \langle \chi_3 | \hat{h}^{KS} | \chi_4 \rangle & \langle \chi_3 | \hat{h}^{KS} | \chi_5 \rangle \\ \langle \chi_4 | \hat{h}^{KS} | \chi_1 \rangle & \langle \chi_4 | \hat{h}^{KS} | \chi_2 \rangle & \langle \chi_4 | \hat{h}^{KS} | \chi_3 \rangle & \langle \chi_4 | \hat{h}^{KS} | \chi_4 \rangle & \langle \chi_4 | \hat{h}^{KS} | \chi_5 \rangle \\ \langle \chi_5 | \hat{h}^{KS} | \chi_1 \rangle & \langle \chi_5 | \hat{h}^{KS} | \chi_2 \rangle & \langle \chi_5 | \hat{h}^{KS} | \chi_3 \rangle & \langle \chi_5 | \hat{h}^{KS} | \chi_4 \rangle & \langle \chi_5 | \hat{h}^{KS} | \chi_5 \rangle \end{pmatrix} \quad (23)$$

The atoms of the molecular system can be classified as belonging to the contact 1, the contact 2, or the molecule (*M*). For illustration, the atoms conforming the

contact 1, the contact 2, and the molecule are modeled by the χ_2; χ_3, χ_4; and χ_1, χ_5 basis functions, respectively. After reordering and partitioning H^{KS} into submatrices we have:

$$H_{11} = \left(\langle \chi_2 | \hat{h}^{KS} | \chi_2 \rangle \right) \tag{24}$$

$$H_{22} = \begin{pmatrix} \langle \chi_3 | \hat{h}^{KS} | \chi_3 \rangle & \langle \chi_3 | \hat{h}^{KS} | \chi_4 \rangle \\ \langle \chi_4 | \hat{h}^{KS} | \chi_3 \rangle & \langle \chi_4 | \hat{h}^{KS} | \chi_4 \rangle \end{pmatrix} \tag{25}$$

$$H_{MM} = \begin{pmatrix} \langle \chi_1 | \hat{h}^{KS} | \chi_1 \rangle & \langle \chi_1 | \hat{h}^{KS} | \chi_5 \rangle \\ \langle \chi_5 | \hat{h}^{KS} | \chi_1 \rangle & \langle \chi_5 | \hat{h}^{KS} | \chi_5 \rangle \end{pmatrix} \tag{26}$$

$$H_{1M} = \begin{pmatrix} \langle \chi_2 | \hat{h}^{KS} | \chi_1 \rangle & \langle \chi_2 | \hat{h}^{KS} | \chi_5 \rangle \end{pmatrix} \tag{27}$$

$$H_{M1} = \begin{pmatrix} \langle \chi_1 | \hat{h}^{KS} | \chi_2 \rangle \\ \langle \chi_5 | \hat{h}^{KS} | \chi_2 \rangle \end{pmatrix} \tag{28}$$

$$H_{2M} = \begin{pmatrix} \langle \chi_3 | \hat{h}^{KS} | \chi_1 \rangle & \langle \chi_3 | \hat{h}^{KS} | \chi_5 \rangle \\ \langle \chi_4 | \hat{h}^{KS} | \chi_1 \rangle & \langle \chi_4 | \hat{h}^{KS} | \chi_5 \rangle \end{pmatrix} \tag{29}$$

$$H_{M2} = \begin{pmatrix} \langle \chi_1 | \hat{h}^{KS} | \chi_3 \rangle & \langle \chi_1 | \hat{h}^{KS} | \chi_4 \rangle \\ \langle \chi_5 | \hat{h}^{KS} | \chi_3 \rangle & \langle \chi_5 | \hat{h}^{KS} | \chi_4 \rangle \end{pmatrix} \tag{30}$$

where H_{MM} is the submatrice representing the isolated molecule (restricted molecule). The other submatrices represent the couplings between the molecule (subscript *M*) and the atoms of the contact (subscripts 1 and 2).

Then, we create an ordered Hamiltonian matrix (*H*) and the respective overlap matrix (*S*) in the following way

$$H = \begin{pmatrix} H_{11} & H_{1M} & H_{12} \\ H_{M1} & H_{MM} & H_{M2} \\ H_{21} & H_{2M} & H_{22} \end{pmatrix} \tag{31}$$

$$S = \begin{pmatrix} S_{11} & S_{1M} & S_{12} \\ S_{M1} & S_{MM} & S_{M2} \\ S_{21} & S_{2M} & S_{22} \end{pmatrix}$$

This Hamiltonian matrix for the extended molecule (*H*) can also be recalculated in case of an external field in order to account for the reorganization of the molecular electronic structure due to the presence of such field, including among others the effects of charge transfer between the molecule and the contacts. Notice that the molecule itself does not have an integer charge for any of the charge states of the extended molecule because the charge distributes between the isolated molecule and the metal atoms. Charge transfers between molecule and contact occur even at zero bias voltage and also as a result of an externally applied field. Certainly, this charge transfer is limited due to the small number of metal atoms attached to the molecule, which is not a major problem since it is clearly demonstrated from theoretical as well as experimental information (*64-66*) that the connection of the molecule to the metal is only through one or two metal atoms as concluded in reference (*64*); however, the interactions with the atoms located beyond these nearest neighbors are very small and truncated; this constitutes the strongest approximation of our procedure. Fortunately, there is strong evidence that it is an acceptable approximation because it precisely considers the

chemistry and physics of the actual local attachment or bonding of the molecule to the catalyst atoms (*64*, *65*).

The coupling between atoms of the catalyst atoms and those of the molecule yields the self-energy term, Σ_j.

$$\Sigma_j = H_{Mj} g_j H_{jM} \qquad j = 1,2 \tag{32}$$

where it depends on the complex Green function, g_j, describing the contact j. The complex g_i can be obtained from any source as long as it can be represented in matrix form of the appropriate dimensions; it provides the information from the contact to the DFT-GF formalism. We choose to generate the Green function for the catalyst using Crystal 03 since it allows obtaining a high-level electronic structure of a bulk system of any shape using DFT. This complex function is defined as

$$g_j(E) = -\pi\sqrt{-1}\begin{pmatrix} g_j^1 & \cdots & 0 \\ \vdots & \ddots & \vdots \\ 0 & \cdots & g_j^{n_j} \end{pmatrix} \qquad j = 1,2 \tag{33}$$

where each value of the diagonal matrix is proportional to the local density of states DOS, which has been calculated in 2.3.

$$g_j^k(E) = \begin{pmatrix} \mathrm{DOS}_j s^k(E) & 0 & 0 & 0 \\ 0 & \mathrm{DOS}_j p^k(E) & 0 & 0 \\ 0 & 0 & \mathrm{DOS}_j d_{t_2g}^k(E) & 0 \\ 0 & 0 & 0 & \mathrm{DOS}_j d_{e_g}^k(E) \end{pmatrix} \tag{34}$$

In order to keep consistency in the matrix dimensions of Eq. 57, the index k runs over all the interfacial atoms that represent contact j (k = *1*,..,n_j). Each diagonal

term of Eq. 34 is again another diagonal matrix, in such a way that the size of $\mathrm{DOS}_j s^k(E)$ is equal to the number of *s*-type basis functions use to model the electronic structure of the type of atom that composes contact *j*.

The coupling of the molecule to the contacts is obtained from molecular calculations (H_{iM} and H_{Mi} in the extended molecule Hamiltonian, shown in Eq. 31) that consider the atomistic nature of the contact-molecule interface. The interaction terms defined in Eq. 32 are added to the molecular Hamiltonian to account for the effect of the catalyst on the molecule:

$$H_e = \begin{pmatrix} H_{11} & H_{1M} & H_{12} \\ H_{M1} & H_{MM} + \Sigma_1 + \Sigma_2 & H_{M2} \\ H_{21} & H_{2M} & H_{22} \end{pmatrix} \tag{35}$$

To account for the non-orthogonality of the basis set, the overlap matrix (*S*) modifies the Hamiltonian into

$$H_e^{'} = S^{-1} H_e = \begin{pmatrix} H_{11}^{'} & H_{1M}^{'} & H_{12}^{'} \\ H_{M1}^{'} & H_{MM}^{'} & H_{M2}^{'} \\ H_{21}^{'} & H_{2M}^{'} & H_{22}^{'} \end{pmatrix} \tag{36}$$

This modified Hamiltonian is used to obtain the Green function for a molecule attached to two contact tips,

$$G_M(E) = (E1 - H_{MM}^{'})^{-1} \tag{37}$$

Finally, the Density of States (DOS) of the molecule subjected to the effect of the two contacts is calculated as:

$$DOS = \frac{\sqrt{-1}}{2\pi} * Trace(G_M - G_M^{\dagger}) \tag{38}$$

Within the Green function formalism, two separated and independent calculations are needed. First, molecular calculations on the molecule of interest plus a few atoms like those in the contact. Second, a calculation of the density of states of each contact; those calculations can be performed at any level of theory; however it is desirable to choose *ab initio* methods known to provide chemical accuracy, such as DFT using generalized gradient approximation or better.

2.5 Application example: Study of a molecule-metal interface*

Here we simplify the DFT-GF formalism described in 2.4 to the special case of both contacts being the same, i.e., contact 1 = contact 2. In other words, the molecule is attached to a contact at two different bonding sites instead of being attached to two different contacts. In this way, we study the problem of a single molecule lying on top of substrate material. The specific problem is the electroreduction and dissociation of molecular oxygen, O_2. This problem is at the heart of the proton-exchange membrane (PEM) fuel cell technology. The molecular oxygen fed to the fuel cell needs to be dissociated and negatively charged, as described for the proposed first one-electron equation:

$$O_2 + e^- \xrightarrow{catalyst} \left(O_2^-\right)_{adsorbed} \tag{39}$$

* Most of the results have been published in reference 47. P. B. Balbuena, D. Altomare, L. Agapito, J. M. Seminario, *Journal of Physical Chemistry B* **107**, 13671-13680 (2003).

In this case, the substrate bulk material exerts strong influence on the molecular oxygen to undergo a conformational and electronic change of its structure (chemisorption), which is generically described as the catalytic effect. However, the mechanism by which the catalyst exerts its influence is not totally understood.

One of the aims of the present work is to propose a mechanism for the effect of the catalyst on the oxygen dissociation. Fig. 10 shows a schematic of O_2 (red atoms) chemisorbed on a catalytic platinum substrate. The density of states of the Pt-Pt-O-O molecule, under the presence of a Pt background, is calculated for different O-O distances and plotted on the right side of Fig. 10. A second aim of this work is to search for catalysts alternative to platinum; alloys of Pt with less expensive metals such as Co, Ni and Cr are investigated. The DOS of the discrete systems O_2NiNiPt, O_2CoCoPt, and O_2PtPtPt under the influence of platinum background is calculated and shown in Fig. 11.

A general trend is noticed in Fig. 10 (right), the two DOS peaks around the Fermi level of Pt (-5.93 eV) merge into one as the O-O distance is being increased. In the total dissociation limit (O-O distance ~5 Å), there is not oxygen-oxygen interaction and each oxygen behaves as an "isolated" atom, presenting a unique DOS peak (doubly degenerated) at same energy. Then, the closer the DOS peaks, the better the O-O dissociation. Therefore, the shape of the DOS for the adsorbed molecule can be used as a figure of merit to assess the effectiveness of a substrate to dissociate the molecular oxygen.

Comparing the relative position of the DOS peaks in Fig. 11, it is concluded that O_2NiNiPt induces the worst oxygen dissociation and O_2CoCoPt the best.

In a metal, the electrons at the Fermi level are considered "free" electrons, which are available for conduction. In the present case, the "free" electrons are readily transferred from the substrate to the molecular oxygen. The DOS, at the Fermi level, of the O_2 molecule under the influence of the substrate gives a qualitative estimation of the number of electrons that are transferred from the substrate to the O_2 molecule.

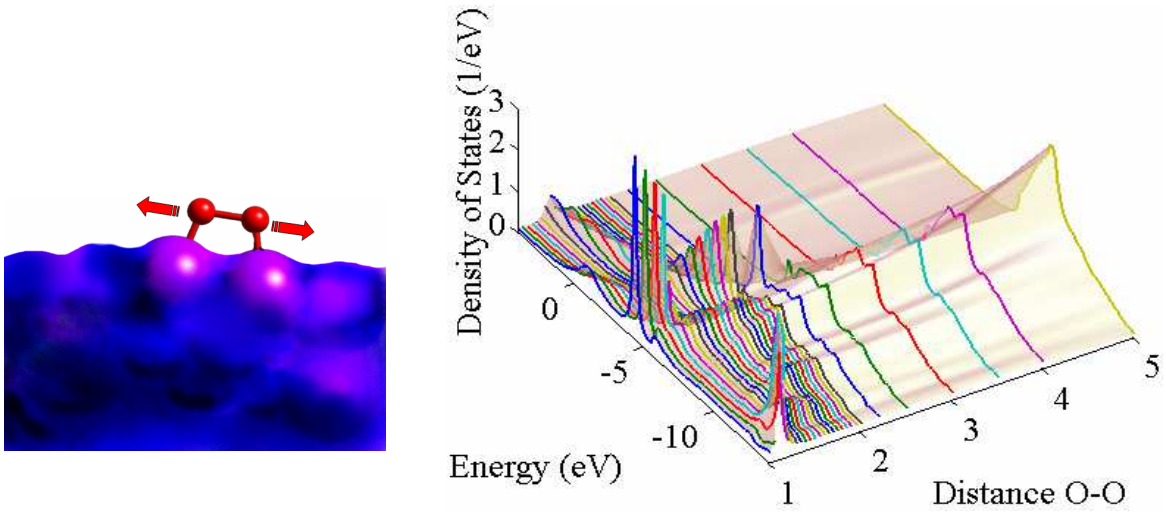

Fig. 10. The center of the O-O bond is located at 2.10 Å from the center of the Pt-Pt bond. The Pt-Pt (2.47 Å) and the Pt-O bond distances are kept constant, whereas the O-O bond length is varied progressively from the gas phase O-O bond length, 1.2 Å, to 5 Å, under the influence of a Pt background. From reference (*47*).

From Fig. 11, we observe that at the Fermi level the O_2NiNiPt system (blue) has lower density of states than the system alloyed with Co (pink). The O_2PtPtPt system (green) presents a value of DOS intermediate between the Co and the Ni alloys. Then, a catalyst of Pt alloyed with Co allows for higher transfer of electrons between the substrate and the O_2; therefore, it is more helpful for the required electroreduction reaction pointed in Eq. 39.

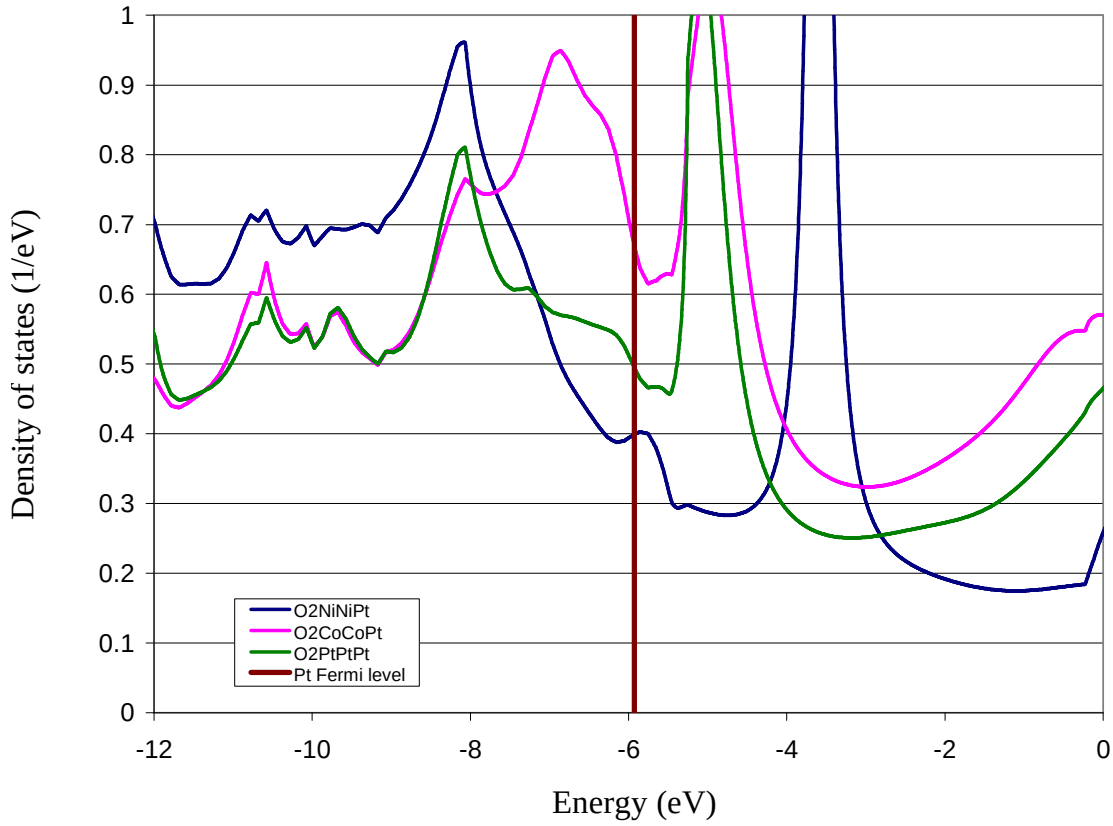

Fig. 11. DOS for the O_2NiNiPt, O_2CoCoPt, and O_2PtPtPt, all embedded in a Pt metal. The occupied states of all the systems are qualitatively similar; however, they all differ considerably in the proximity of the Fermi level. Note the decrease in the amount of the available states for O_2NiNiPt (not a good promoter of O_2 electroreduction), in contrast with the case of O_2CoCoPt. The first peak corresponding to the unoccupied states for O_2CoCoPt and O_2PtPtPt is located in the same range of energies, but for O_2CoCoPt the proximity of this peak with the one at the left of the Fermi level is found to be a signal of O_2 dissociation being favored by this system. From reference (*47*).

Several bimetallic systems are investigated as listed in the second column of Table 2. All molecular geometries and wavefunctions are optimized using the B3PW91 DFT method and a combined LANL2DZ/6-31G basis set. The first group of systems, where O_2 is adsorbed on a Pt-Pt bond with both Pt atoms bonded to a foreign metal (Co, Ni, Cr), does not represent an improvement over the pure Pt case. A good degree of dissociation is found for the second group, where O_2 bonds to a Pt-X metal with both Pt and X bonded to a Pt atom, except when X = Ni. Not much improvement is obtained for the third group, where O_2 is chemisorbed on a PtX site with both Pt and X bonded to an

X atom. The best promoter of O_2 dissociation and electroreduction is found to be the case of O_2 adsorbed to a Co-Co bond, where both Co are connected to a Pt atom. The worst case is O_2 adsorbed to a Ni-Ni bond, both Ni are connected to a Pt atom, in all cases the small systems in Table 2 is embedded in a Pt metal background.

Fig. 11 illustrates these concepts for three systems; one in which the active sites are Pt atoms (O_2PtPtPt) is compared with the "worst" O_2NiNiPt and the "best" O_2CoCoPt cases.

Table 2. Density of states (DOS) of each molecule-metal system as indicated in the first column, the metal background is Pt. The difference in energy (Δ*E*) between the main peak of the occupied states located at the left of the Pt Fermi level, and the main peak of the virtual states located at the right of the Pt Fermi level, provides an indication of the degree of O_2 dissociation, as shown in Fig. 10. From reference (*47*).

Group	System	DOS at Pt Fermi level (1/eV)	Δ*E* between peaks at both sides of Pt Fermi level (eV)	O-O distance at the chemisorbed state (Å)
1	O_2PtPtPt	0.50	3.0	1.41
	O_2PtPtCo	0.52	4.0	1.38
	O_2PtPtNi	0.50	4.0	1.38
	O_2PtPtCr	0.60	3.5	1.37
2	O_2PtCoPt	0.55	2.5	1.45
	O_2PtNiPt	0.50	3.8	1.40
	O_2PtCrPt	0.60	1.5	1.47
3	O_2PtCoCo	0.55	3.8	1.40
	O_2PtNiNi	0.55	3.3	1.41
	O_2PtCrCr	0.52	3.8	1.41
4	O_2CoCoPt	0.65	2.0	1.49
	O_2NiNiPt	0.40	4.3	1.38
	O_2CrCrPt	0.72	1.5	1.41

2.6 Conclusions

An atomistic formalism, DFT-GF, is presented to calculate the distribution of electronic states of a single molecule under the influence of two macroscopic contacts. The contacts are semi-infinite molecular systems with a continuous distribution of electronic states. The formalism accounts for the transfer of electrons between the contacts and the adsorbed molecule.

The DFT-GF formalism is applied to investigate the behavior of active catalytic sites including the effect of the bulk environment on the reaction. The procedure is illustrated for O_2 dissociation on bimetallic active sites in which Co, Cr, or Ni atoms are mixed with Pt atoms all embedded in a Pt matrix.

We show that the DOS of the O_2 embedded in a substrate can be used to predict qualitatively the catalytic power of the substrate. Two main properties are required from a good catalyst for fuel-cell applications: electroreduction (to transfer electrons from the substrate to the O_2 molecule) and dissociation of the O_2 molecule (to breakge the O-O bond). We establish that the higher value of the DOS at the Fermi level the better the electroreduction of the O_2. Also, the closer the two DOS peaks at the Fermi level, the more dissociated the O_2 is. This analysis permits us to identify the best ensembles of bimetallic active sites that favor O_2 dissociation. It is found that O_2 chemisorption on O_2XXPt (X = Co and Cr) are the best active sites to promote O_2 dissocation. On the other hand, ensembles involving Ni atoms produce similar degrees of O_2 dissociation as those of pure Pt.

In short, O_2CoCoPt (O_2 adsorbed to a Co-Co bond and both Co connected to the Pt atom) is the best alloy for catalyst and the worst case is O_2NiNiPt (O_2 adsorbed to a Ni-Ni bond and both Ni connected to a Pt atom). Both systems are immersed in a Pt background.

CHAPTER III

ELECTRON TRANSPORT IN MOLECULAR ELECTRONIC DEVICES*

3.1 Introduction

The ability to calculate the current-voltage through a single molecule is essential for engineering molecular electronic devices (*67*). Because quantum-mechanical effects are prevailing in atomistic sizes, standard mesoscopic descriptions of electron transport cannot be applied in molecular systems.

In order to evaluate the use of single molecules as electronic devices, we need to attach them to contacts to be able to measure their electrical properties. The presence of macroscopic contacts influences greatly the electrical properties of a single molecule (*32*); therefore, there is a need to test the metal-molecule-metal junction as an independent unit instead of evaluating the isolated molecule. Experimentally, it has been challenging to measure metal-molecule-metal junctions, where the metallic contacts are separated by a distance of ~20 Å. Only few experiments until now have claimed to have been able to address a single molecule between two macroscopic gold contacts (*33*).

Fortunately, quantum-chemistry techniques can be used to study precisely isolated molecules. We use the DFT of quantum chemistry to determine the electronic properties of molecules; a mathematical formalism based on the Green function (GF), is used to account for the effect of the contacts.

The electron transport in junctions of atomic sizes is coherent. In the coherent regime, the electrons travel, with a given probability, sequentially one after the

* Part of this chapter is reprinted with permission from J. M. Seminario, Y. Ma, L. A. Agapito, L. Yan, R. A. Araujo, S. Bingi, N. S. Vadlamani, K. Chagarlamudi, T. S. Sudarshan, M. Myrick, P. E. Colavita, P. D. Franzon, D. P. Nackashi, L. Cheng, Y. Yao,

other through the molecule without electron-electron or phonon-electron interactions. This kind of transport is described by the Landauer formalism (*68*). Here, we use our DFT-GF technique, which is explained in the previous chapter, to make an atomistic adaptation of the Landauer formalism for the calculation of current through molecular junctions.

Specifically, we focus our study in the nitroOPE molecule, which has been proposed as a candidate for a molecular electronic device (*31*). Similar OPE molecules, attached to gold contacts, have shown two distinctive states of conductance, namely, a high- and a low- conductance state. Those states can be used to encode information as logic "0" and "1," hence, their importance. Switching between both states of the molecule is attributed to two different mechanism: changes in charge state (*31*) and changes in conformational state (*69*). We use the DFT-GF formalism to calculate the conductance through metal-nitroOPE-metal junctions in several charge and conformational states. Two different metallic materials are evaluated: the commonly used gold and the promising (4,4) CNT.

We also use our adaptation of the Landauer formalism to explain the leakage current observed in discontinuous gold films.

3.2 Calculation of current through a molecular junction

We model our molecular system as a generic two-port network, shown in Fig. 12B. The bias voltage is defined as: $V = V_1 - V_2$. Thus, contact 1 is considered the positive electrode and contact 2 the negative one. At contact 1, we define i_1^- as the current* flowing from contact 1 towards the molecule and i_1^+ as the backscattered current,

---

J. M. Tour, *Journal of Nanoscience and Nanotechnology* **4**, 907 (2004).

* Throughout this work, the term "current" will refer to "current of electrons," not to the conventional "current of positive charges."

which flows from the molecule to the contact. Likewise, at contact 2, we have i_2^+ flowing from contact 2 to the molecule, and i_2^- flowing from the molecule to contact 2.

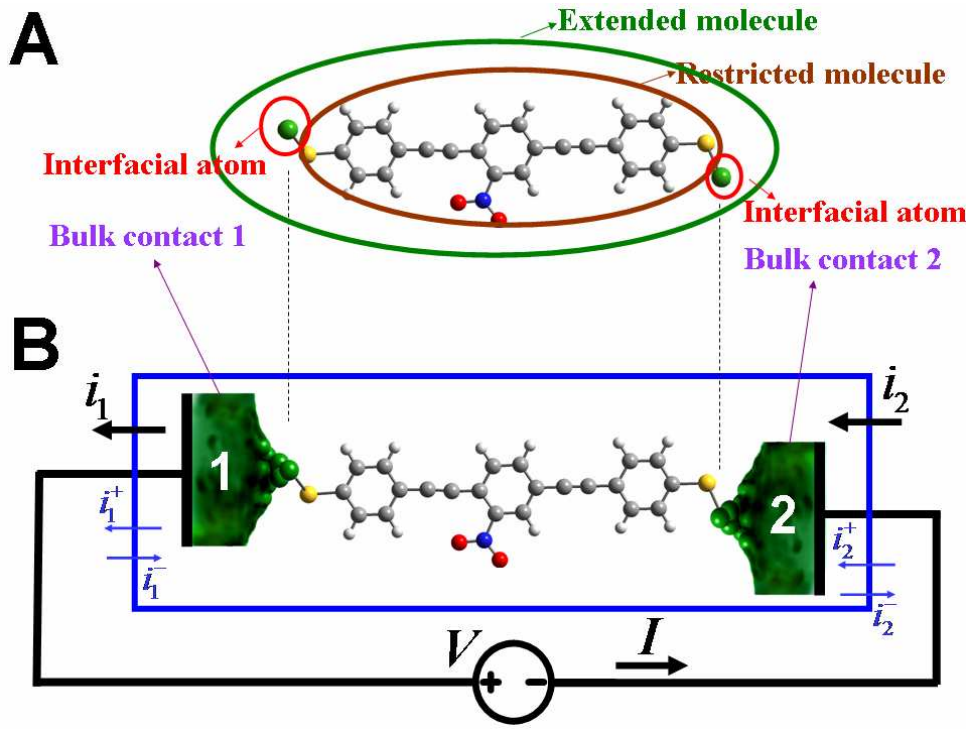

Fig. 12. (A) Terminology used in our electron transport calculations. The *bulk* contacts are pictorial representations of the two macroscopic tips that approach the molecule. A *restricted* molecule corresponds to the model under study itself; it includes the *alligator* atoms, such as sulfur, if they are present. *Interfacial* atoms correspond to atoms of the type belonging to the bulk contacts. The *extended* molecule is composed of the restricted molecule and some atoms of the type belonging to each contact material. (B) Convention used for the direction of the currents and the polarity of the bias voltage.

The associated scattering matrix for such two-port network is

$$\begin{pmatrix} i_1^+ \\ i_2^- \end{pmatrix} = \begin{pmatrix} s_{11} & s_{12} \\ s_{21} & s_{22} \end{pmatrix} \begin{pmatrix} i_1^- \\ i_2^+ \end{pmatrix} \tag{40}$$

where the elements of the scattering matrix are defined as

$$s_{21} = \left.\frac{i_2^-}{i_1^-}\right|_{i_2^+=0} \tag{41}$$

$$s_{12} = \left.\frac{i_1^+}{i_2^+}\right|_{i_1^-=0} \tag{42}$$

$$s_{22} = \left.\frac{i_2^-}{i_2^+}\right|_{i_1^-=0} \tag{43}$$

$$s_{11} = \left.\frac{i_1^+}{i_1^-}\right|_{i_2^+=0} \tag{44}$$

From Eq. 41, s_{21} is interpreted as the number of electrons that can reach contact 2 (considering contact 2 as reflectionless, $i_2^+ = 0$), per each electron that is injected from contact 1. In other words, it is the probability for an electron to cross the molecular junction from contact 1 to contact 2. Analogously, s_{12} represents the probability for an electron to cross the junction from contact 2 to contact 1. At equilibrium, the probability for a particle to tunnel through a barrier would be the same whether it crosses the barrier from left to right or from right to left. We define this quantity as the transmission probability, $\overline{T}$.

$$s_{21} = s_{12} = \overline{T} \tag{45}$$

From Eq. 43, s_{22} is the number of backscattered electrons per each electron that goes through contact 1, considering no reflection at contact 2. Then it is the

probability for an electron injected through port 2 to be reflected, which is the complement of the transmission probability.

$$s_{11} = s_{22} = 1 - \bar{T} \tag{46}$$

Then, Eq. 40 becomes

$$\begin{pmatrix} i_1^+ \\ i_2^- \end{pmatrix} = \begin{pmatrix} 1-\bar{T} & \bar{T} \\ \bar{T} & 1-\bar{T} \end{pmatrix} \begin{pmatrix} i_1^- \\ i_2^+ \end{pmatrix} \tag{47}$$

Eq. 47 ensures the conservation of total current in the two-port network, i.e., $I = i_1 = i_2$, where

$$i_1 = i_1^+ - i_1^-$$

$$i_2 = i_2^+ - i_2^-$$

At a given energy *E*, the current per mode per unit energy (as a result of an occupied state in one contact leaking into the molecule) is given by $\frac{2e}{h}$*. For a partially occupied state, such current needs to be corrected by the Fermi distribution factor (*f*) of the contact. The total current leaking from contact 1 into the molecule is given by

$$i_1^-(E) = \frac{2e}{h} M(E) f_1(E) dE \tag{48}$$

* Throughout this work, the value of *e* refers to the charge of a proton $+1.602177 \times 10^{-19}$

where $M(E)$ is the number of transmission modes allowed for the molecule at the energy E. Analogously, the number total current leaking from contact 2 into the molecule before reaching equilibrium is

$$i_2^+(E) = \frac{2e}{h} M(E) f_2(E) dE \tag{49}$$

When a small bias voltage ($V \neq 0$) is applied between the contacts of the junction, the molecular system is taken out of equilibrium and the electrons start flowing. The application of a positive bias voltage between the contacts shifts down the ECP of contact 1 and shifts up the ECP of contact 2. In both cases, the shifts are by an equal amount of $0.5 \times e \times V$ with respect to the equilibrium ECP of the extended molecule (μ_{EM}) (*65*), in the following way

$$\mu_2^* = \mu_{EM} + \frac{1}{2} eV \tag{50}$$

$$\mu_1^* = \mu_{EM} - \frac{1}{2} eV \tag{51}$$

Consequently, the Fermi distribution functions of both contacts are shifted whenever a bias voltage (V) is applied to the junction; this makes the Fermi distributions dependent on the applied bias voltage.

$$f_2(E - \mu_{EM} - \frac{1}{2} eV) = \frac{1}{1 + e^{\frac{E - \mu_2^*}{kT}}} \tag{52}$$

$$f_1(E - \mu_{EM} + \frac{1}{2} eV) = \frac{1}{1 + e^{\frac{E - \mu_1^*}{kT}}} \tag{53}$$

Combining Eqs. 47, 48, 49, 52, and 53, we obtain

$$i(E,V) = \frac{2e}{h} M(E)\bar{T}(E)[\, f_2(E - \mu_{EM} - \frac{1}{2}eV) - f_1(E - \mu_{EM} + \frac{1}{2}eV)]dE \qquad (54)$$

Defining the transmission function as $T(E) = M(E)\bar{T}(E)$ and integrating over energy we have that the total current of electrons flowing between the contacts is:

$$I(V) = \frac{2e}{h} \int_{-\infty}^{+\infty} T(E,V)[\, f_2(E - \mu_{EM} - \frac{1}{2}eV) - f_1(E - \mu_{EM} + \frac{1}{2}eV)]dE \qquad (55)$$

The transmission function, *T*, is obtained from the chemistry of the molecular junction. It is defined as (*70*):

$$T(E,V) = \frac{1}{N} Trace(\Gamma_2 G_M \Gamma_1 G_M^{\dagger}) \qquad (56)$$

where *N* is the number of basis functions used to represent the restricted molecule and *V* is the bias voltage applied between the contacts. The coupling (Γ_j) between the molecule and the contact *j* is defined as

$$\Gamma_j = \sqrt{-1}(\Sigma_j - \Sigma_j^{\dagger}) \qquad j = 1,2 \qquad (57)$$

where the self-energy term, Σ_j (Eq. 32), depends on the Green function of the contacts. The Green function *g*(*E*) (Eq. 33) depends on the ECP of the contact, which varies with the applied voltage according to Eqs. 50 and 51. Consequently, the Green function of

each contact, the self-energy terms Σ_j, the coupling terms Γ_j, and the transmission function are a function of the applied voltage, i.e, $T(E,V)$.

3.3 Metal-molecule-metal junctions

3.3.1 Metal-benzene-metal junction

We aim to study the conductance of the nitroOPE molecule, which is composed of three benzene rings (Fig. 4A), attached to metallic CNT tips. We start the analysis with a simpler case, a single benzene molecule between two CNT tips (CNT-benzene-CNT junction). The Au-S-benzene-S-Au junction has been studied before (*61, 71*); in those calculations, the adsorption of the benzene to the gold contacts is possible by use of a sulfur atom connecting a carbon and a gold atom (thiol bond). Recent research has shown the possibility of direct attachment of benzene to carbon nanotubes (*37-39, 72*); this opens the possibility of employing metallic CNTs as contacts to organic molecules.

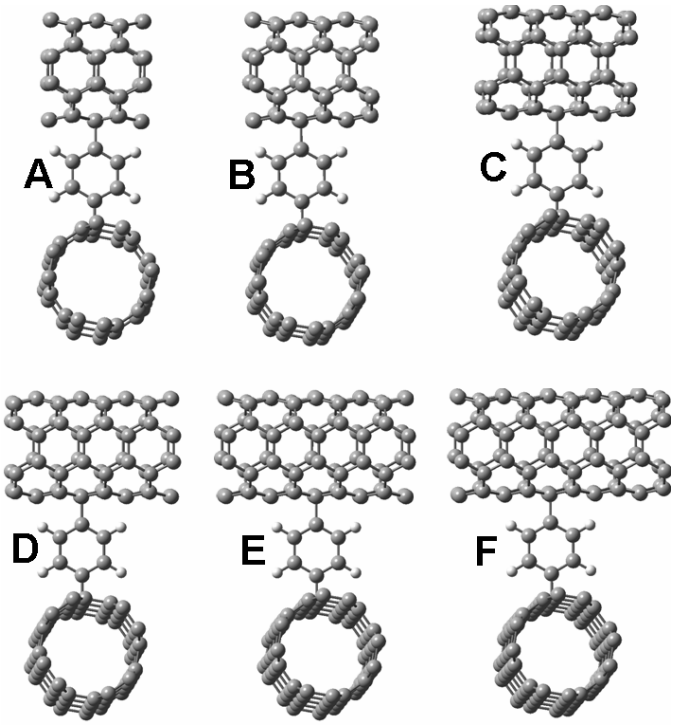

Fig. 13. Molecular junctions of the type metal-benzene-metal. The pieces of (4,4) CNTs (metal) are shown above and below the benzene. A ring of the metallic CNT is defined to be composed by 8 carbon atoms. The total number of atoms belonging to the top and bottom CNTs is increased progressively, both contacts are constructed to have the same number of carbon atoms. (A) is composed by 5 rings in the top and also 5 rings in the bottom contact, (B) by 6, (C) by 7, (D) by 8, (E) by 9, and (F) by 10. The molecular junction shown in (F) is indexed as Molecule 4.

The first step in simulating the benzene connected to two infinitely long CNT contacts is the inclusion of interfacial carbon atoms, representing the CNT contacts, in the extended molecule (see terminology in Fig. 12). It is known that an infinitely long (4,4) CNT shows metallic behavior (*53*), but small pieces of (4,4) CNT need not necessarily show a metallic character. Therefore, the CNT has to be modeled by an adequate number of atoms such that metallic behavior is reached. The second step is to include the effect of the continuum of electronic states provided by the infinitely long nature of the (4,4) CNT contacts; this is accomplished by the use of the DFT-GF approach described in 2.4.

We test several junctions in which each CNT contact is modeled by 40, 48, 56, 64, 72, and 80 carbon atoms, corresponding to Fig. 13A, B, C, D, E, and F respectively. The DOS for the (4,4) CNT, which is shown in Fig. 9, and the electronic structures of all the molecular junctions are calculated using the B3PW91 DFT method combined with the 6-31G basis set. The calculation of the I-Vs (Fig. 14) shows that all the junctions present consistently similar values of current, indicating that even 40 carbon atoms suffice to model each CNT contact. Moreover, in a previous work (*73*), we demonstrated that small pieces of CNT, composed of 80 atoms, did behave as expected for their infinitely long counterparts, i.e., metallic character for the (4,4) and the (9,0), and semiconducting character for the (8,0) CNT.

All the junctions show ohmic behavior, with a constant resistance of ~2 MΩ, for small bias voltages (< ~3 V). The ohmic behavior at low bias voltages agrees with the theoretical calculations reported by Derosa (*61*) and Di Ventra (*71*).

Gold has more electrons available for conduction per atom than the metallic (4,4) CNT has (~10 times higher at their ECPs, see Fig. 5 and Fig. 9); which in principle should make the Au-S-benzene-S-Au junction more conducting that the CNT-benzene-CNT junction. However, the current in the CNT-benzene-CNT junction, at 2 V, is found to be higher than the values reported by Derosa (*61*) and Reed (*33*) for the Au-S-benzene-S-Au junction. We attribute that higher current to the better (seamless) chemical bond between the benzene and the CNT than the Au-S-benzene bond.

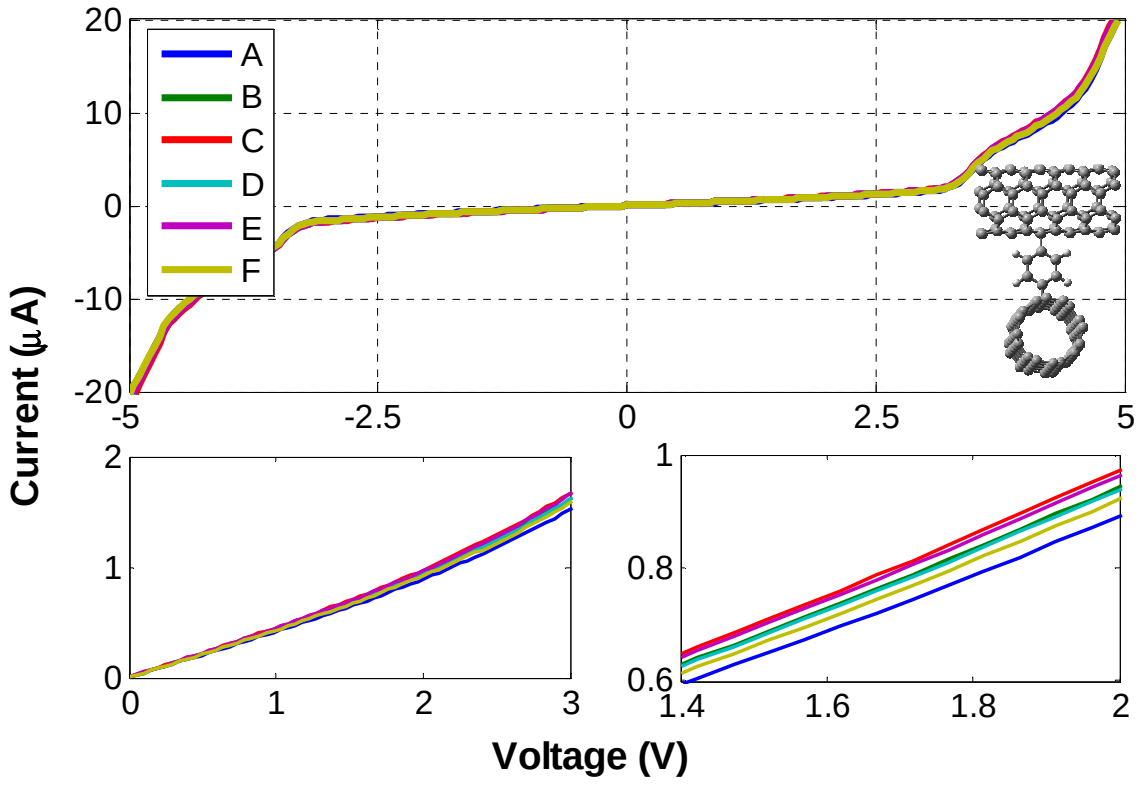

Fig. 14. Current-voltage characteristics for six junctions of the form CNT-benzene-CNT (shown in Fig. 13). In each junction a different number of carbon atoms is used to model the CNT contact (40, 48, 56, 64, 72, and 80 carbon atoms corresponding to the junctions A, B, C, D, E, and F, respectively). The inset shows the geometry of the junction F. The plots on the bottom part are two amplifications of the ohmic region.

3.3.2 Metal-nitroOPE-metal junction

We calculate junctions containing the nitroOPE molecule under metallic contacts such as Au and the (4,4) CNT. These results will be considered as references for subsequent calculations, which will include semiconducting contacts.

Gold has been the preferred contact material for the experiments on molecular conduction either as a vapor-deposited top contact, such as in a nanopore device, or as the tip of an STM (*74*). Here, we study two cases in which the nitroOPE is bonded to gold contacts, the Au_6-nitroOPE-S-Au_1 and the Au_1-S-nitroOPE-S-Au_1 junction.

In the Au_6-nitroOPE-S-Au_1 junction, the bottom contact is modeled by one interfacial gold atom. The nitroOPE is bound to the gold atoms by a thiol bond (C-S-Au). The top contact is modeled by six interfacial gold atoms that are not chemically bonded to the nitroOPE. This type of physical bond is expected to be found in experimental measurements of molecular I-V that use an STM tip as top contact. The geometry of the extended molecule is shown in the lower right corner of Fig. 15B.

The neutral, the first charge state (anion) and the perpendicular conformational state are calculated for this Au_6-nitroOPE-S-Au_1 junction. Also, two different and possible geometrical conformations are calculated. In the coplanar conformation, the three phenyl rings in the nitroOPE are lying in the same plane; however, in the perpendicular conformation, the middle phenyl ring is perpendicular to the other two. The calculation establishes the coplanar conformation as more stable than the perpendicular conformation, with a rotational barrier of -0.20 eV (-4.7 kcal/mol) for the middle phenyl ring. The current-voltage calculations for the coplanar, perpendicular and anion states are reported in Fig. 15A.

In the Au_1-S-nitroOPE-S-Au_1 junction, one gold atom is used to represent each contact. The attachment of the nitroOPE molecule to both gold atoms is through thiol bonds. The geometry of this junction is shown in the lower right corner of Fig. 16A. The current-voltage characteristic for the coplanar, perpendicular, and anion states for this junctions are shown in Fig. 16.

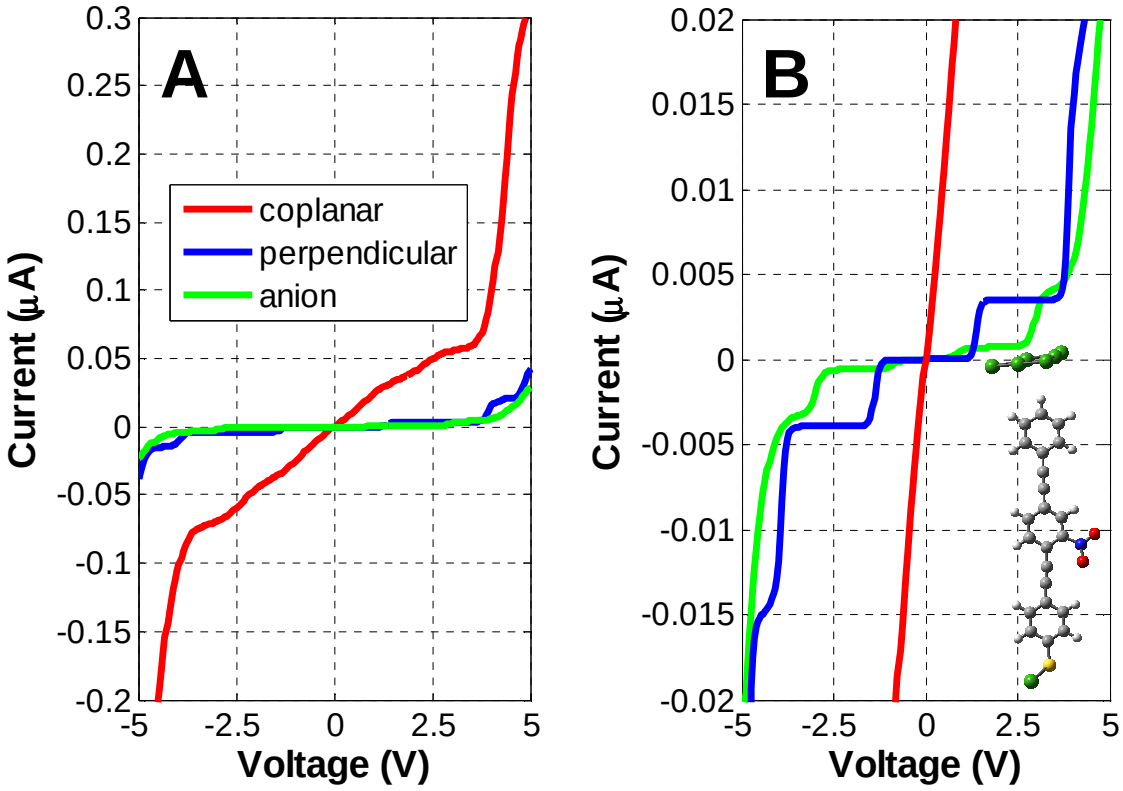

Fig. 15. (A) Current-voltage characteristic for Au_6-nitroOPE-S-Au_1 junction shown in Fig. 4C. (B) Amplification of the low-current region of (A). The coplanar conformation of the molecular junction is shown in the lower part of (B). The C, H, S, N, O, and Au atoms are colored grey, white, yellow, blue, red, and green, respectively.

For both junctions, the Au_6-nitroOPE-S-Au_1 and the Au_1-S-nitroOPE-S-Au_1, two distinct states of conductance are observed, high conductance (red curve) and low conductance (green and blue curves). The neutral molecule (charge = 0) presents high conductance whereas the anion (charge = -1) and the perpendicular state show low conductance. Moreover, the high-conductance state of the junctions shows ohmic behavior at low bias voltage, which agrees with previous results reported for similar molecules (*31*, *62*, *69*).

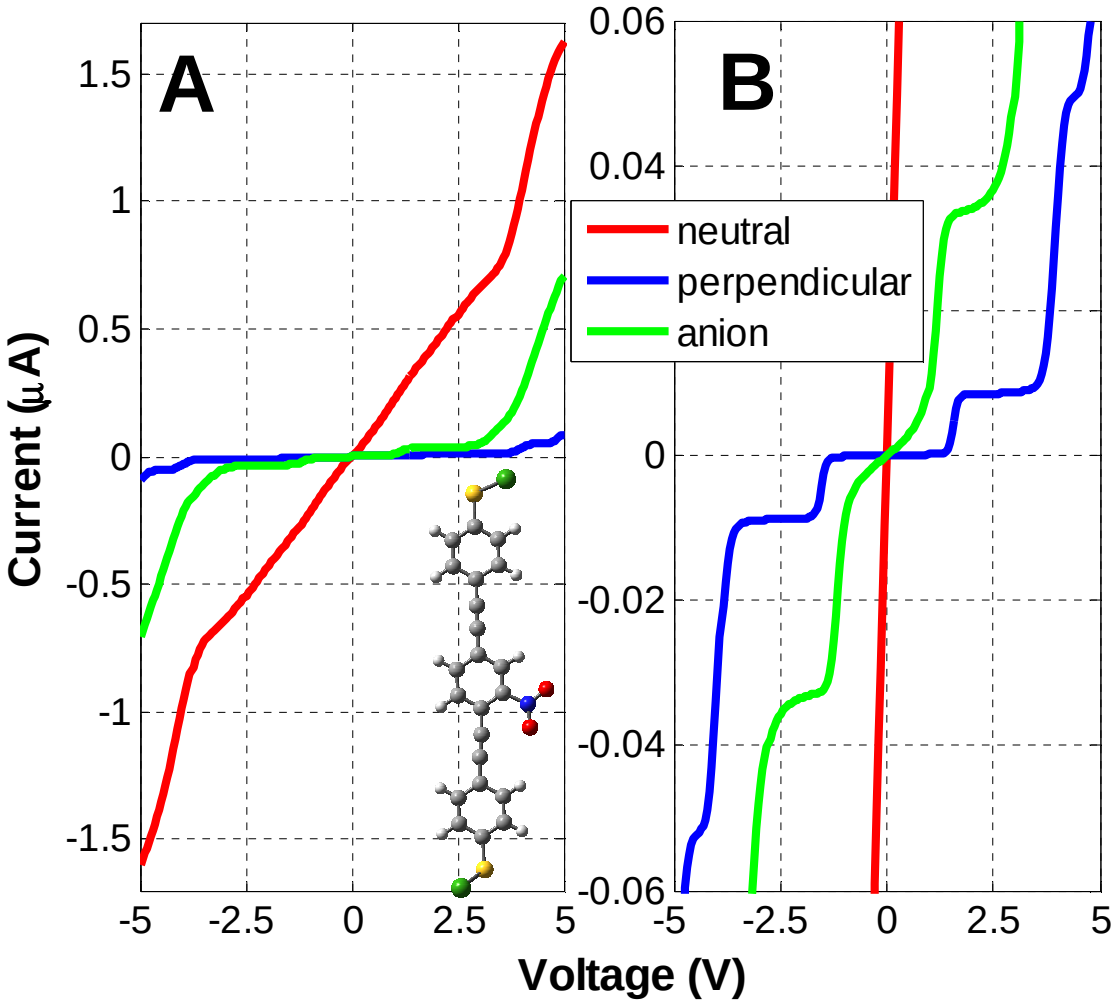

Fig. 16. (A) Current-voltage characteristic for the nitroOPE under two gold tips (green). Sulfur atoms (yellow) have been included too. (B) Amplification of (A). The coplanar conformation of the molecular junction is shown in the lower right corner of (A).

The Au_1-S-nitroOPE-S-Au_1 junction allows for significantly higher current (~5 times) than the Au_6-nitroOPE-S-Au_1. The physical bond, present between the nitroOPE and the six-gold plane, is a gap of atomistic size that obstructs the flow of electrons. It is effectively a thin tunneling barrier for the electrons to overcome. The thiol bond in the top contact of the Au_1-S-nitroOPE-S-Au_1 junction allows more transfer of electrons than the physical bond in the top contact of the Au_6-nitroOPE-S-Au_1

junction. In this regard, Cui *et al*. have experimentally demonstrated (*75*) a difference of four orders of magnitude between the current in a chemisorbed junction ("glued" by covalent bonds) and the current in a physisorbed junction ("glued" by physical bonds).

We study metallic CNTs as prospective contacts for molecular junctions. Eighty carbon atoms are used to model a piece of the (4,4) CNT. The geometry of the coplanar conformation of the CNT-nitroOPE-CNT junction is shown in the lower right corner of Fig. 17A. The calculated current-voltage characteristics for the coplanar, perpendicular, and anion states are reported in Fig. 17.

Similar to the case when having gold contacts, the two distinct states of conductance attributed to the nitroOPE molecule are still found for the CNT-nitroOPE-CNT junction. The coplanar conformation (red) exhibits high conductance whereas the perpendicular and anion states (blue and light green respectively) exhibit low conductance.

Despite the fact that gold has more electrons per atom available for conduction than the metallic (4,4) CNT has, the CNT-nitroOPE-CNT allows higher current than the Au_6-nitroOPE-S-Au_1 junction. This is a consequence of the tunneling gap around the top contact of the Au_6-nitroOPE-S-Au_1 junction, which obstruct the flow of electrons.

Although thiol bonds are chemically easy to work with, they present a disadvantage from the electrical point of view. Thiol bonds are highly polar, and polar bonds introduce undesirable capacitive effects that restrict the flow of electrons. Vondrak *et al*. used two-photon photoelectron spectroscopy to show that the S atom, in C-S-Cu thiol bonds, acts as insulators, obstructing the flow of electrons (*76*). Thiol bonds should be considered as thin tunneling barriers. The Au crystal has ~10 times higher density of states than the (4,4) CNT crystal does; however, the Au-S-nitroOPE-S-Au junction exhibits only ~3 times higher current than the CNT-nitroOPE-CNT junction does. This is an indication that the C-C bonds in the CNT-nitroOPE-CNT are electrically superior to the thiol bonds in the Au_1-S-nitroOPE-S-Au_1 junction.

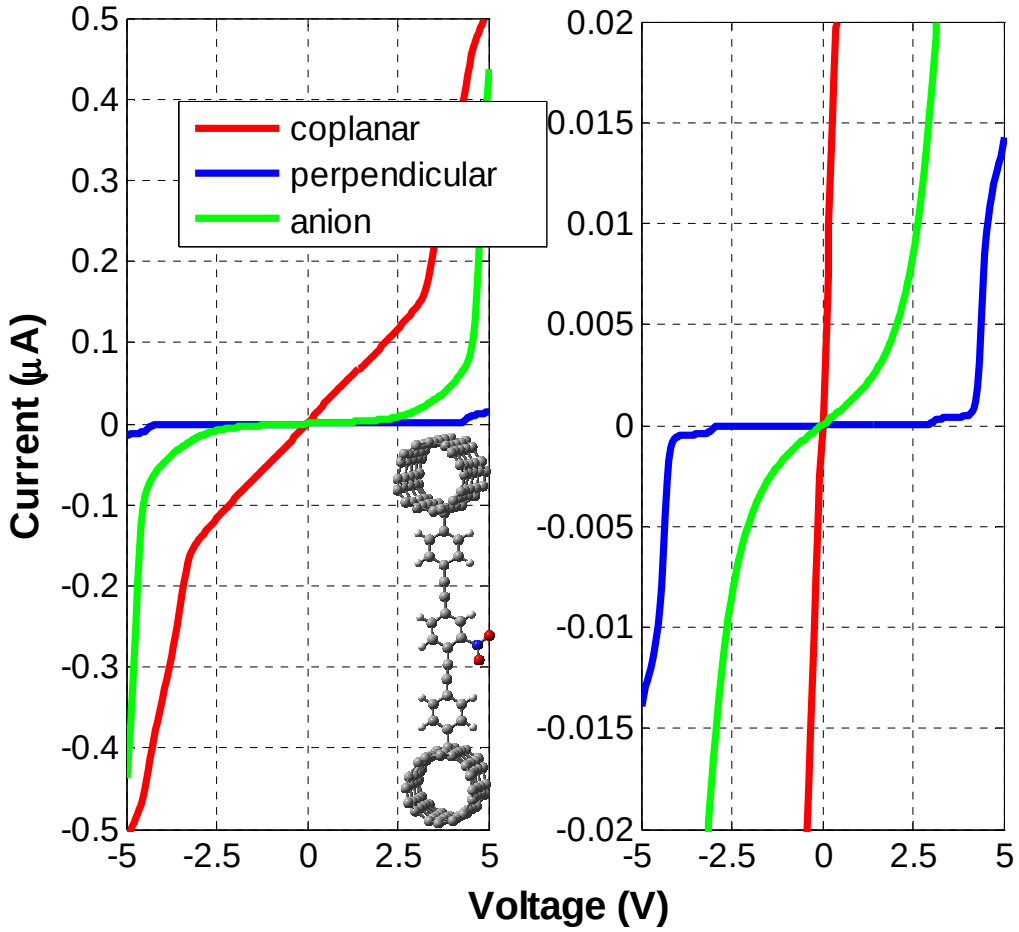

Fig. 17. Left: Current-voltage characteristic for the coplanar, perpendicular, and anion states of the CNT-nitroOPE-CNT junction. The coplanar conformation of the molecular junction is shown in the lower right corner. Right: Amplification of the low-current region.

From another point of view, the Au_1-S-nitroOPE-S-Au_1 and the Au_6-nitroOPE-S-Au_1 junctions can be thought of as a nitroOPE isolated by two thin tunneling barriers at each end, resembling the particle-in-a-box problem. The quantum confinement preserves the discrete nature of the molecular electronic states. The DOS of the perpendicular Au_1-S-nitroOPE-S-Au_1 junction shows the presence of an isolated and narrow peak in the proximity (a channel for conduction) of its ECP. The junction is not conducting until enough bias voltage (energy) is applied to reach the energy of that channel; electron transport takes place by resonant tunneling using that isolated channel.

Moreover, the current does not change with the increase of voltage until another molecular channel is reached. This phenomenon is reflected in the steplike shape of the I-V curve (Fig. 15B). The perpendicular Au_1-S-nitroOPE-S-Au_1 junction shows steplike I-V characteristic (Fig. 16B), too. The steplike variation of the current has also been experimentally observed in molecular systems (*77, 78*).

In summary, metal-nitroOPE-metal junctions are found to have isolated and narrow DOS peaks, which is reflected in steplike I-V curve, whenever they meet two conditions: first, they are in a state of low-conductance (perpendicular conformation or anion); and second, they contain tunneling barriers (physical or thiol bonds). Junctions in states of high conductance (coplanar conformations) and junctions that do not contain tunneling barriers (CNT-nitroOPE-CNT) do not show steplike I-V curve.

3.4 Application example: Study of clustering of nanoparticles in discontinuous gold films

The NanoCell architecture was conceived (*12, 14, 79, 80*) to allow the use of single molecules as the switching building blocks for creating complex logic circuitry (*81*). Recent implementations of NanoCells possess two main components: the gold islands (with a pattern based either on nanoclusters or on discontinuous films) and the interlinking molecules (which bridge two gold islands). Furthermore, simulations have shown that logic gates can be implemented using a NanoCell chip (*14*).

Electrical measurements of these NanoCells show some memory effects; it has been proposed that not only the interlinking molecules (*82*), but also the gold islands might be contributing to the NanoCell NDR-like effects through nanometer-sized filaments interconnecting the gold islands (*12, 83-85*). The primary goal of this study is to isolate the contributions of the gold islands from the NDR effects by studying the NanoCells without the effect of interlinking molecules.

3.4.1 Experimental results

A bare NanoCell device (*12*), which is shown in Fig. 18A, is composed of a patterned region of discontinuous gold film (burgundy) formed by physical vapor deposition onto SiO_2 (dark blue) and electrodes patterned on opposing sides of the NanoCell device (yellow). The discontinuous gold film is zoomed in in Fig. 18B, where the gold islands can be appreciated. The islands are insulated from each other by silicon dioxide gaps (dark gaps) of about 10 nm in average. In principle, the electrical measurement of the NanoCell device from electrode to electrode should yield an open circuit; however, parasitic current has been found. A single NanoCell chip contains several NanoCell devices.

Two kinds of molecules (Fig. 19) are used in this work. Molecule 1 is 4,4'-di(ethynylphenyl)-2'-nitro-1-benzenethiolate, which self-assembles on the discontinuous gold film (*86*, *87*). Molecule 2 is octyltrichlorosilane, which self-assembles on SiO_2 (*88*, *89*). The acetyl group in the thiols protects against reaction with oxygen, and it is removed in situ during the self-assembly process under acid conditions (CH_2Cl_2/MeOH/H_2SO_4), which is reported to yield better results than the traditional NH_4OH/THF mixture (*90*).

Four different ensembles (Fig. 20) are prepared and tested in this work. The first ensemble has only the discontinuous gold film; the second one has Molecule 1 self-assembled on the gold islands of the discontinuous gold film; the third ensemble has Molecule 2 self-assembled on the silicon oxide of the substrate; the fourth one has Molecule 1 and Molecule 2 self-assembled on the gold islands and SiO_2, respectively.

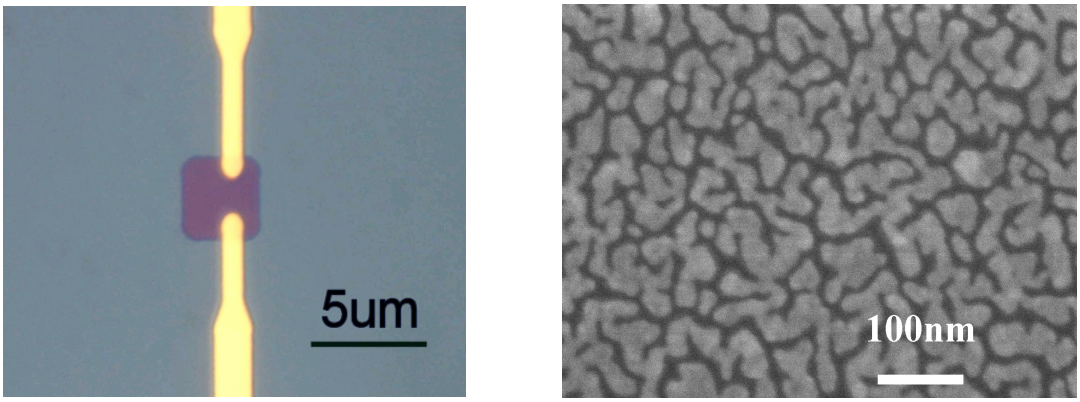

(**A**) (**B**)

Fig. 18. (A) Simple NanoCell used for the measurements are composed of a discontinuous gold film (burgundy) and two leads (yellow) of 2 μm width placed at 1-5 μm deposited on a SiO_2 substrate (blue) using conventional lithography methods (*12*) (B) SEM image of the discontinuous gold film (clear islands) deposited on a SiO_2 substrate (dark regions) in a NanoCell. The typical separation between the gold islands may range from 0 to 10 nm. Filaments between islands are not visible. From reference (*48*).

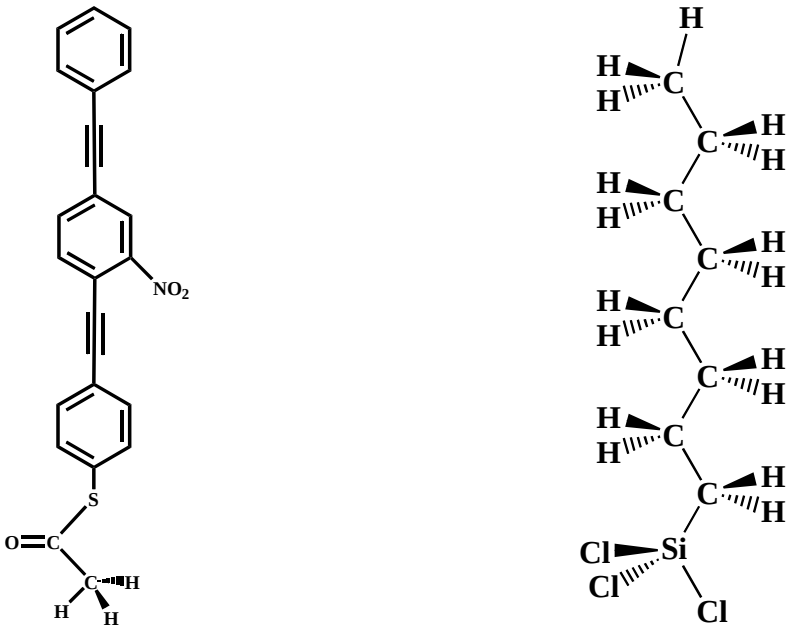

(**A**) (**B**)

Fig. 19. Molecules used for self-assembling on the chips. Molecule 1 generates the 4,4'-di(ethynylphenyl)-2'-nitro-1-benzenethiolate during self-assembly wherein the acetyl group (-$COCH_3$) is cleaved and the sulfur attaches to the gold islands. Molecule 2 is the octyltrichlorosilane. During the self-assembly process, the three chlorine atoms are displaced by surface hydroxyls on the SiO_2 substrate. From reference (*48*).

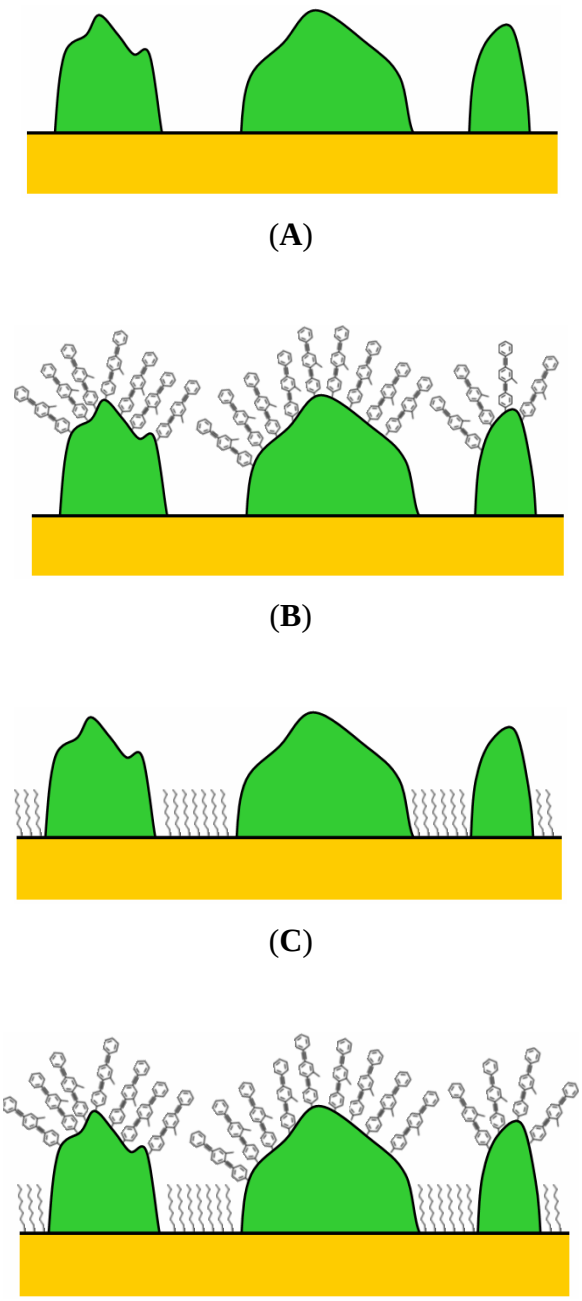

Fig. 20. Schematic drawings (lateral views) of four ensembles of the NanoCells with (A) only the discontinuous gold film (green) on SiO_2 (orange); (B) molecule 1 (the NO_2 is represented by a stick) deposited on the discontinuous gold film islands; (C) molecule 2 deposited on the silicon oxide surface; (D) molecules 1 and 2 deposited on gold and SiO_2, respectively. From reference (*48*).

Thirty NanoCell devices containing only discontinuous gold film (first ensemble, Fig. 20A) have been tested. No NDR behavior is found initially in the NanoCells, instead, linear I-V patterns are found before NDR appeared. From the NanoCells that were tested, 12 exhibited behavior like the one shown in Fig. 21. During the first voltage sweep from 0 V to 5 V, the NanoCell exhibits repeatable linear I-Vs (curves 1 and 2 in Fig. 21A). When the voltage sweeps from 0 V to 10 V, the current drops sharply at a certain voltage V_{th1} = ~6.8 (curve 3 in Fig. 21A). In the next voltage sweep from 0 V to 10 V, the current is very low (~10^{-9} A) at low voltage (< 6 V). Above 6 volts, the current increases ~3 orders of magnitude (Fig. 21B), and we define this voltage as the threshold voltage V_{th2}. Repeatable NDR-like characteristics appear in the subsequent voltage sweeps (Fig. 21C). This sequence of events is referred to as the first observed behavior, which is composed of an initial (Fig. 21A), a transitional (Fig. 21B), and an NDR-like (Fig. 21C) I-V characteristic. For the other six NanoCell devices, the transitional I-V does not occur before NDR appears; whereby, the NDR appears immediately after the sharp drop in the linear I-V.

The other 12 of the measured NanoCells exhibit behaviors similar to those shown in Fig. 22. This is different from the first observed behavior because no linear region is found upon the first voltage sweep. In other words, when a voltage sweep from 0 V to 10 V is applied, nonlinear I-V curves appear (curves 1 and 2 in Fig. 22A). Although the current enhances with increasing voltage, it remains in a low conductance state ($I < 10^{-10}$ A). This behavior persists in subsequent sweeps, until a threshold voltage of ~V_{th2}, at which the current suddenly increases to 10^{-4} A (curve 3 in Fig. 22A). After the bias voltage reaches this threshold (V_{th2}), NDR-like characteristics appear in the subsequent sweeps (curves 4 and 5 in Fig. 22B). This sequence of events, which is composed of the transitional and the NDR-like characteristics, is referred to as the second observed behavior.

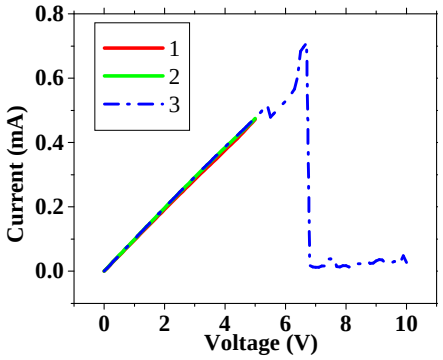

(A)

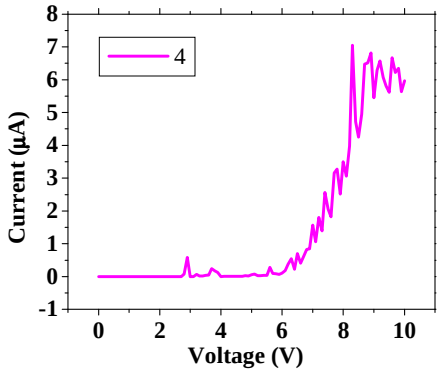

(B)

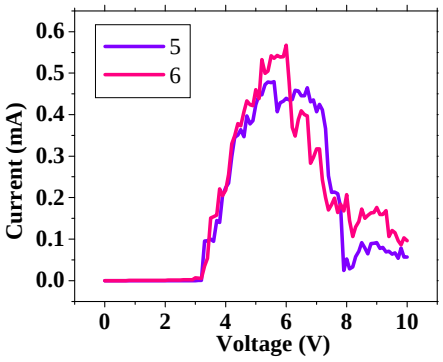

(C)

Fig. 21. First observed I-V behavior of NanoCell device consists of (A) Repeatable (initial) linear I-Vs from 0 to 5 V and their breakdown once the bias voltage exceeds ~6.8 V; (B) Transitional I-V follows the breakdown, low current increases sharply at about 6 V; (C) NDR-like behavior appears in the following sweeps. (The numbers in the legend represent the sequence of the measurement). From reference (*48*).

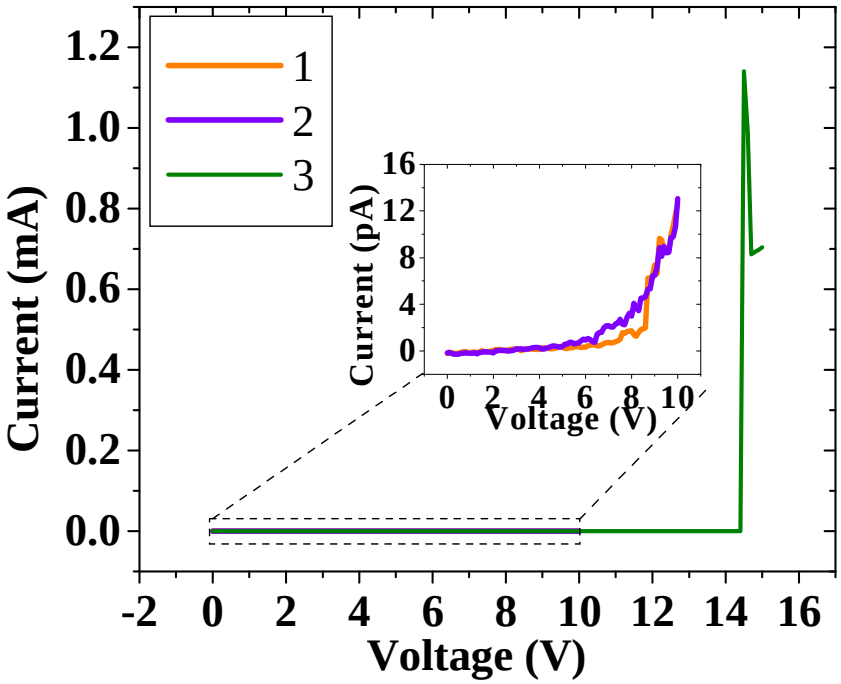

(A)

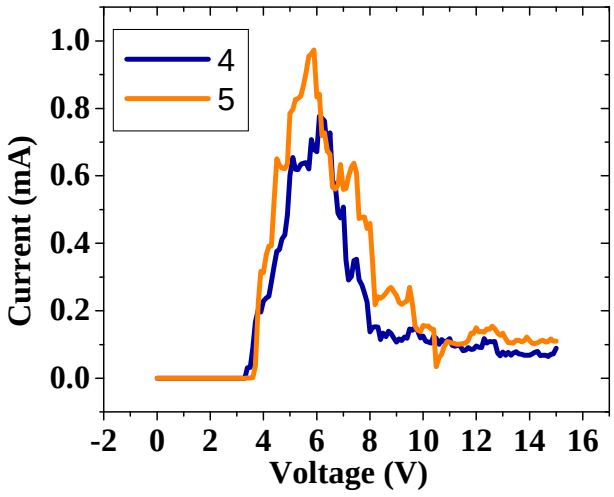

(B)

Fig. 22. Second observed I-V behavior: (A) Repeatable low conduction state (inset) transits to (B) NDR-like state if threshold voltage V_{th2}=14.5 V is applied. (The numbers in the legend represent the sequence of the measurement). From reference (*48*).

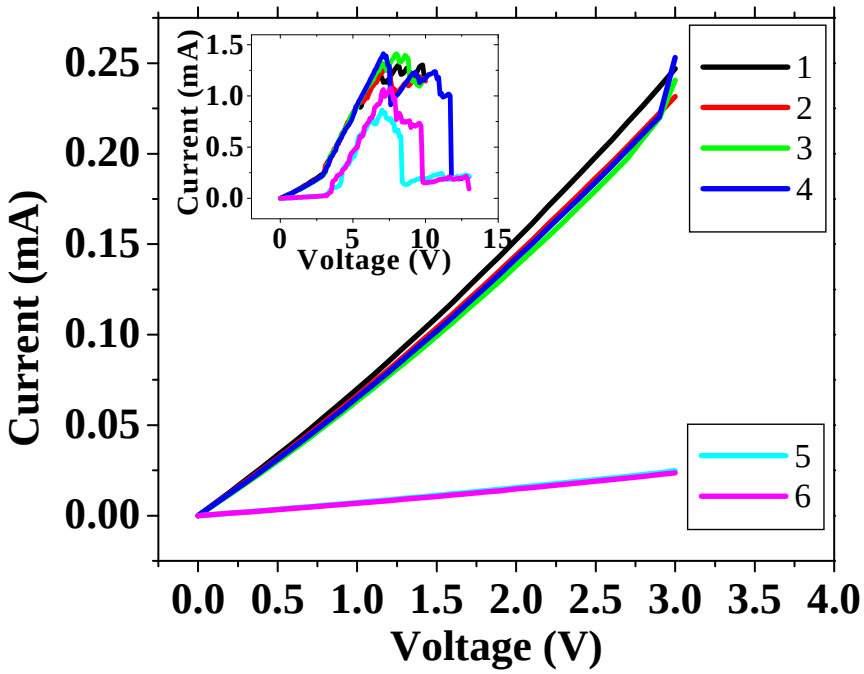

Fig. 23. Repeatable memory effect observed below 3 V. 1-4 represent a high conductance state, and 5-6 represent the low conductance state. To write a low conductance state, a complete drop of current (inset) is required; otherwise, a high conductance state persists. (The numbers in the legend represent the sequence of the measurement. From reference (*48*).

Once NDR is detected, a repeatable memory feature is observed in the NanoCells. Two conductance states are distinguished in the voltage range from 0 to 3 V (which can be used as read voltages): high conductance of ~8 × 10^{-5} S and low conductance of ~8 × 10^{-6} S states. As shown in Figure 6, if a write voltage sweep is applied such that the NDR is observed in the I-V, a low conductance state is read in the following voltage sweeps (curves 5 and 6 in Fig. 23). However, if the write voltage is such that only a raising I-V is observed (i.e., making the voltage sweep not too large to reach the peak of the NDR but large enough to go beyond the reading voltages), the high

conductance state is read with the following reading voltage sweeps (curves 1-4 in Fig. 23).

Although the NanoCell NDR-like characteristic is detected in most experiments, once it appears, the NanoCell cannot be switched back to the original state by the application of a bias voltage. In addition, on unbiased NanoCell devices, negative voltage sweeps also induce similar sequences of I-Vs, including the NDR-like behavior. However, on biased NanoCells, after the NDR has appeared in the forward bias range, it also shows up in the negative bias range without the initial and transitional sequence of I-Vs, and vice-versa.

The gold islands in the NanoCells are removed when a chip with discontinuous gold film is immersed in piranha solution (a mixture of H_2SO_4 and H_2O_2, in a ratio of 3:1) for 30 min. The temperature in this exothermic reaction rises to 130ºC. However, we find that only the gold filaments and clusters can be removed without significantly damaging the discontinuous Au film if the chip is immersed for a much shorter time. An experiment is carried out in which one chip with only the discontinuous gold film (Fig. 20A) is immersed in piranha solution for 45 s. On this chip, prior to the piranha bath treatment, some of the NanoCells have yielded NDR behavior. After the piranha bath, we find no NDR behavior in these NanoCells. Instead, the two types of observed behavior (first and second) are found again; therefore, the NanoCell can be reset to its original conduction state through the bathing process. Moreover, the NanoCell does not have memory of its previous behavior; in other words, a NanoCell, which initially exhibits the first observed behavior, may exhibit the second observed behavior after the piranha bathing, and vice versa (i.e., second behavior, piranha bath, and first behavior). Then, the same NanoCell chip is immersed in piranha for another 2 min and then 90% of the NanoCells do not show any current in excess of the noise (~0.1 pA) even when they are biased up to 100 V and observations under an optical microscope indicate that the discontinuous gold film (gold islands) is not removed.

In order to study the influence of molecules on the NanoCells electrical behavior, one of the chips with NanoCells featuring NDR, is cut into two pieces. Molecule 1 (Fig. 19A) is deposited on one half of the chip and Molecule 2 (Fig. 19B) on the other half of the chip. The NanoCells with Molecule 1 (Fig. 20B) exhibit similar switching characteristics like the NanoCells with only the discontinuous gold film (Fig. 20A), including a similar threshold voltage and NDR peak value. This further demonstrates that only the formed gold filaments are responsible for the NDR behavior or at least that the contribution of the Molecule 1 is negligible compared to the contribution of the filaments. The NanoCells with Molecule 2 (Fig. 20C) show increases in threshold voltage V_{th2} (~10 V higher). This means that the Molecule 2**,** self-assembled on SiO_2, blocks the formation of new gold filaments. After reaching this voltage, Molecule 2 is probably burned out, and we obtain a NDR characteristic similar to those found without any molecule or with only Molecule 1. Knowing that the contribution of the gold filaments to NDR is blocked by Molecule 2, we carry out deposition of Molecule 2 on the chips already containing Molecule 1 (Fig. 20D). Since this fourth ensemble (Fig. 20D) exhibits behavior similar to the third ensemble (Fig. 20C), we can conclude that Molecule 1 is not participating in bridging gold islands; thus, it is consistent that the I-Vs of the NanoCell with and without Molecule 1 are very similar. To further investigate the influence of Molecule 1, we deposit Molecule 1 on a chip where no current is found. After deposition, there is still no current. This, again, proves that Molecule 1 have no significant influence on the I-Vs of the NanoCells.

3.4.2 Theoretical results

The DFT-GF approach is used to calculate the electrical characteristic of the gold nanoclusters thought to be formed between the gold islands in the NanoCell device. A linear chain Au-Au_7-Au, shown in Fig. 24A, is optimized using the B3PW91 method and the LANL2DZ basis set. The effect of the continuum is added through the Green function approach described in 2.4.

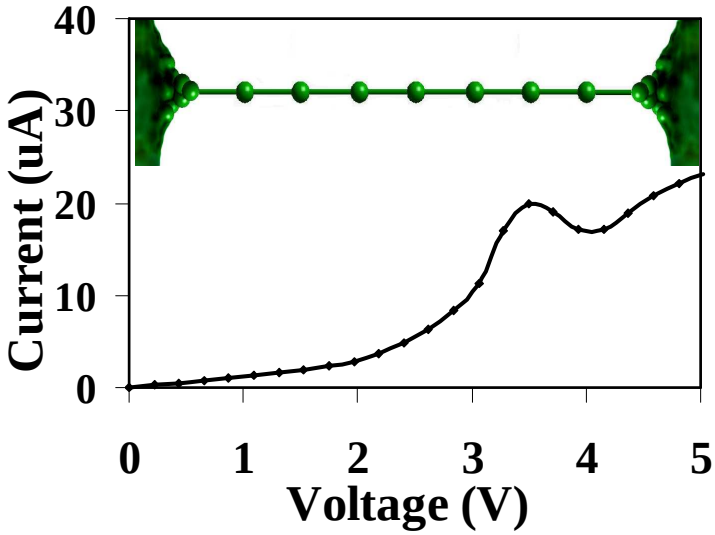

(A)

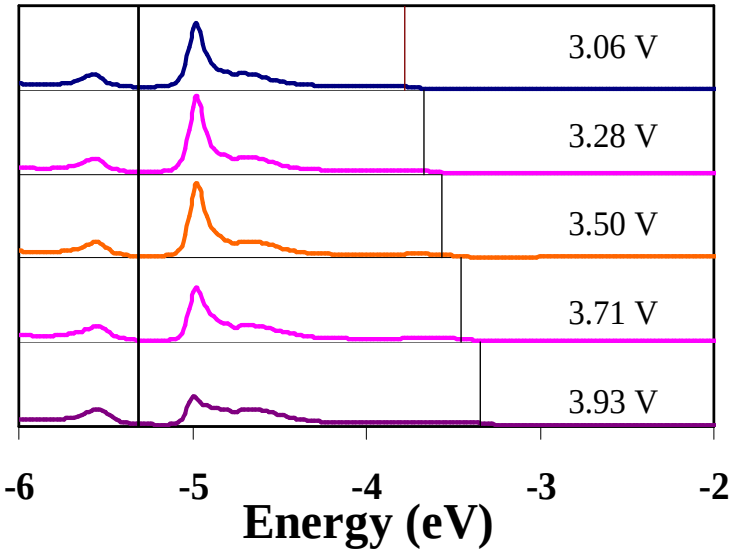

(B)

Fig. 24. I-V characteristic (A) and transmission function (B) for the anion of the Au-Au$_7$-Au cluster at bias voltages *V* = 3.06, 3.28, 3.50, 3.71, and 3.93 V. The left vertical line marks the Fermi level, and the separation between the Fermi energy and the right line determines half of the integration interval used to obtain the current through the molecule. (*64, 91*). The NDR at ~3.5 V is because the peak at ~5 eV tends to disappear as the bias voltage increases beyond 3.50 V. From reference (*48*)

We find out NDR-like behavior with a peak at ~3.5 V when the Au-Au_7-Au nanocluster is negatively charged (q = -1). This NDR is intrinsic to the nature of the charged species, and its mechanism can be easily explained using Fig. 24B depicting the transmission function (*T*) for the negative cluster as the bias voltage increases. The *T* for bias voltages at 3.06 V, 3.28 V and at the location of the current peak at 3.50 V changes smoothly reflecting an increase in current from 10 μA to 20 μA. For bias voltages of 3.71 and 3.93 V the *T*s have a perceptible decrease in their peak magnitude (Fig. 24B) which results in a decrease in the current (19, 17 μA, respectively), and hence the NDR-like I-V characteristic. Therefore, NDR-like I-V characteristics could be the result of nanocluster formation between the gold islands of the NanoCell device.

This NDR feature has also been observed experimentally in OPE molecular wires (*34*, *92-94*). The physical interpretation is the same than for the Au-Au_7-Au wire; i.e., NDR is a consequence of the changes in the electronic structure of the wire produced by the applied electric field (*95*, *96*).

3.5 Conclusions

The transport of current through a molecular junction comprises the study of a molecular system that presents both a finite and an infinite character. The finite part (single molecule) is calculated precisely from the fundamental Schrödinger equation. The effect of macroscopic contacts (infinite part) is included following the DFT-GF approach. At the scale of the molecular junctions considered in this work, the transport of electrons is coherent and is described by the Landauer formalism.

A DFT-GF implementation of the Landauer formalism is used to calculate the I-V of metal-nitroOPE-metal junctions in different conformational and charge states. Gold and the (4,4) CNT are tested as metallic contacts and in both cases the metal-nitroOPE-metal junction presents high conductance when the nitroOPE is in its coplanar conformation. The calculations predict low conductance for the perpendicular

conformation and for the charge states (anion, dianion, trianion) of the nitroOPE. It is observed that the states of high conductance exhibit ohmic I-V at low bias voltage.

The CNT-nitroOPE-CNT junction has values of current similar to the junctions containing gold contacts, despite the fact that CNT has ~10 times lower density of states than gold. This result encourages the use of CNT as an alternative to gold in molecular devices; however, technological challenges remain regarding the manipulations of single CNTs. The rationale for the high conductance of the junction containing CNT is the direct C-C bond between the CNT and the nitroOPE; instead, the thiol bonds (Au-S-C) in the Au_1-S-nitroOPE-S-Au_1 junction behave as undesired interfacial capacitors at the interfaces, isolating the nitroOPE from the contacts. Moreover, the calculation shows that the gold atoms at the top contact of the Au_6-CNT-S-Au_1 junction form a physical bond with the nitroOPE. The physical bond is effectively a tunneling gap, which deters even more the flow of electrons. For the Au_6-CNT-S-Au_1 junction, the current is lower than for the CNT-nitroOPE-CNT junction.

The DFT-GF approach is used in an application example to calculate the I-V characteristic of gold nanoclusters, which are formed within the insulating gaps in the discontinuous gold films. Leakage current showing NDR is found in electrical measurements of these films. The I-V calculations indicate that charged gold nanoclusters (q = -1) do present NDR, which is intrinsic to the electronic structure of the cluster. This finding offers an alternative mechanism to the appearance of NDR in discontinuous gold films. Furthermore, the effect on the leakage current caused by removing the nanoclusters and self-assembling molecules is analyzed. The removal of the nanoclusters, by immersing the sample in piranha solution, erases the leakage current. Two different molecules are self-assembled on the discontinuous gold film: Molecule 1, which attaches only to the gold islands, has no significant influence on the formation of gold nano clusters. However, Molecule 2, which attaches to SiO_2, blocks the leakage current.

CHAPTER IV

ELECTRON TRANSPORT IN METAL-MOLECULE-SEMICONDUCTOR JUNCTIONS

4.1 Introduction

The semiconductor industry entered the nanometer regime (< 100 nm) in 2000 and continues today in the race for miniaturization. The first commercial single-molecule-based device is most likely to be built around Si.

At sizes approaching the quantum-confinement regime, the electrical properties of silicon, and any other material, diverge from the bulk properties. For example, studies have shown the increase of the bandgap with the decrease of the size of the semiconducting nanostructure (*6-8*). For silicon nanowires (SiNWs), theoretical calculations have shown the quantum effects are substantial at diameters below than 3 nm (*97-102*). Quantum-mechanical calculations of the type presented in this work are necessary for devices containing Si nanostructures in the quantum-confinement regimen.

In the previous chapter, we have described the distinctive impedance states of the metal-nitroOPE-metal junctions. Advances in synthetic chemistry have allowed the direct attachment of organic molecules on Si substrates (*40, 41*), opening the door for hybrid organic-semiconducting devices. In this chapter, we consider the effect of Si contacts on the bistable properties of the nitroOPE.

A Schottky diode, which is formed when a metal and a semiconductor are in intimate contact, acts as a current rectifier. Therefore, in a macroscopic metal-device-semiconductor junction, the simultaneous use of a semiconducting and a metallic contact implies a tremendous change in the properties of the device. In other words, the electrical behavior of the device may be overruled by the rectifying behavior of the contacts. The challenge is to use Si as one of the contacts in metal-nitroOPE-Si molecular junctions without destroying the bistable characteristics attributed to the nitroOPE molecule. The rectifying behavior has been experimentally observed to vanish

as the size of the metal-semiconductor junction approaches the nanometer regime, i.e., ultra-small Schottky diodes (*103-105*). This gives hope for using Si as a righteous contact material in single-molecule-based electronic devices; we perform quantum-mechanical calculations to assess the ability of metal-nitroOPE-Si junctions to keep the high- and low-impedance states found in metal-nitroOPE-metal junctions. Our study considers the different charge states (neutral, anion, dianion, and trianion) as well as the coplanar and perpendicular conformations of the nitroOPE molecule. Both gold and (4,4) CNT are tested as metallic contacts.

4.2 Significance of the electronic chemical potential (ECP) for a single molecule

The electrochemical potential is a property traditionally defined, for macroscopic systems, as the variation of the total energy with respect to the number of particles in the ensemble. This concept needs to be extended to be able to determine the ECP of a single molecule.

The ECP for a molecule is synonymous with minus the electronegativity, which is defined as the average of the *IP* and the *EA* (Mulliken electronegativy)

$$\mu = -\frac{IP + EA}{2} \tag{58}$$

where the electron affinity (*EA*) is defined as the amount of energy needed by the molecule (or atom), in its neutral state, to accept an extra electron. The ionization potential (*IP*), also called ionization energy, is the energy needed to strip out one electron from molecule (or atom). *EA*s and *IP*s can be calculated computationally as the difference between the self-consistent field (SCF) energies of the charge states of the molecule.

$$EA = E_{\text{anion}} - E_{\text{neutral}}$$

$$IP = E_{\text{cation}} - E_{\text{neutral}}$$

This approach is called ΔSCF; recent studies show than DFT methods are able to achieve 0.1-0.2 eV of accuracy to calculate *EA*s and *IP*s (*106-108*).

A more direct approach to calculate the molecular ECP is based on a quantum-mechanical extension of the traditional definition of chemical potential(*109-111*).

According to the first Hohenberg-Kohn theorem (*49*), the ground-state energy (E_0) is a functional of the density, $\rho_0(r)$

$$E_0 = E_v[\rho_0(r)] = \int \rho_0(r) v(r) + F[\rho_0(r)] \tag{59}$$

where ρ_0(r) is the ground-state electron density. For any other trial electron density, $\rho(r)$, we get another energy

$$E' = E_v[\rho(r)] = \int \rho(r) v(r) + F[\rho(r)] \tag{60}$$

The second Hohenberg-Kohn theorem establishes that the energy of Eq. 60 cannot be lower than the energy in Eq. 59. In other words, the minimization of Eq. 60 with respect to variations of the electron density, $\rho(r)$, yields the ground-state energy (E_0) and ground-state electron density, ρ_0(r)

$$\int \rho(r) d\tau = N \tag{61}$$

with N being the number of electrons in the molecular system. This minimization problem is commonly tackled by the introduction of a Lagrange multiplier μ

$$\delta\{E_v[\rho(r)] - \mu\int \rho(r)d\tau\} \tag{62}$$

which results in the following Euler-Lagrange equations

$$\mu = \left[\frac{\delta E[\rho(r)]}{\delta\rho(r)}\right]_{\rho=\rho_0} \tag{63}$$

$$\mu = \frac{\partial E}{\partial N} \tag{64}$$

The similarity of Eq. 64 to the traditional, thermodynamical, definition of chemical potential in macroscopic systems reassures that the chosen Lagrange multiplier constant, μ, corresponds indeed with the ECP (*111*). Moreover, Eq. 64 gives a direct relationship of the ECP with the total energy functional and the ground-state electron density.

Combining Eqs. 58 and 63, we obtain the following relation

$$\mu = \left[\frac{\delta E[\rho(r)]}{\delta\rho(r)}\right]_{\rho=\rho_0} = -\frac{IP + EA}{2} \tag{65}$$

Based on Eq. 63 Perdew *et al.* (*109*, *110*) have shown that the ionization potential (*IP*) is exactly minus the energy of the highest occupied Kohn-Sham molecular orbital energy (ε_{HOMO}), for the exact energy functional.

$$IP = -\varepsilon_{HOMO} \tag{66}$$

The ground-state energy of a molecule varies continuously with fractional variations in the number of electrons in the system. For integer variations on the number

of electrons, the exact exchange-correlation potential component of the total energy jumps by a constant, i.e. it has a derivative discontinuity at any integer number of electrons. However, the exact exchange-correlation functional may never be found and the approximations that are in use cannot account for these discontinuities. The smoothing of the curve introduces errors that make ε_{HOMO} deviate from the ideal relation in Eq. 66. Surprisingly, it has been shown (*112*) that the accumulation of errors makes the energy of the HOMO tend to the average of the *IP* and the *EA* instead of the *IP*. Then

$$\varepsilon_{HOMO} \approx -\frac{IP + EA}{2} \tag{67}$$

Combining Eq. 66 and 67, we finally get an expression to find the ECP of a molecule as approximately the energy of the Kohn-Sham HOMO.

$$\mu \approx \varepsilon_{HOMO} \tag{68}$$

4.3 "Fermi-level alignment" in metal-semiconductor interfaces

One of the paramount issues in the study of metal-semiconductor junctions relates to the electronic equilibration of charges across the interface. When having two materials with different ECPs in direct contact, electrons flow from the material with higher ECP to the one with lower ECP until equilibrium is reached. At equilibrium, it is said that junction have a unique ECP throughout the two materials, the "Fermi-level alignment" rule.

The rearrangement of charges produces a built-in electric field at the interface, which helps to maintain the equilibrium at the interface. The distribution of charges is expressed as a built-in electrostatic potential profile $V_{bi}(x)$ across the junction.

This potential modifies the original ECP to produce an effective ECP (EECP), μ^*, in the following way

$$\mu^* = \mu + eV_{bi}(x) \tag{69}$$

Then, "Fermi-level alignment" refers strictly to the alignment of the EECPs of the materials conforming the junction, not to the alignment of the ECPs.

Our method of studying the interfaces is schematized in Fig. 25. Zones I and V corresponds to the regions of the junction where both contacts (contact 1 and contact 2) behave as bulk materials and their effect on the junction is accounted using the Green function method. The critical part of a junction is the region where both bulk materials are in direct contact; the formation and breakage of molecular bonds takes place in this region, resulting in a new material (material 3) that is neither contact 1 nor contact 2 (see the nomenclature in Table 3). The electronic properties of the junction depend mostly on the character of this interface; thus, a high degree of accuracy is needed in modeling this region. This region is treated as a separate new molecule, which is the extended molecule defined in Fig. 12, and calculated quantum-mechanically. The extended molecule is comprised of the zones II, III, and IV (Fig. 25). Several atoms belonging to the contacts (interfacial atoms, zones II and IV) are included as part of the extended molecule. In other words, our model considers the original two-contact junction as a junction composed of three different materials, material 1 (the contact 1), material 3 (the extended molecule), and material 2 (the contact 2). These three distinct materials reach and stay in equilibrium. Their EECPs are aligned to the value of the ECP of the extended molecule, as shown in Fig. 25C. According to Eq. 68, the ECP of the extended molecule corresponds to the energy of the Kohn-Sham HOMO.

In order to read/write information from/in the molecule, an external bias voltage, *V*, needs to be applied between the contacts. Upon the application of the external voltage, the junction gets out of equilibrium. As a first approximation, the EECPs of both contacts are affected by the external voltage as shown in Fig. 25. This

gradient of EECPs along the junction produces a flow of electrons between the contacts, i.e. current.

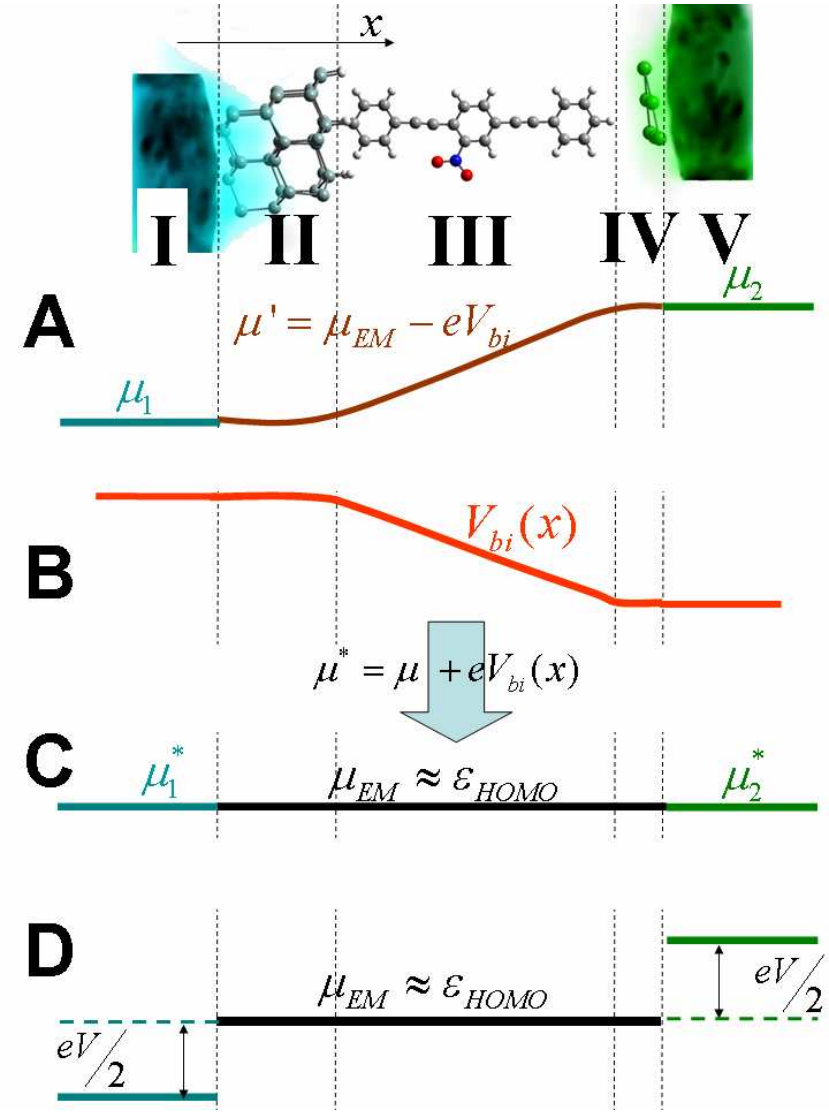

Fig. 25. (A) Schematic of the electrochemical potential (ECP) distribution, $\mu(x)$, along the x axis, perpendicular to the junction. Zone I corresponds to bulk CNT, region V to the silicon bulk, and zones II, III, and IV to the extended molecule. (B) Spatial distribution of the electrostatic potential (ESP), $V_{bi}(x)$, for the CNT-molecule-Si junction. (C) Spatial distribution of the effective electrochemical potential (EECP), $\mu^*(x)$, across the junction. (D) Shifting of the effective electrochemical potential (EECP) across the junction upon the application of an external bias voltage V.

Table 3. Parallel between several equivalent names given to the components of a junction. The extended molecule is composed of the interfacial atoms and the restricted molecule.

Junction components		Molecule	Fig. 25A	Fig. 12
Material 1	Contact 1	Au DOS	I	Bulk contact
Material 3	Interface	Au atoms	II	Interfacial atoms
	Interface	nitroOPE	III	Restricted molec.
	Interface	Si atoms	IV	Interfacial atoms
Material 2	Contact 2	Si DOS	V	Bulk contact

4.4 Quantum-mechanical calculation

4.4.1 Gold contact

The Au-nitroOPE-Si junction (Fig. 26C) is composed of six interfacial Au atoms, which model the top contact, and 38 Si atoms, which model the bottom contact. The geometry for this extended molecule is obtained by performing separately quantum-mechanical optimizations of the top and bottom components of the junction.

To find an appropriate geometry for the bottom part of the junction, we optimize the nitroOPE molecule perpendicularly bonded to a hydride-passivated Si (111) surface, which is modeled by 52 silicon atoms (Fig. 26A). Hydrogen atoms are added to saturate the boundary Si atoms. This molecule presents a total dipole moment of 5.08 D (+2.72 D in the direction of the junction). The optimized C-Si bond length is 1.913 Å.

The top part of the junction is found by optimizing the nitroOPE molecule and six gold atoms (Fig. 26B). We run several calculations with increasing number of Au atoms (from 1 to 6); those geometry optimizations show that the gold atoms tend to a planar conformation and that there is no chemical bond between the gold atoms and the nitroOPE molecule. For compatibility, the optimization of the top (Fig. 26B) and bottom (Fig. 26A) parts of the junction are performed using the same level of theory, B3PW91, and basis set, LANL2DZ.

Fig. 26C shows the final assembly of the Au-nitroOPE-Si junction from the optimized bottom and top parts. Due to the computationally expensive nature of the geometry optimizations, the assembled geometry of the junction (Fig. 26C) is kept fixed (not fully optimized) for all subsequent calculations. Also, notice that the number of total silicon atoms is reduced to 38 with respect to Fig. 26A. The total dipole moment for this junction is 9.03 D (+7.8 D in the direction of the junction).

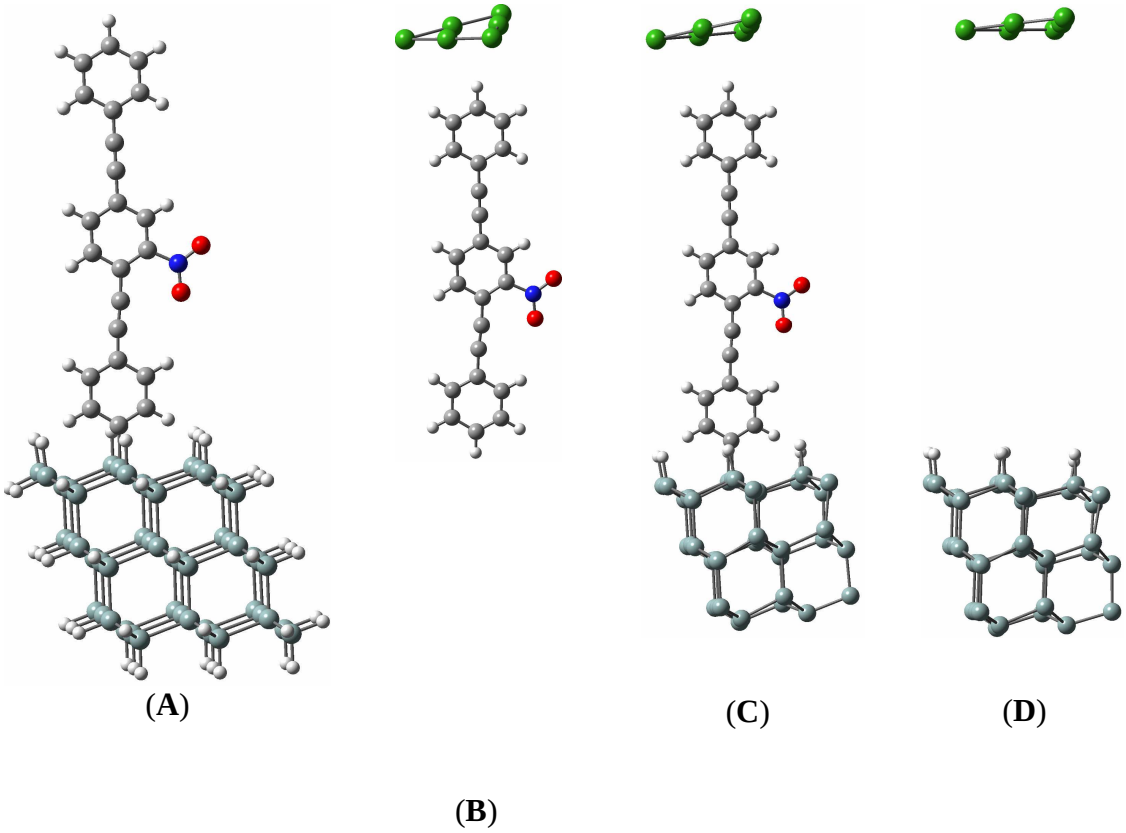

Fig. 26. (A) Optimization of the bottom part of the junction (Molecule 16). (B) Optimized geometry corresponding with the top part of the junction (Molecule 3). (C) Final assembly of the Au-nitroOPE-Si junction (Molecule 5). (D) Associated Au-Si tunneling junction. For higher compatibility all calculations are performed under the same DFT method and basis set (B3PW91/LANL2DZ).

We also calculated an alternative geometry, the perpendicular conformation. In that conformation the middle phenyl ring, which contains the nitro group is rotated 90° with respect to the plane of the other two phenyl rings. If the opposite is not stated explicitly, the default conformation corresponds to "coplanar", where all the phenyl rings are contained in a plane, as seen in Fig. 26C.

The calculations of both conformations, shown in Table 4, predict that the Au-nitroOPE-Si junction is more stable in the perpendicular conformation than in the coplanar conformation, with an energetic barrier of 0.19 eV (4.3 kcal/mol, ~7 *kT*) for rotation of the middle phenyl ring.

Table 4. Summary of the calculation for the Au-nitroOPE-Si junction (Molecule 5).

	Coplanar conformation	Perpendicular conformation
Calculation type	single point	single point
Calculation method	UB3PW91	UB3PW91
Basis set	LANL2DZ	LANL2DZ
Total electronic energy	-2014.57326 Ha	-2014.58015 Ha
Dipole moment	9.03 D	9.52 D

4.4.2 (4,4) CNT contact

Recently, several procedures have been reported for attaching covalently aromatic hydrocarbons (arenes) to CNTs (*37-39*). Manipulation of CNTs has been limited since they are synthesized as bundles or ropes. Because of the tendency to agglomerate, CNTs present low solubility and dispersion when placed in polymer matrices (*113*). The ability to attach arene "handles" to CNTs, allows direct manipulation of this amazing form of carbon, opening new possibilities for using individual CNTs as molecular devices.

Moreover, several functionalization techniques have been reported to react faster in metallic CNTs rather than in semiconducting ones (*72, 114, 115*), which has

allowed the separation of CNTs based on their electronic properties, i.e., metallic from semiconducting (*72*). These advances have opened the possibility of using metallic CNTs as tips for contacting organic molecules.

On the other hand, the synthesis of nitroOPE molecules perpendicularly assembled on a hydride-passivated Si (111) substrate, with the top end covalently attached to a metallic CNT, i.e., the metallic CNT-nitroOPE-Si junction shown in Fig. 27A, has been reported recently (*54*). Computationally, the use of atoms with smaller atomic number, such as carbon instead of gold, has the advantage of allowing a full-electron study of the system, which leads to a more precise calculation.

We optimize the geometry of the (4,4) CNT-nitroOPE-Si junction by parts. The top part of the geometry is obtained by optimizing a piece of (4,4) CNT with a benzene ring covalently bonded to it (Molecule 14). The piece of the armchair (4,4) CNT is composed of 10 carbon rings, each ring containing 8 carbon atoms. The positions of the CNT atoms away from the benzene-CNT bond are kept fixed. The bottom part is obtained as described for the Au-nitroOPE-Si junction. The geometry of the assembled (4,4) CNT-nitroOPE-Si junction is shown in Fig. 27A. Due to computational restrictions, this geometry is kept fixed for all subsequent calculations.

We calculated the coplanar (Fig. 27A) and the perpendicular (Fig. 27B) conformations. Contrary to the case when having a gold top contact, the coplanar conformation of the CNT-nitroOPE-Si junction turns out to be slightly more stable than the perpendicular conformation (Table 5), with a rotational barrier of 0.17 eV (4 kcal/mol).

The calculated total dipole moment is 130.46 D (-130.16 D in the direction of the junction) for the coplanar configuration. The perpendicular configuration presents a similar dipole moment, 133.37 D (-133.03 D in the direction of the junction).

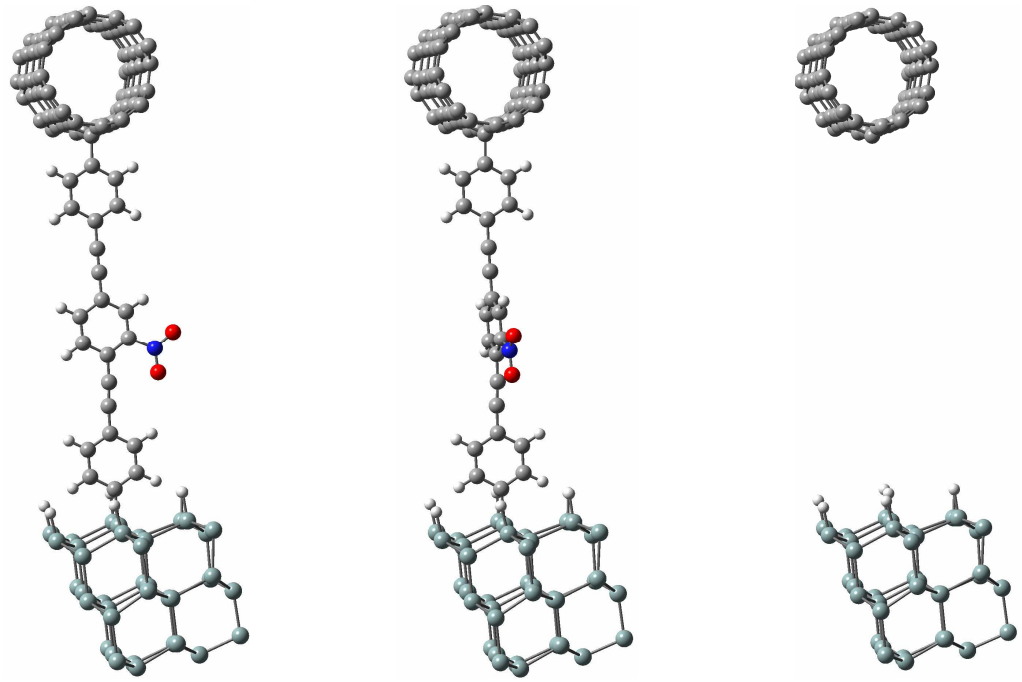

(**A**) (**B**) (**C**)

Fig. 27. (A) Coplanar and (B) perpendicular configuration of the (4,4) CNT-nitroOPE-Si junction (Molecule 9). (C) The (4,4) CNT-Si tunneling junction has the interfacial atoms in the same position tas (A) and (B), but without the nitro-OPE molecule between them. The Gaussian 03 geometry file for (A) is given in the Appendix 4.

Table 5. Summary of the calculation for the (4,4) CNT-nitroOPE-Si junction (Molecule 9).

	Coplanar configuration	Perpendicular configuration
Calculation type	single point	single point
Calculation method	UB3PW91	UB3PW91
Basis set	6-31G(d)	6-31G(d)
Total electronic energy	-15097.75352 Ha	-15097.74713 Ha
Dipole moment	130.46 D	133.37 D

Because of the larger spatial extension of d-electrons over p-electrons, the wavefunction of gold can tunnel farther into the vacuum than the wavefunction of a CNT contact. The variation of the ESP (Fig. 28B and D) along metal-Si tunneling junctions (Fig. 28A and C) corroborates the fact that the wavefunction of gold can tunnel

farther, yielding higher tunneling currents. Gold would apparently be a superior choice for metallic contact than the (4,4) CNT would for a nitroOPE-based molecular device. However, the CNT has the advantage of forming a covalent bond with the nitroOPE whereas the gold forms a physical bond.

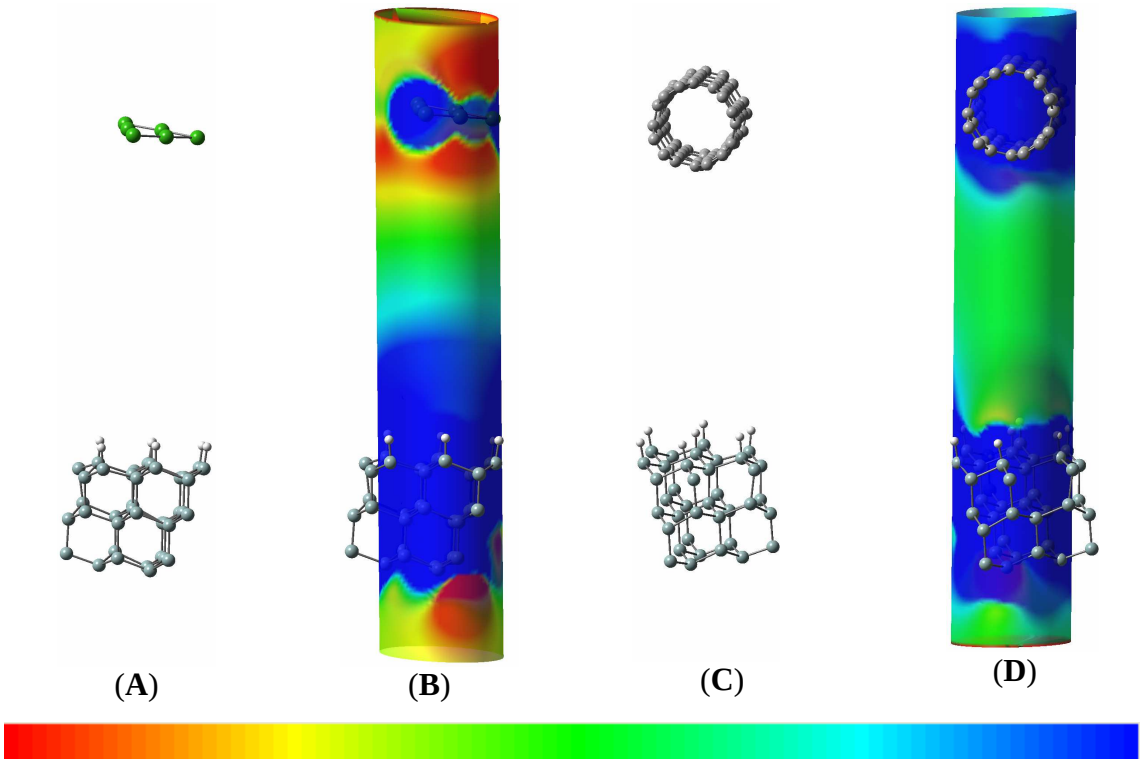

Fig. 28. (A) Geometry of the Au-Si tunneling junction (Molecule 8). The position of the gold and silicon atoms are kept the same as in the Au-nitroOPE-Si junction (Molecule 5). (B) Distribution of the ESP for (A). The spatial region corresponds to the same cylindrical surface shown in Fig. 34C. (C) CNT-nitroOPE- Si junction. (D) Distribution of the ESP for (C). The spatial region for all the figures corresponds to a cylinder of radius 4 Å. The color scale for all the figures ranges from -0.1 V (red) to 0.1 V (blue).

4.4.3 Mulliken charges

The distribution of charges is computed based on the recipe given by Mulliken (*116-119*), which starts from the calculated wavefunction of the molecular system.

The analysis of Mulliken atomic charges (Table 6) shows a strong rearrangement of charges taking place in the (4,4) CNT-nitroOPE-Si junction; for the coplanar neutral state of this junction, the CNT loses 0.97*e*, the Si loses 1.09*e* and the nitroOPE gains 2.06*e*. The high rearrangement of charges accounts for the high dipole moment of the (4,4) CNT-nitroOPE-Si junction, -130.16 D in the direction of the junction.

Table 6. Distribution of Mulliken charges for the (4,4) CNT-nitroOPE-Si junction in its coplanar conformation. The Si contact includes the hydrogen atoms adsorbed on it. The units of the charges are in *e*, the absolute value of the charge of an electron.

	Neutral	Anion	Dianion	Trianion
CNT contact	0.97	0.19	0.00	0.00
nitroOPE	-2.06	-0.33	-0.98	-1.22
Si contact	1.09	-0.86	-1.02	-1.78
total charge	0	-1	-2	-3

The optimization of the gold atoms in the top contact of the Au-nitroOPE-Si junction shows a gap between the plane of gold atoms and the nitroOPE molecule (Fig. 26B). This gap obstructs the free displacement of charges between the Au contact and the rest of the junction, explaining the very low charge rearrangement throughout the Au-nitroOPE-Si junction (Table 7). Most of low charge transfer takes place between the nitroOPE and the Si contact with an almost-null transfer between the nitroOPE and the Au contact, 0.03*e*. This also explains the relatively low dipole moment that is found for the Au-nitroOPE-Si junction (7.80 D in the direction of the junction).

Table 7. Distribution of Mulliken charges for the Au-nitroOPE-Si junction in its coplanar conformation. The Si contact includes the hydrogen atoms adsorbed on it. The units of the charges are in *e*, the absolute value of the charge of an electron.

	Neutral	Anion	Dianion	Trianion
Au contact	-0.03	-0.03	-0.08	-1.64
nitroOPE	-0.10	-0.17	-0.19	-0.26
Si contact	0.13	-0.80	-1.73	-1.10
total charge	0	-1	-2	-3

The Metal-Si junctions (Fig. 28A and C) present a gap of ~20 Å, which is large enough to obstruct any transfer of charges between the contacts. The lack of charge displacement results in the negligible dipole moment found for the CNT-Si, 1.31 D in the direction of the junction, and the Au-Si tunneling junction, 2.85 D in the direction of the junction.

4.5 Current-voltage calculation

The calculation of current assumes electrons being injected from the top contact (negative electrode) to the bottom contact (positive electrode). At zero bias voltage ($V = 0$), the most energetic electrons in the top and bottom bulk contacts have the same energy; therefore, the junction is in equilibrium, without net flow of electrons. This is called "Fermi-level alignment" as described in 4.3. The most intimate part of the junction is modeled by an extended molecule, which contains atoms representing both contacts; the ECP of the extended molecule gives an approximation of the ECP of the macroscopic junction. The quantum-mechanical calculations allow to find the ECP of the extended molecule, which correspond to the energy of the HOMO, as discussed in 4.2.

The applied bias voltage (V) is defined such that the semiconducting contact is positively biased with respect to the metallic contact, $V = V_{semic} - V_{metal}$. Therefore, after applying a bias voltage between the contacts, the EECP of the metal is shifted up

whereas the EECP of the Si contact is shifted down (by an equal amount of $0.5\times e\times V$) with respect to the equilibrium ECP of the extended molecule(μ_{EM}), in the following way

Metal: $$\mu_2^* = \mu_{EM} + \frac{1}{2}eV \quad (70)$$

Semiconductor: $$\mu_1^* = \mu_{EM} - \frac{1}{2}eV \quad (71)$$

The values of current reported here refer to "current of electrons" and is defined as positive when flowing from the metal (contact 2) to the semiconductor (contact 1).

4.5.1 Gold contact

The ECPs for the Au-nitroOPE-Si junctions (μ_{EM}) are calculated as the energy of the HOMO (ε_{HOMO}) of the extended molecule. The calculated values for the ε_{HOMO} and the ε_{LUMO} of several Au-nitroOPE-Si junctions are reported in Table 8

The Green function, $g(E)$, for the metallic contact is based on the density of states for the FCC gold crystal which is calculated under the same level of theory (B3PW91) and basis set (LANL2DZ) as the junction. The DOS for Au used for the current-voltage calculations is shown in Fig. 5. For compatibility, we use a Si DOS calculated using the combination B3PW91/LANL2DZ (Fig. 8).

The calculation of the current-voltage characteristic for the junction with the nitroOPE in its coplanar conformation is shown in Fig. 29A. Only the contribution of α-electrons is taken into account for the I-V calculation.

Table 8. Summary of the α-HOMO and α-LUMO energies for the different charge states and conformations of the Au-nitroOPE-Si (Molecule 5). The calculations are performed using the B3PW91 method and the LANL2DZ basis set.

Conformation	Charge	μ_{EM} (ε_{HOMO} in eV)	ε_{LUMO} in eV
Coplanar	0	-5.45	-4.75
	-1	-2.96	-2.86
	-2	-1.67	-1.04
	-3	0.36	0.50
Perpendicular	0	-5.37	-4.70
	-1	-3.00	-2.77
	-2	-1.47	-0.92

4.5.2 (4,4) CNT contact

We test several (4,4) CNT-nitroOPE-Si junctions, which include the coplanar, perpendicular, and charge states. The quantum-mechanical calculation of the values for the ECPs are performed using the B3PW91 method and the full-electron 6-31G(d) basis set. These values are reported in Table 9.

The Green functions, $g(E)$, for the Si and CNT contacts are based on B3PW91/6-31G(d) calculations of the DOS using the Crystal 03 commercial software. The Si DOS is shown in Fig. 7, it is calculated using the 6-31G(d) basis set. We point out that the Si DOS use for the Au-nitroOPE-Si junction is calculated using a different basis set, LANL2DZ basis. The DOS of the (4,4) CNT is shown in Fig. 9.

Since the molecule is connected to a half of the Si bulk, we consider that only half of the total Si electronic states are available to leak into the molecule through the bottom contact. Then, a DOS factor (a scaling factor) of 0.5 is applied to the silicon DOS, mostly on intuitive geometrical grounds (*61*). Interestingly, the atoms in a CNT are both surface and bulk atoms at the same time; therefore, DOS per atom of the bulk material corresponds to the DOS of the atom to which the nitroOPE molecule is adsorbed and no factor needs to be applied to the CNT DOS. The current-voltage characteristic for the coplanar (4,4) CNT-nitroOPE-Si junction is reported in Fig. 29B.

For both metal-nitroOPE-semiconductor junctions, we notice a flat region in the I-V curve at low bias voltage (approximately from -1.4 to 1.4 V). This flat region of ~ zero conductance has also been observed in experimental calculations of semiconductor-molecule-metal (metallic STM tip) junctions (*43-46*) and in insulator-molecule-metal junctions (*15*), Al/AlO_x/molecule/Ti/Al. The flat region in the I-V curve constitutes the most notorious difference with respect to the metal-nitroOPE-metal junctions (Fig. 15 and Fig. 16).

Table 9. Summary of the α-HOMO and α-LUMO energies for the different charge states and conformations of the (4,4) CNT-nitroOPE-Si junction (Molecule 9).

Conformation	Charge	μ_{EM} (ε_{HOMO} in eV)	ε_{LUMO} in eV
Coplanar	0	-4.83	-4.50
	-1	-3.06	-3.06
	-2	-1.58	-1.53
	-3	0.07	0.12
Perpendicular	0	-4.81	-4.48
	-1	-3.18	-3.01
	-2	-1.57	-1.52
	-3	-0.11	0.19

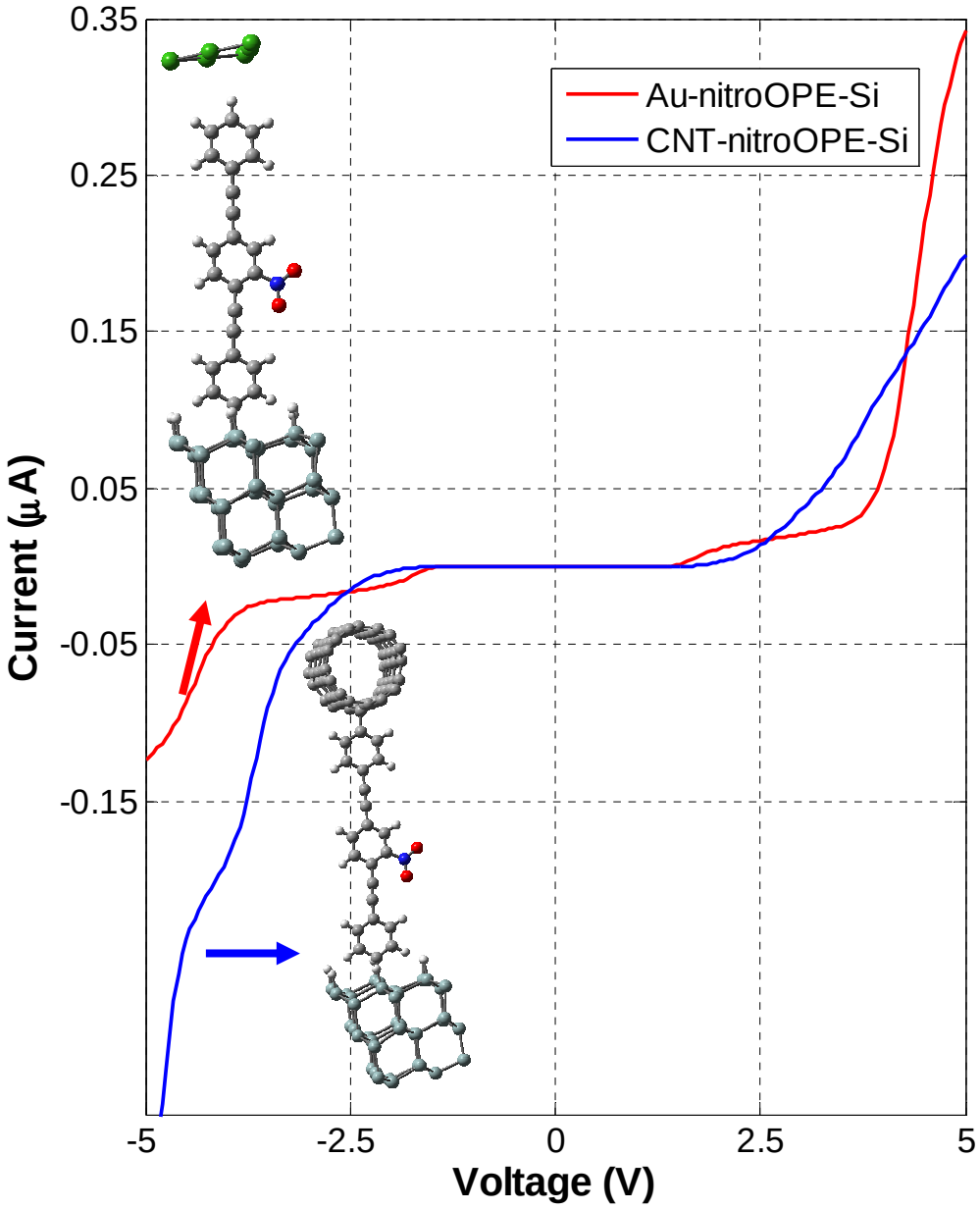

Fig. 29. (A) Current-voltage characteristic for the Au-nitroOPE-Si (Molecule 5) in linear scale. (B) I-V for the (4,4) CNT-nitroOPE-Si junction (Molecule 9).

Despite the fact that gold is a metal with higher density of states than the (4,4) CNT (~10 times higher at their respective ECPs), the current in the CNT-nitroOPE-Si junction is similar or higher than the current in the Au-nitroOPE-Si junction. This indicates that a better chemical contact between the molecule and the metallic contact can make up for the lower density of electrons of the (4,4) CNT.

Any junction composed of a metallic and a semiconducting contact is a simple Schottky diode. The interface between the metal and the semiconductor gives rise to a potential barrier, which was first explained by Schottky. The Schottky barrier obstructs the transport of carriers in one direction of the junction, acting as an electrical rectifier. The rectifying behavior is most characteristic features associated with macroscopic Schottky diodes; however, lack of rectifying behavior in Schottky diodes of nanometer sizes has been experimentally observed (*103-105*). Likewise, no rectifying behavior is seen in our I-V calculations of molecular metal-molecule-semiconductor junctions (Fig. 29).

Three mechanisms for electron transport can take place in a junction: thermionic emission, tunneling, and diffusion. Thermionic emission and tunneling are the most important mechanism in Schottky diodes. The thermionic transport depends mostly on the height of the Schottky barrier whereas the tunneling transport depends on both the height and the thickness of the barrier. The thermionic contribution to the current is given by the following equation

$$I \propto T^2 e^{-\frac{\phi_B}{kT}} [e^{\frac{eV}{kT}} - 1] \tag{72}$$

where ϕ_B is the height of the barrier and T temperature. The tunneling current, for a triangular barrier, is given by

$$I \propto \Theta \quad ; \Theta = e^{-\frac{4}{3}\frac{\sqrt{2m\phi_B}}{\hbar} L} \tag{73}$$

where Θ is the tunneling probability, *m* the effective mass, and *L* is the thickness of the barrier.

Smit *et al*. used a theoretical model based on the Poisson equation to track the behavior of the Schottky barrier for diodes of arbitrary sizes, from macroscopic to ultra-small dimensions. Following that top-down methodology, he demonstrated that for diodes smaller than a characteristic length (associated with the doping level of the semiconductor), the thickness of the potential barrier no longer depends on the concentration of the dopant in the semiconductor but on the size and shape of the diode (*120, 121*). "Molecular Schottky diodes" exhibit thin potential barriers ; therefore, the tunneling contribution to conduction outweighs the thermionic contribution (*103, 104*). Then, contrary to macroscopic diodes, the I-V of molecular diodes does not exhibit the characteristic diode-like shape of Eq. 72.

Because of the small length of molecular junctions, the electron transport is coherent. Our DFT-GF is built upon the Landauer formalism, which deals with coherent transport. In coherence transport, the electrons travel non-interactively from one contact to the other in a single quantum-mechanical process whose probability can be calculated directly from the fundamental equations. The transport in molecular junctions can be seen as a probability for an electron to cross from one side of the molecule to the other, which is a tunneling process. Eq. 55, used in our formalism to calculate the current-voltage characteristic, reflects the fact that tunneling is the main mechanism for electron transport through molecular junctions.

It is interesting to see how Smit *et al*., by using a top-down approach, reached the conclusion that electron transport in ultra-small Schottky diodes is predominantly by tunneling. This conclusion arises naturally when using an atomistic (bottom-up) approach, such as our DFT-GF interpretation of the Landauer formalism.

4.6 Changes in the conformation and charge states

4.6.1 Gold contact

We also analyze the perpendicular conformation of the Au-nitroOPE-Si junction. For that, we rotate 90° the atoms of the middle phenyl ring and keep all the other simulation parameters the same as for the coplanar conformation.

Our result predicts a drastic difference in conductance between the coplanar and perpendicular conformations (Fig. 30). Such change in conductance has been attributed to the rupture of the π-orbital network (*122*). When the phenyl rings are coplanar, they form a conducting path across the molecule; however, when the phenyl rings are perpendicular to each other, this conducting path is broken, decreasing tremendously the conductance.

This huge change of conductance was observed by Donhouser (*74*) in STM electrical measurement of several types of OPE molecules, including the nitroOPE, over time.

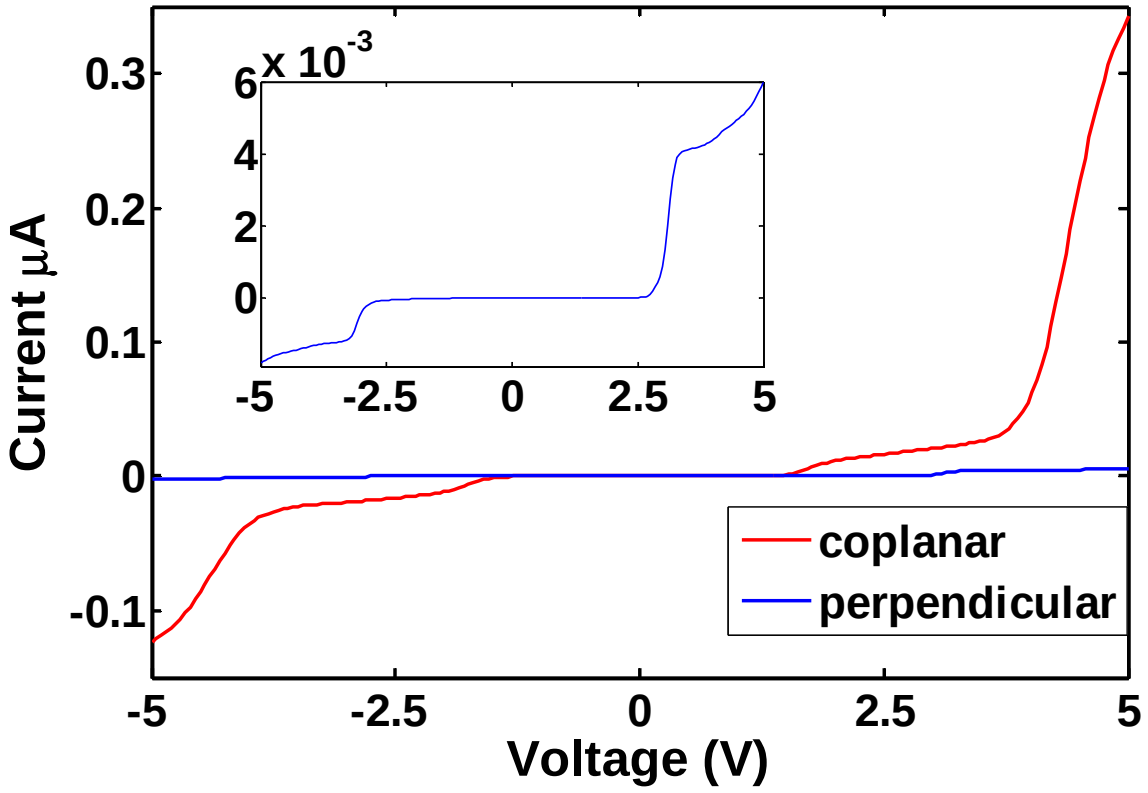

Fig. 30. Current-voltage characteristic for two different geometrical conformations of the Au_6-nitroOPE-Si (Molecule 5). The planar conformation is referred to when the three rings are coplanar, and the perpendicular conformation refers to the case when the ring containing the nitro group is perpendicular to the other two. The inset shows a zoomed view of the I-V characteristic for the molecule in its perpendicular conformation.

Charge trapped in the molecular junction has been thought to cause a strong change in the conductance of molecular junctions (*15*, *31*); we investigate that by calculating the I-V of Au-nitroOPE-Si junctions containing an extra number of electrons (anion, dianion, and trianion). In the coplanar conformation, we observe a strong decay in conductance when the extended molecule gets negatively charged (Fig. 31A). The anion and dianion states present similar low conductance, but the trianion is seen to have the lowest conductance. At 3.3 V the neutral junction conduces 23.6 nA, which is 34.6, 75.3, and 23.6 times the current conduced by the anion, the dianion, and the trianion states respectively. At 1.0 V the ratios are even better, $I_{neutra/} / I_{anion} = 88.5$, $I_{neutra/} / I_{dianon} = 123.4$, $I_{neutra/} / I_{trianion} = 246.2$, where $I_{neutra/} = 5.5 \times 10^{-13}$ A.

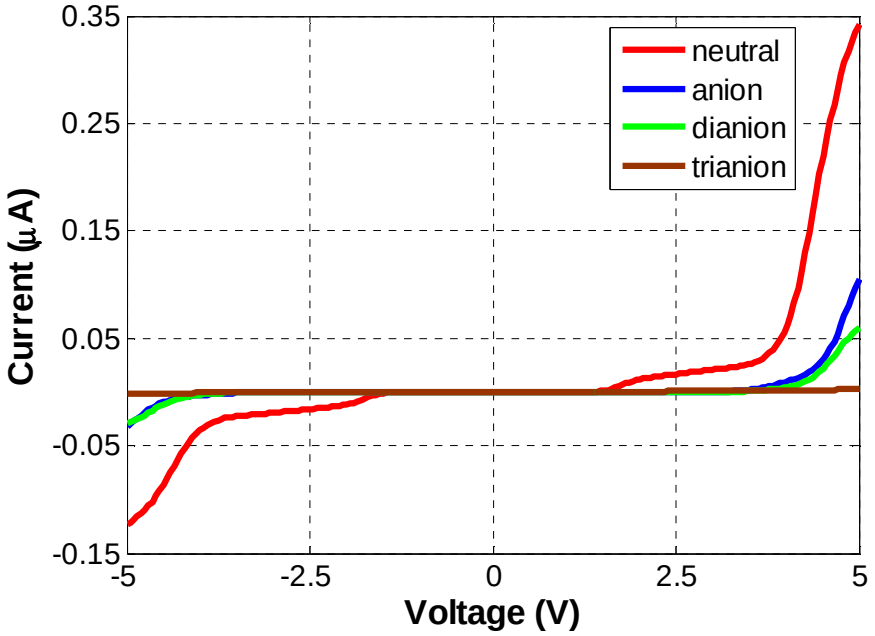

(**A**)

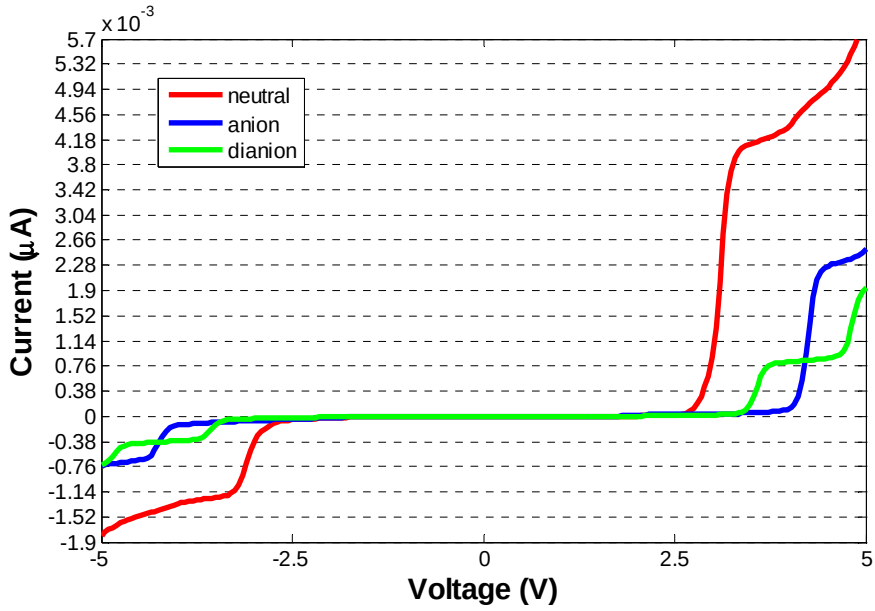

(**B**)

Fig. 31. (A) Current-voltage characteristic for different charge states of the Au-nitroOPE-Si junction in their coplanar conformation (Molecule 5). Only the contribution of α electrons is shown. (B) Current-voltage characteristic for the different charge states of the Au-nitroOPE-Si junction in its perpendicular conformational state.

High ratios of the currents ($I_{neutra/}$ / $I_{charged}$) are encouraging for the design of a bistable electronic device. Although the absolute current values are too small (~10^{-13} A) to be measured by present equipment; we point out that those values correspond to the conduction through a single molecule, in reality, thousands of molecules are expected to be self-assembled on parallel, with the net current being also thousand times higher.

In the perpendicular conformation, the junctions already have a much lower conductance for the neutral state with respect to the coplanar configuration, as seen in Fig. 30. The addition of charge to the perpendicular conformation lowers even more the conductance as reported in Fig. 31B.

4.6.2 (4,4) CNT contact

We calculate the I-V for the perpendicular conformation of the (4,4) CNT-nitroOPE-Si junction (Molecule 9). Fig. 32 shows a comparison of the conductance between the coplanar and the perpendicular conformations. The calculation confirms that the strong change in conductance between both conformational states is still present if we use the metallic CNT instead of gold.

For instance, at 3.3 V the molecule in its coplanar conformation conducts 53 nA, which is 496 times the current that we find for the perpendicular conformation.

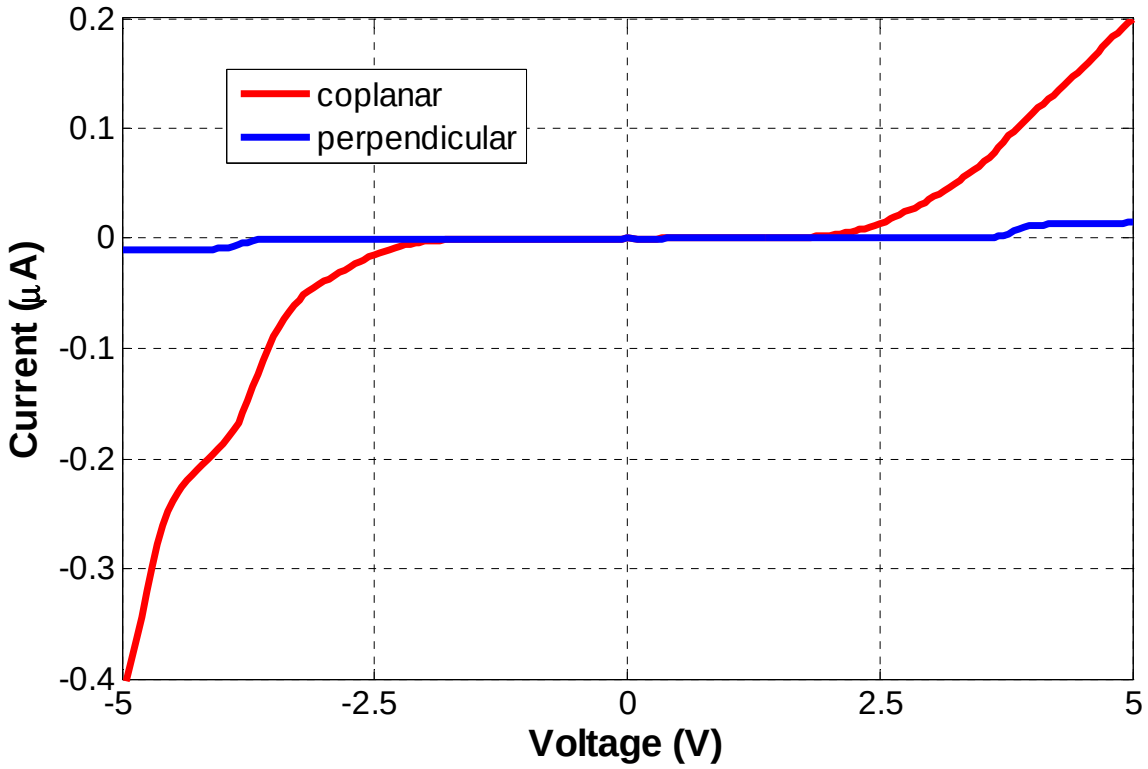

Fig. 32. Comparison of the current-voltage characteristics of the coplanar and perpendicular configurations for the (4,4) CNT-nitroOPE-Si junction (Molecule 9).

We calculate the I-V characteristic for several charge states (charge -1, -2, and -3) for the coplanar and perpendicular configurations of the (4,4) CNT-nitroOPE-Si junction (Molecule 9), as summarized in Fig. 33. The geometries of the charge states are kept fixed to the geometry of the neutral molecule, only the wavefunctions are optimized. The optimization of all the conformational and charge states is performed using the combination of B3PW91 level of theory and the 6-31G(d) basis set.

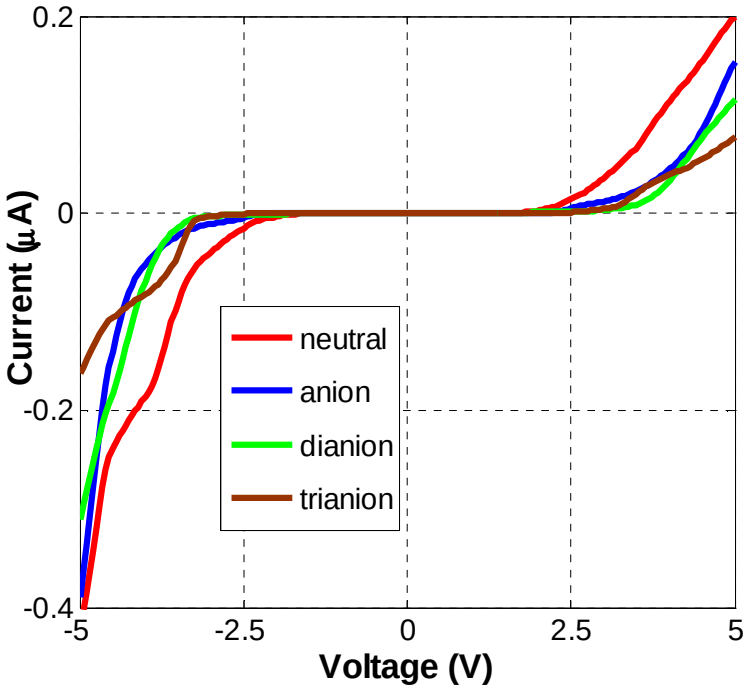

(**A**)

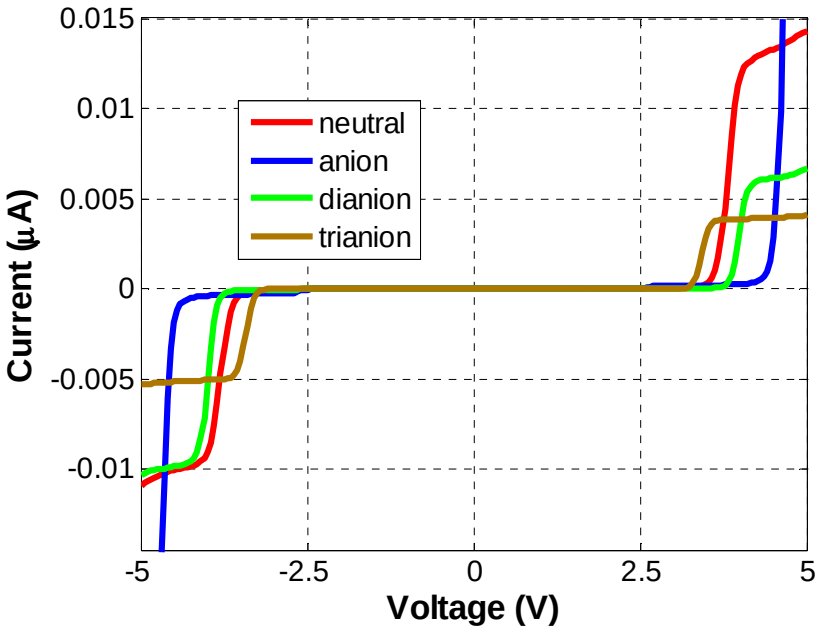

(**B**)

Fig. 33. (A) Current-voltage characteristic for different charge states of (4,4) CNT-nitroOPE-Si (Molecule 9) in its coplanar conformation. (B) Current-voltage characteristic for different charge states of the (4,4) CNT-nitroOPE-Si in its perperdicular conformation. For all cases, only the contribution of α electrons is shown.

Our I-V calculations for the negatively charged states of the coplanar (4,4) CNT-nitroOPE-Si junction show a reduction in conductance with respect to the neutral (Fig. 33A). The anion, dianion, and trianion present similar values of conductance, which is clearly distinctive from the neutral. For instance; at 3.3 V, the neutral molecule conducts 52.9 nA, the anion 17.4 nA, the dianion 5.9 nA, and the trianion 10 nA. The reduction in conductance is not as drastic as when using Au for the top contact.

4.6.3 ESP distribution along the junction

We compare the ESP distribution between the neutral and anion states of the coplanar nitroOPE junctions. The ESP distributions for the neutral states of the Au-nitroOPE-Si and the CNT-nitroOPE-Si are shown in Fig. 34A and Fig. 34C, respectively. The value for the ESP in the junction ranges from positive (blue) to negative (red) values; however, for the anion states (Fig. 34, B and D) mostly regions of negative values are found within the junction. Because of electrostatic repulsion, negatively charged particles are scattered from regions of negative ESP (red). Therefore, the negatively charged junctions (negative ions) behave as nearly closed channels for electron transport, which explains the noticeable reduction of current in the charged junctions as compared to their neutral states.

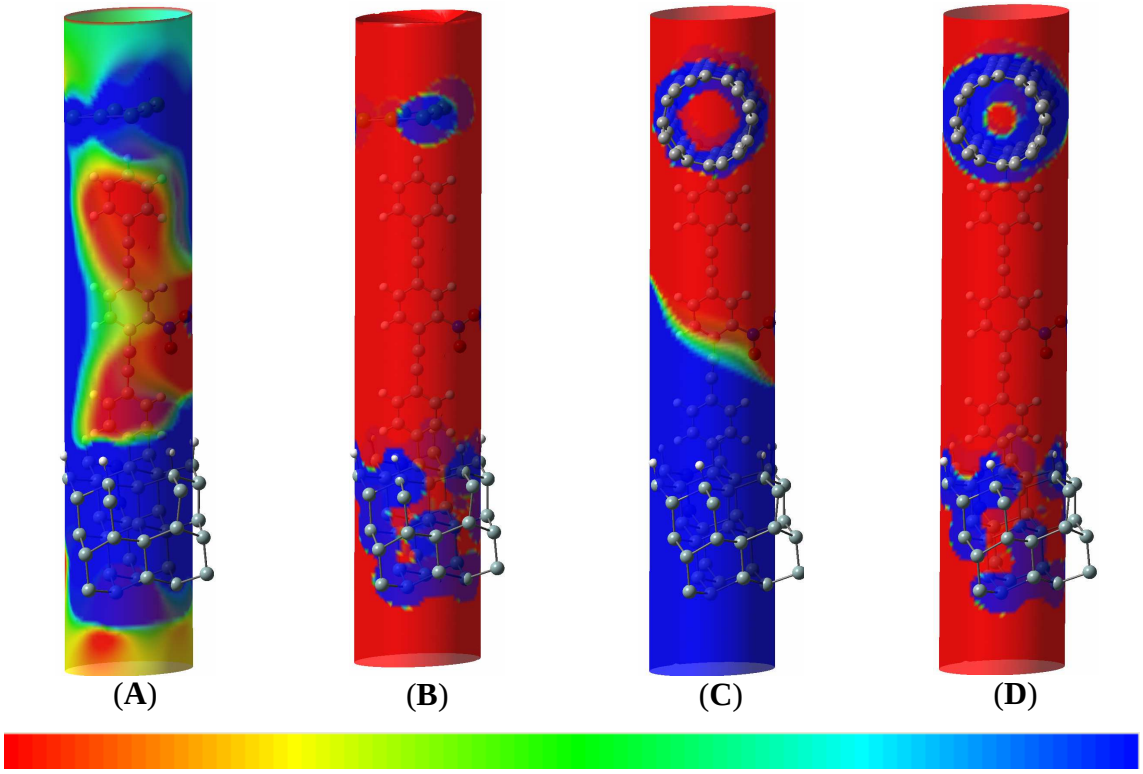

Fig. 34. Distribution of the ESP for the neutral (A) and anion (B) states of the coplanar Au-nitroOPE-Si junction (Molecule 5). Distribution of the ESP for the neutral (C) and anion (D) charge states for the coplanar (4,4) CNT-nitroOPE-Si junction (Molecule 9). The spatial region corresponds to a cylinder of radius 4 Å centered on the main C-C axis. The scale ranges from -0.1 (red) to 0.1 (blue) V.

4.6.4 Analysis of the molecular orbitals

Molecular orbitals (θ_i^{KS}) are the mathematical solutions to the one-electron Kohn-Sham equation, given in Eq. 6. Despite controversies regarding their physical reality, MOs have extensively been used as important qualitative indicators of the conductance of molecular systems (*31, 69, 123*). An MO that is delocalized throughout the molecular junction represents a conducting channel; an MO that is localized only on specific regions of the molecular junctions is not a good conducting channel. As a qualitative rule, the more delocalized a molecular orbital is, the more conducting the channel it represents.

In the resonant tunneling picture, an electron from one contact jumps into an unoccupied MO (HOMO, HOMO-1, …) then it jumps again from that MO to the other contact, freeing the way for another electron to repeat the process. The transport of electrons can also take place through the occupied MOs (LUMO, LUMO+1, …). In this case, the electron occupying the MO jump first into one contact, with a given tunneling probability. Then, an electron from the other contact can jump into the available MO. The tunneling probability depends not only on the shape of the MO, which indicates how localized or delocalized the MO is, but also on the proximity of the energy of the MO to the ECP of the molecular junction. As a qualitative rule, the MOs whose energies are closest to the ECP of the molecule are more conducting than the ones whose energies farther apart.

A simple electrostatic explanation suffices to account for the change in conductance due to charge state, as discussed in 4.6.3. However, we could not find a direct electrostatic explanation for the change in conductance observed between the coplanar and the perpendicular. The explanation rests more in the quantum-mechanical nature of the system. We use the MOs to explain the change in conductance between the coplanar and the perpendicular conformational states.

Since the ECP of the molecular junction is taken as the energy of the HOMO, we expect most of the electron transport to take place through the HOMO.

For the Au_1-S-nitroOPE-S-Au_1 junction, the HOMO for the coplanar conformation is totally delocalized between the metallic contacts and the nitroOPE, as seen in Fig. 35. This explains the high conductance of the coplanar configuration and the low conductance of the perpendicular configuration.

Similar results are found for the Au_6-nitroOPE-S-Au_1, shown in Fig. 36. The HOMO for the coplanar configuration is delocalized across the nitroOPE and the bottom Au atom; however, it does not cover the top Au_6 contact, reflecting the absence of a chemical bond. Because of that, the conduction through the HOMO is not as high as for the Au_1-S-nitroOPE-S-Au_1 junction, where a chemical bond is present. However, this is compensated by the presence of three delocalized orbitals (the HOMO, HOMO-1, and

HOMO-2) instead of only one. The frontier MOs for the perpendicular configuration are localized, accounting for the low conductance observed in the I-V calculation.

The MOs for the CNT-nitroOPE-CNT junction are shown in Fig. 37. The population of the MOs at both CNT-nitroOPE interfaces gives an indication of the seamless chemical attachment of an organic molecule to the CNT, which reflects an electronically superior contact. We observe four delocalized MOs (LUMO, HOMO, HOMO-3, HOMO-4), which enhance the conduction in the coplanar conformation. Conversely, the MOs for the perpendicular conformation are localized.

For the coplanar Au_6-nitroOPE-Si junction, the MOs (Fig. 38) close to the HOMO are localized but two delocalized MOs (HOMO-3, HOMO-4) are found at lower energies. This agrees with the flat region observed in the I-V curve of the coplanar junction, where current is found upon the application of higher voltages. All the MOs for the perpendicular conformation are localized.

The frontier MOs for the CNT-nitroOPE-Si junction are reported in Fi.g 39. The MOs are localized for the perpendicular conformation and delocalized for the coplanar conformation, accounting for the difference in conductance found between both conformational states.

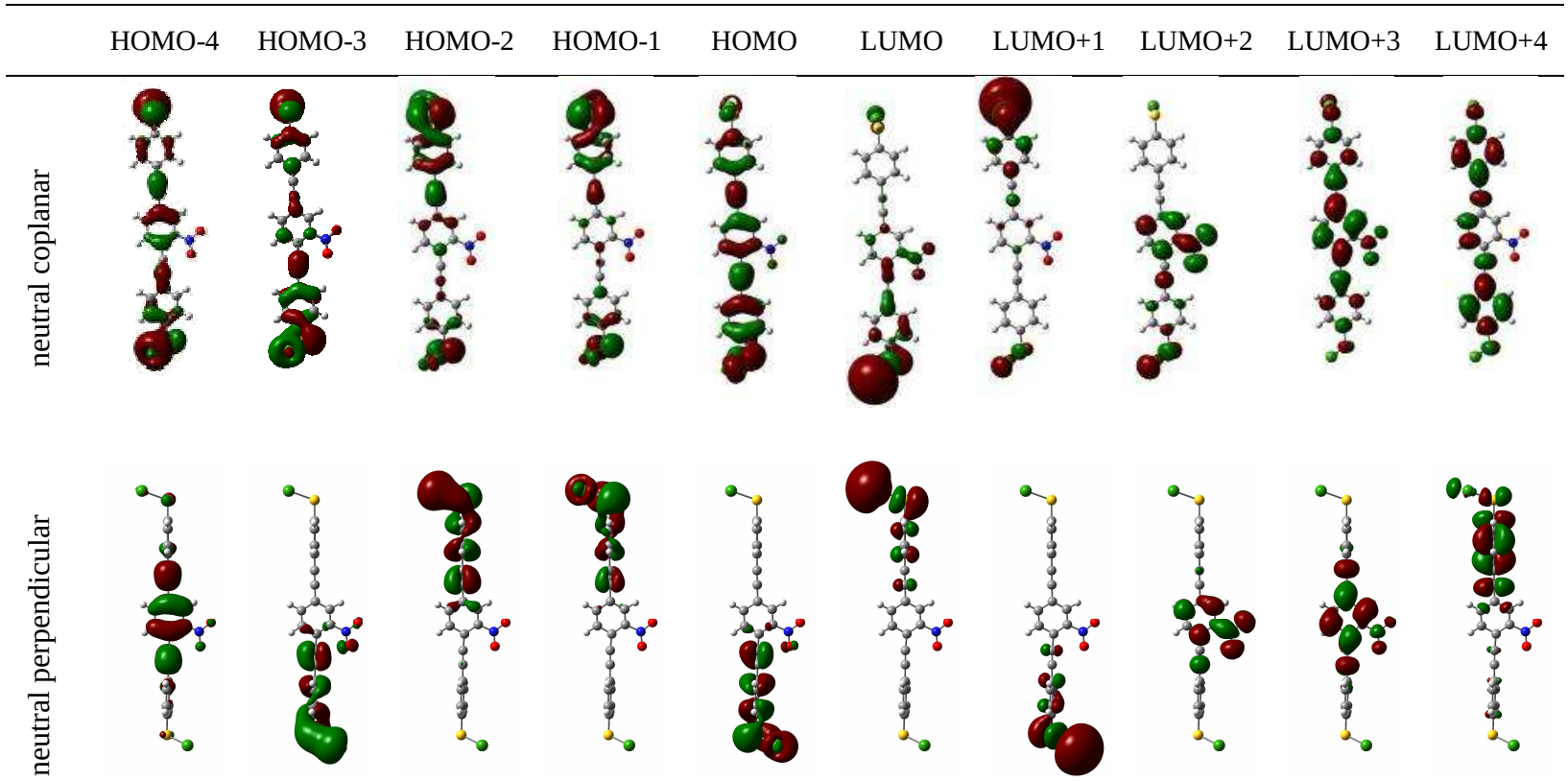

Fig. 35. Molecular orbitals for the coplanar and the perpendicular conformations of the Au_1-S-nitroOPE-S-Au_1 junction. An isosurface of value 0.02 is used for all the plots.

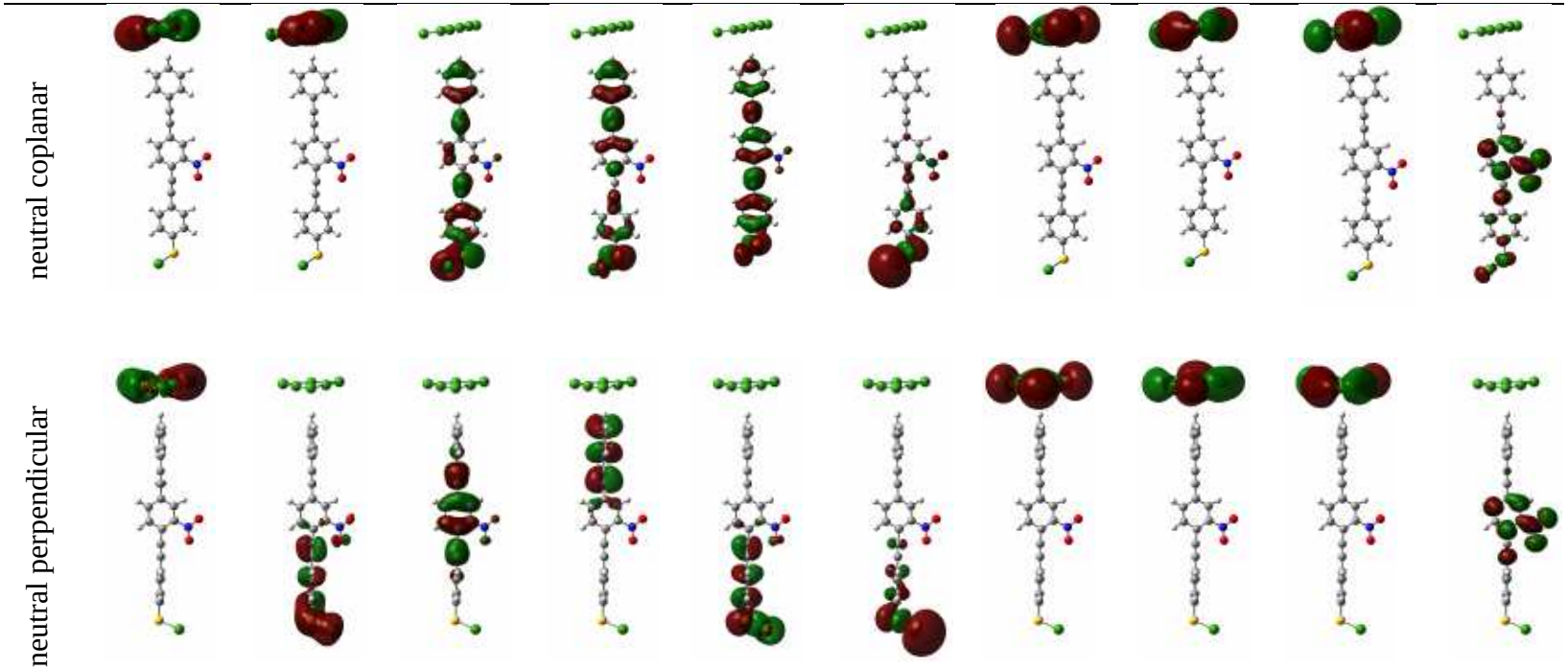

Fig. 36. Comparison of the molecular orbitals for the coplanar and the perpendicular conformations of the Au-nitroOPE-Au junction. An isosurface of value 0.02 is used for all the plots.

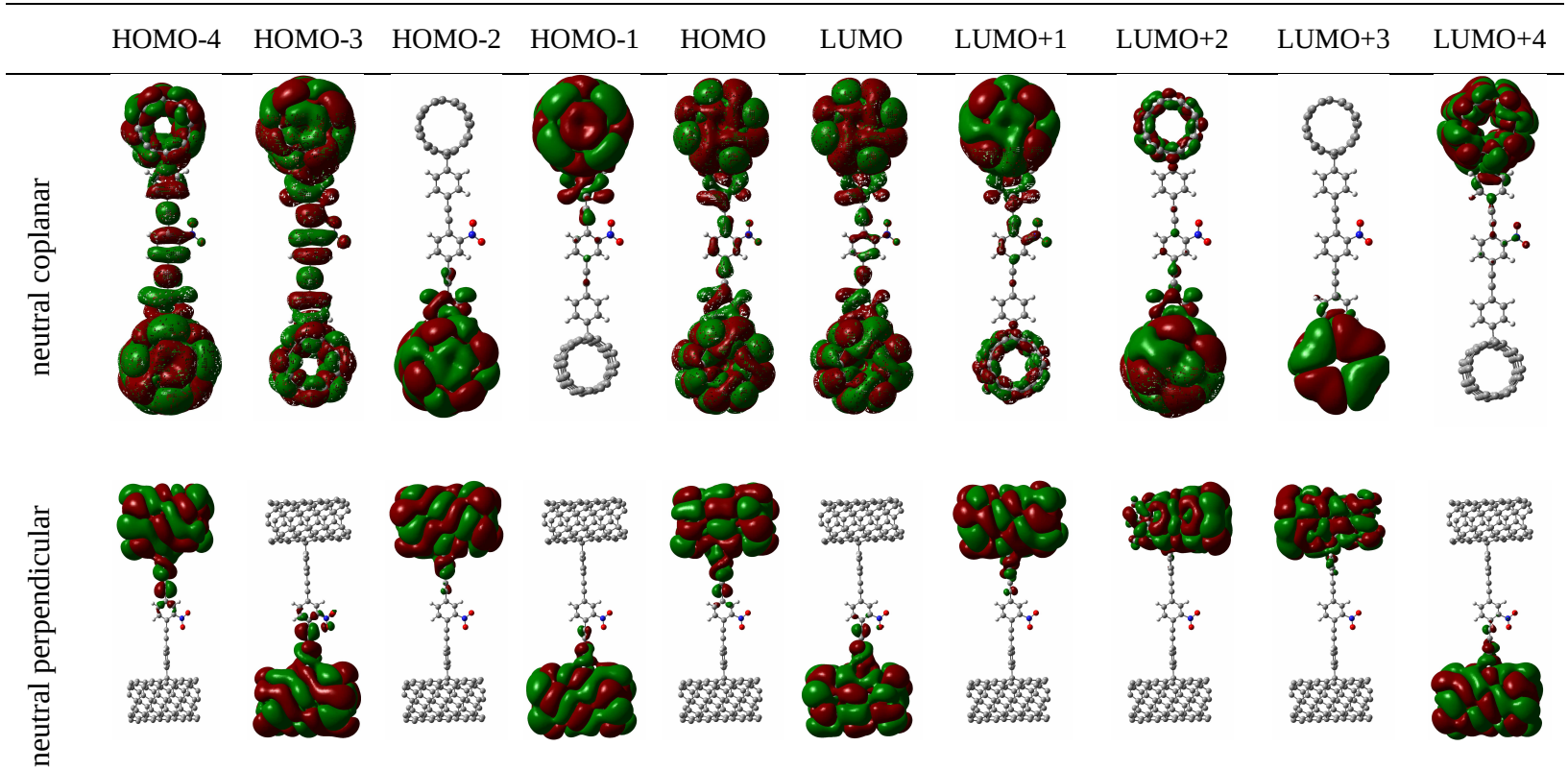

Fig. 37. Molecular orbitals for the coplanar and the perpendicular conformations of the CNT-nitroOPE-CNT junction. An isosurface of value 0.001 is used for all the plots.

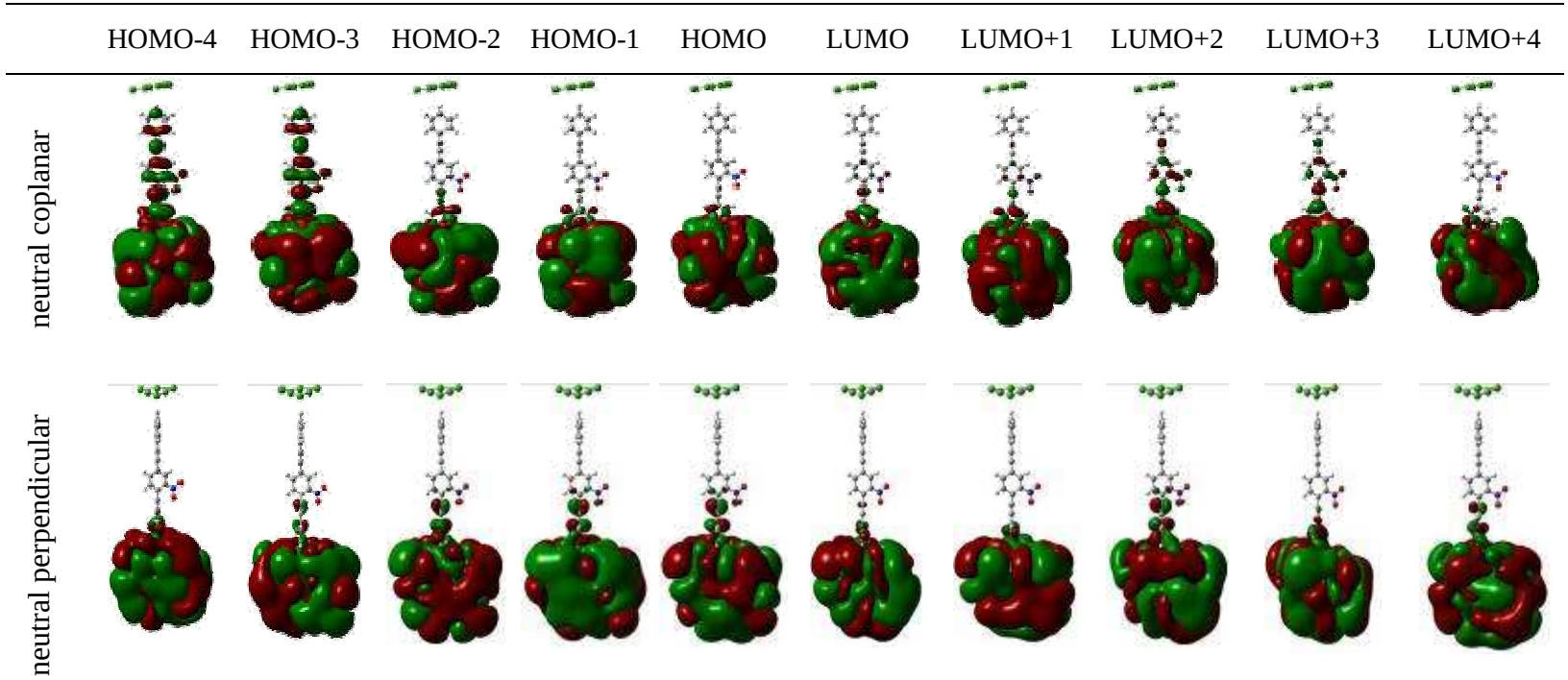

Fig. 38. Molecular orbitals for the coplanar and the perpendicular conformations of the Au_6-nitroOPE-Si junction. An isosurface of value 0.001 is used for all the plots.

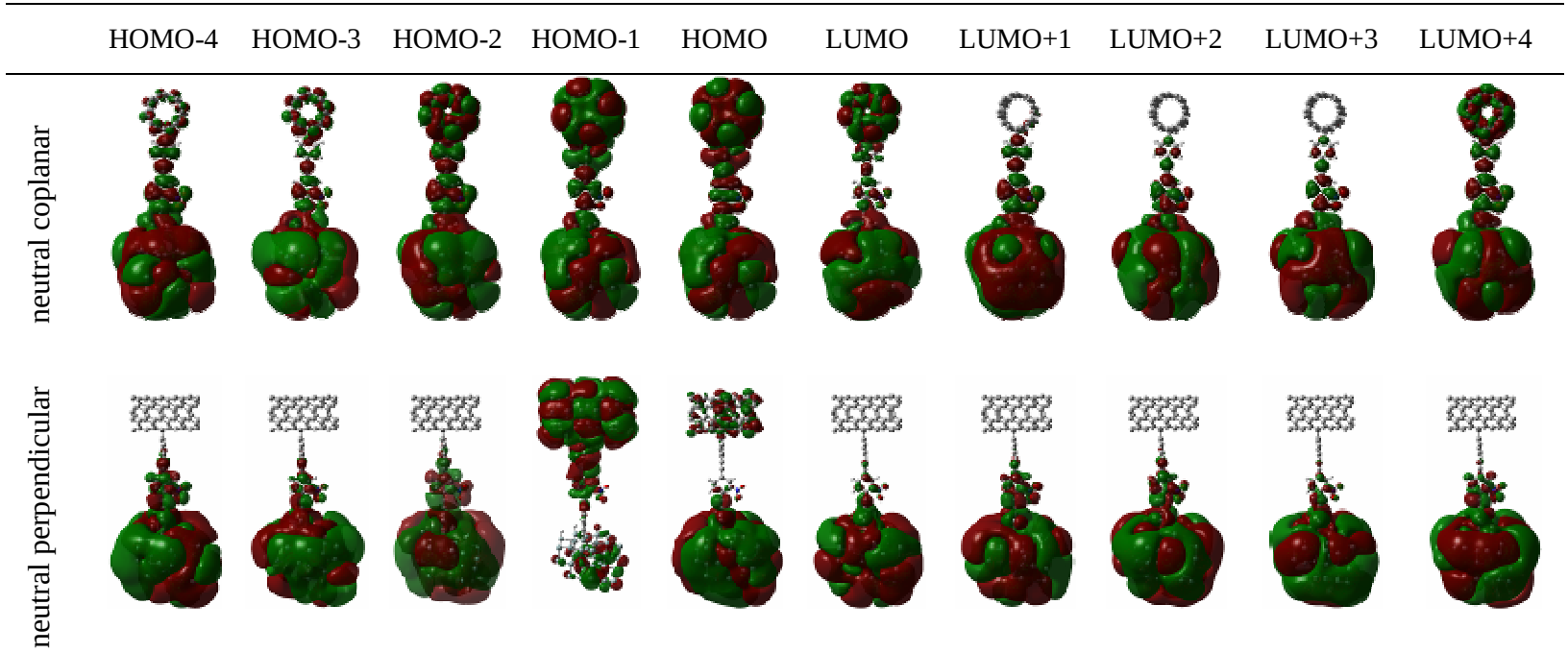

Fig. 39. Comparison of the molecular orbitals for the coplanar and the perpendicular conformations of the CNT-nitroOPE-Si junction. An isosurface of value 0.0001 is used for all the plots.

4.7 Conclusions

The miniaturization of conventional electronic devices can change drastically their electrical characteristics due to the predominance of quantum-mechanical effects at atomistic dimensions. Because of its technological importance, the use of silicon in molecular electronic devices is desirable. Macroscopically, metal-semiconductor junctions are known to behave as electrical rectifiers (Schottky diodes); this is apparently a drawback for the use of a semiconductor material as a contact for single-molecule-based devices. However, our calculation of metal-nitroOPE-semiconductor junctions corroborated previous predictions that a "molecular Schottky diode," contrary to its macroscopic counterpart, does not present rectifying behavior. This is due to the predominance of the tunneling over the thermionic transport mechanisms at atomistic sizes.

We determined that the low- and high-conductance states, observed for metal-nitroOPE-metal junctions, could still be obtained from a metal-nitroOPE-semiconductor junction. The switch between both states of conductance is produced by conformational and charge-state changes of the molecular junctions. However, the operating point of the device should be set at higher bias voltages since a flat region of zero current is predicted to appear at low bias voltages.

The change of conductance of the metal-nitroOPE-Si junctions due to charging effects can be accounted by a simple electrostatic explanation. For the negatively charged junctions, the ESP distribution along the junction reveals a region of negative electrostatic potential, which repels the electrons, thus, it obstructs the flow of carriers.

Changes in conductance between the coplanar and the perpendicular conformation of all the analyzed junctions can be explained by looking at the shape and spatial distribution of their molecular orbitals. The coplanar conformations have molecular orbitals that are more delocalized than the ones belonging to the perpendicular conformations. This indicates that the molecular orbitals for coplanar conformations are

more conductive than those from the perpendicular conformation. Therefore, explaining the higher conductance of the coplanar junctions.

CHAPTER V

CONCLUSIONS

5.1 Summary and conclusions

Molecules can be used as electronic circuits to storage binary information encoded in two molecular bistable states; for instance, a state of high conductance and a state of low conductance. Molecules can be arranged in crossbar architectures to create logic or memory electronic devices. In both cases, the desirable property of bistability depends not only on the molecule but also on the type and geometry of the contacts. Therefore, our calculations consider the molecule and few atoms of the contacts as an entwined unit, a molecular junction.

Advances in Density Functional Theory and the increase in computational power of modern computers have allowed us to perform full-quantum-mechanical calculations of molecular junctions composed of up to a few hundred atoms. The continuum of electronic states, derived from the semi-infinite nature of the contacts, has been added to the molecular junction by using a mathematical formalism based on the Green function.

We have estimated the conductance of molecular junctions composed of the nitroOPE molecule and two contacts of materials such as Au, Si, and carbon nanotubes. These results are summarized in Fig. 35. Two very well defined states of conductance, requisite for digital electronics, are obtained from the nitroOPE by changing the conformation and charge states of the molecule. The nitroOPE molecule is found to conduct higher current (logic “1”) when all its phenyl rings are coplanar rather than when the middle phenyl ring is perpendicular to the other two (logic “0”). In addition, bistable states can be obtained by charging the molecule. When the nitroOPE is in its neutral state, it conducts higher current (logic “1”) than when the molecule is negatively charged (logic “0”).

We determined that when two gold contacts are used to address the molecule, the bistable states of conductance are readily available at any bias voltage. However, when a combination of one semiconducting and one metallic contact is used, the bistable states are lost at low bias voltages. We found a nearly flat region in the current-voltage characteristic of metal-nitroOPE-semiconductor junctions in the low bias voltage region. Instead of presenting two distinguishable states, all the conformation and charge states of the metal-nitroOPE-semiconductor junctions (coplanar, perpendicular, anion, dianion, and trianion) showed almost indistinguishable zero conductance in the flat region. These indicate that when a semiconducting contact is used, we must move the operating point of the device to higher bias voltages.

Our calculations demonstrated that the recently synthesized CNT-nitroOPE-Si junction (*54*) presents the same potential as a bistable device that the Au-nitroOPE-Si junction does. However, for the former case, charging of the junction does not lead to two very distinguishable states; therefore, the two bistable states to consider should come from the neutral coplanar (logic "1") and the neutral perpendicular ("0").

Quantum-mechanical effects cannot be disregarded whenever dealing with electronic devices of atomistic dimensions. For instance, we corroborated that a "molecular Schottky diode" does not present the rectifying behavior associated with a macroscopic Schottky diode. It is most likely that future electronic devices will be purposely engineered to take advantage of the most exotic quantum-mechanical properties for applications such as quantum computation, quantum teleportation, quantum cryptography. Consequently, computational tools derived from the fundamental equation of quantum mechanics, the Schrödinger equation, will be mandatory.

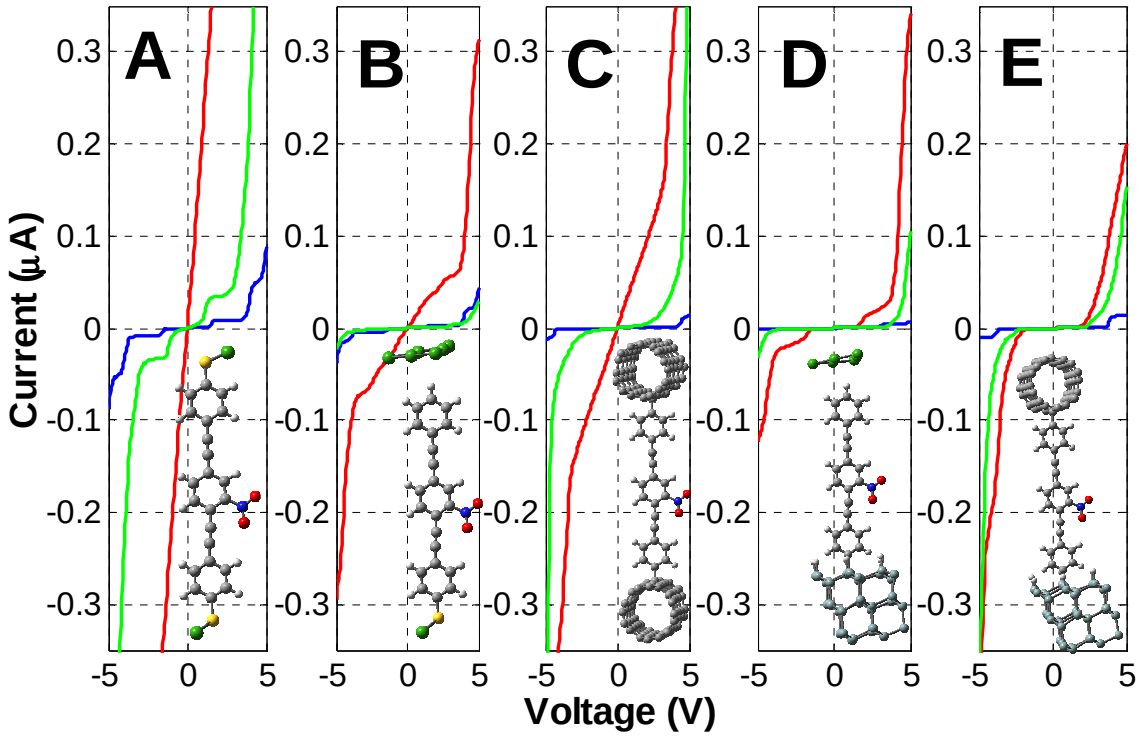

Fig. 40. Summary of current-voltage characteristics for the following molecular junctions: (A) Au_1-S-nitroOPE-S-Au_1, (B) Au_6-nitroOPE-S-Au_1, (C) CNT-nitroOPE-CNT, (D) Au_6-nitroOPE-Si, and (E) CNT-nitroOPE-Si.

5.2 Future work

Our methods add the effect of the semi-infinite contacts to the molecular junction by considering the density of states of the bulk material. We have considered intrinsic Si as the bottom contact; we suggest extending the calculations to consider doped Si. Different levels of doping could be simulated by varying the position of the Fermi level within the bandgap according to the desired concentration of dopants.

In all our calculations, the wavefunction of the molecular junction has been calculated as one of an isolated molecule in vacuum. We suggest extending our calculation to include the effect of the applied bias voltage in the electronic structure by

computing the Hamiltonian of the molecular junction in the presence of an external electric field.

We suggest calculating molecular junctions composed of a metallic CNT contact, an organic molecule, and a semiconducting CNT. Each carbon atom in the CNT is a surface and bulk atom at the same time. Therefore, in the singular case of CNT contacts, the organic molecule is attached to a bulk C atom of the CNT. The density of states of bulk atoms can be precisely obtained, increasing the accuracy of current-voltage calculation. These junctions are extremely interesting for the study of the formation of Schottky barriers; however, technical difficulties prevented us from obtaining quantum-mechanically the density of states for the semiconducting (8,0) CNT.

REFERENCES AND NOTES

1. M. Leong, B. Doris, J. Kedzierski, K. Rim, M. Yang, *Science* **306**, 2057-2060 (2004).
2. B. Doyle, R. Arghavani, D. Barlage, S. Datta, M. Doczy *et al.*, *Intel Technology Journal* **06**, 42-54 (2002).
3. Semiconductor Research Corporation, *Research Needs for Device Sciences Modeling and Simulation* (2005); available at http://www.src.org/
4. Semiconductor Industry Association, *International Technology Roadmap for Semiconductors - Executive Summary* (2005); available at http://public.itrs.net
5. Semiconductor Industry Association, *International Technology Roadmap for Semiconductors - Modeling and Simulation* (2005); available at http://public.itrs.net
6. A. D. Yoffe, *Advances in Physics* **42**, 173-266 (1993).
7. A. D. Yoffe, *Advances in Physics* **50**, 1-208 (2001).
8. A. L. Efros, M. Rosen, *Annual Review of Materials Science* **30**, 475-521 (2000).
9. A. G. Cullis, L. T. Canham, *Nature* **353**, 335-338 (1991).
10. D. K. Ferry, S. M. Goodnick, *Transport in Nanostructures* (Cambridge University Press, Cambridge, U.K., 1997).
11. A. Aviram, M. A. Ratner, *Chemical Physics Letters* **29**, 277-283 (1974).
12. J. M. Tour, L. Cheng, D. P. Nackashi, Y. X. Yao, A. K. Flatt *et al.*, *Journal of the American Chemical Society* **125**, 13279-13283 (2003).
13. C. P. Husband, S. M. Husband, J. S. Daniels, J. M. Tour, *IEEE Transactions on Electron Devices* **50**, 1865-1875 (2003).
14. J. M. Tour, W. L. Van Zandt, C. P. Husband, S. M. Husband, L. S. Wilson *et al.*, *IEEE Transactions on Nanotechnology* **1**, 100-109 (2002).
15. C. A. Richter, D. R. Stewart, D. A. A. Ohlberg, R. S. Williams, *Applied Physics A: Materials Science & Processing* **80**, 1355-1362 (2005).
16. C. J. Amsinck, N. H. Di Spigna, D. P. Nackashi, P. D. Franzon, *Nanotechnology* **16**, 2251-2260 (2005).
17. D. B. Strukov, K. K. Likharev, *Nanotechnology* **16**, 888-900 (2005).
18. Y. H. Choi, Y. K. Kim, *Nanotechnology* **15**, 639-644 (2004).

19. M. H. Lee, Y. K. Kim, Y. H. Choi, *IEEE Transactions on Nanotechnology* **3**, 152-157 (2004).

20. G. Y. Jung, S. Ganapathiappan, X. Li, D. A. A. Ohlberg, D. L. Olynick *et al.*, *Applied Physics A: Materials Science & Processing* **78**, 1169-1173 (2004).

21. M. M. Ziegler, M. R. Stan, *IEEE Transactions on Nanotechnology* **2**, 217-230 (2003).

22. K. Likharev, A. Mayr, I. Muckra, O. Turel, *Molecular Electronics III* **1006**, 146-163 (2003).

23. M. M. Ziegler, C. A. Picconatto, J. C. Ellenbogen, A. Dehon, D. Wang *et al.*, *Molecular Electronics III* **1006**, 312-330 (2003).

24. Z. H. Zhong, D. L. Wang, Y. Cui, M. W. Bockrath, C. M. Lieber, *Science* **302**, 1377-1379 (2003).

25. Y. Chen, G. Y. Jung, D. A. A. Ohlberg, X. M. Li, D. R. Stewart *et al.*, *Nanotechnology* **14**, 462-468 (2003).

26. R. J. Luyken, F. Hofmann, *Nanotechnology* **14**, 273-276 (2003).

27. C. Li, D. H. Zhang, X. L. Liu, S. Han, T. Tang *et al.*, *Applied Physics Letters* **82**, 645-647 (2003).

28. Y. Luo, C. P. Collier, J. O. Jeppesen, K. A. Nielsen, E. Delonno *et al.*, *ChemPhysChem* **3**, 519-525 (2002).

29. K. W. Martin, *Digital Integrated Circuit Design* (Oxford University Press, NY, 2000).

30. N. A. Melosh, A. Boukai, F. Diana, B. Gerardot, A. Badolato *et al.*, *Science* **300**, 112-115 (2003).

31. J. M. Seminario, A. G. Zacarias, P. A. Derosa, *Journal of Physical Chemistry A* **105**, 791-795 (2001).

32. A. Nitzan, M. A. Ratner, *Science* **300**, 1384-1389 (2003).

33. M. A. Reed, C. Zhou, C. J. Muller, T. P. Burgin, J. M. Tour, *Science* **278**, 252-254 (1997).

34. J. Chen, M. A. Reed, A. M. Rawlett, J. M. Tour, *Science* **286**, 1550-1552 (1999).

35. J. Chen, W. Wang, J. Klemic, M. A. Reed, B. W. Axelrod *et al.*, *Molecular Electronics II* **960**, 69-99 (2002).

36. C. P. Collier, E. W. Wong, M. Belohradsky, F. M. Raymo, J. F. Stoddart *et al.*, *Science* **285**, 391-394 (1999).

37. C. A. Dyke, J. M. Tour, *Journal of Physical Chemistry A* **108**, 11151-11159 (2004).

38. C. A. Dyke, J. M. Tour, *Chemistry-A European Journal* **10**, 813-817 (2004).

39. C. A. Dyke, M. P. Stewart, F. Maya, J. M. Tour, *Synlett* **1**, 155-160 (2004).

40. J. M. Buriak, *Chemical Reviews* **102**, 1271-1308 (2002).

41. M. P. Stewart, F. Maya, D. V. Kosynkin, S. M. Dirk, J. J. Stapleton *et al.*, *Journal of the American Chemical Society* **126**, 370-378 (2004).

42. M. A. Brook, *Silicon in Organic, Organometallic, and Polymer Chemistry* (Wiley, NY, 2000).

43. N. P. Guisinger, N. L. Yoder, M. C. Hersam, *Proceedings of the National Academy of Sciences of the United States of America* **102**, 8838-8843 (2005).

44. N. P. Guisinger, R. Basu, A. S. Baluch, M. C. Hersam, *Molecular Electronics III* **1006**, 227-234 (2003).

45. N. P. Guisinger, R. Basu, M. E. Greene, A. S. Baluch, M. C. Hersam, *Nanotechnology* **15**, S452-S458 (2004).

46. N. P. Guisinger, M. E. Greene, R. Basu, A. S. Baluch, M. C. Hersam, *Nano Letters* **4**, 55-59 (2004).

47. P. B. Balbuena, D. Altomare, L. Agapito, J. M. Seminario, *Journal of Physical Chemistry B* **107**, 13671-13680 (2003).

48. J. M. Seminario, Y. F. Ma, L. A. Agapito, L. M. Yan, R. A. Araujo *et al.*, *Journal of Nanoscience and Nanotechnology* **4**, 907-917 (2004).

49. P. Hohenberg, W. Kohn, *Physical Review B* **136**, 864-871 (1964).

50. W. Kohn, L. J. Sham, *Phys. Rev. A* **140**, 1133-1138 (1965).

51. A. Szabo, N. S. Ostlund, *Modern Quantum Chemistry: Introduction to Advanced Electronic Structure Theory* (Dover Publications, Mineola, NY, 1996).

52. C. Roetti, in *Quantum-Mechanical Ab-initio Calculation of the Properties of Crystalline Materials* C. Pisani, Ed. (Springer-Verlag, Berlin, 1996), vol. 67.

53. R. Saito, M. Fujita, G. Dresselhaus, M. S. Dresselhaus, *Applied Physics Letters* **60**, 2204-2206 (1992).

54. A. K. Flatt, B. Chen, J. M. Tour, *Journal of the American Chemical Society* **127**, 8918-8919 (2005).

55. M. Ouyang, J. L. Huang, C. L. Cheung, C. M. Lieber, *Science* **292**, 702-705 (2001).

56. M. Ouyang, J. L. Huang, C. L. Cheung, C. M. Lieber, *Science* **291**, 97-100 (2001).

57. R. A. Jishi, J. Bragin, L. Lou, *Physical Review B* **59**, 9862-9865 (1999).

58. C. D. Spataru, S. Ismail-Beigi, L. X. Benedict, S. G. Louie, *Physical Review Letters* **92**, 77402 (2004).

59. C. D. Spataru, S. Ismail-Beigi, L. X. Benedict, S. G. Louie, *Applied Physics A: Materials Science & Processing* **78**, 1129-1136 (2004).

60. P. V. Avramov, K. N. Kudin, G. E. Scuseria, *Chemical Physics Letters* **370**, 597-601 (2003).

61. P. A. Derosa, J. M. Seminario, *Journal of Physical Chemistry B* **105**, 471-481 (2001).

62. J. M. Seminario, P. A. Derosa, *Journal of the American Chemical Society* **123**, 12418-12419 (2001).

63. M. J. Frisch, G. W. Trucks, H. B. Schlegel, G. E. Scuseria, M. A. Robb *et al.*, *Gaussian 03* (Gaussian Inc., Wallingford, CT, 2003).

64. J. M. Seminario, A. G. Zacarias, P. A. Derosa, *J. Chem. Phys.* **116**, 1671-1683 (2002).

65. P. A. Derosa, A. C. Zacarias, J. M. Seminario, in *Reviews in Modern Quantum Chemistry* K. D. Sen, Ed. (World Scientific, Singapore, 2002) pp. 1537-1567.

66. J. M. Seminario, C. E. De la Cruz, P. A. Derosa, *Journal of the American Chemical Society* **123**, 5616-5617 (2001).

67. J. C. Ellenbogen, J. C. Love, *Proceedings of the IEEE* **88**, 386-426 (2000).

68. S. Datta, *Quantum Transport: Atom to Transistor* (Cambridge University Press, NY, 2005).

69. J. M. Seminario, A. G. Zacarias, J. M. Tour, *Journal of the American Chemical Society* **122**, 3015-3020 (2000).

70. S. Datta, *Electronic Transport in Mesoscopic Systems* (Cambridge University Press, Cambridge, U.K., 1995).

71. M. Di Ventra, S. T. Pantelides, N. D. Lang, *Physical Review Letters* **84**, 979-982 (2000).

72. M. S. Strano, C. A. Dyke, M. L. Usrey, P. W. Barone, M. J. Allen *et al.*, *Science* **301**, 1519-1522 (2003).

73. J. M. Seminario, L. A. Agapito, H. P. Figueroa, paper presented at the IEEE-NANO 2002, Arlington, VA 22202 2002.

74. Z. J. Donhauser, B. A. Mantooth, K. F. Kelly, L. A. Bumm, J. D. Monnell *et al.*, *Science* **292**, 2303-2307 (2001).

75. X. D. Cui, A. Primak, X. Zarate, J. Tomfohr, O. F. Sankey *et al.*, *Science* **294**, 571-574 (2001).

76. T. Vondrak, H. Wang, P. Winget, C. J. Cramer, X. Y. Zhu, *Journal of the American Chemical Society* **122**, 4700-4707 (2000).

77. H. Sumi, *Journal of Physical Chemistry B* **102**, 1833-1844 (1998).

78. R. Hasunuma, T. Komeda, H. Tokumoto, *Applied Physics a-Materials Science & Processing* **66**, S689-S693 (1998).

79. J. M. Tour, *Molecular Electronics : Commercial Insights, Chemistry, Devices, Architecture, and Programming* (World Scientific, River Edge, NJ, 2003).

80. J. M. Tour, M. A. Reed, J. M. Seminario, D. A. Allara, P. A. Weiss, in *US Patent 6,430,511*. (2002).

81. J. M. Seminario, *Nature Materials* **4**, 111-113 (2005).

82. J. M. Seminario, P. A. Derosa, J. L. Bastos, *Journal of the American Chemical Society* **124**, 10266-10267 (2002).

83. J. M. Seminario, R. A. Araujo, L. M. Yan, *Journal of Physical Chemistry B* **108**, 6915-6918 (2004).

84. D. L. Allara, T. D. Dunbar, P. S. Weiss, L. A. Bumm, M. T. Cygan *et al.*, *Molecular Electronics: Science and Technology* **852**, 349-370 (1998).

85. J. M. Tour, L. Jones, D. L. Pearson, J. J. S. Lamba, T. P. Burgin *et al.*, *Journal of the American Chemical Society* **117**, 9529-9534 (1995).

86. R. G. Nuzzo, D. L. Allara, *Journal of the American Chemical Society* **105**, 4481-4483 (1983).

87. A. Ulman, *Chemical Reviews* **96**, 1533-1554 (1996).

88. G. J. Kluth, M. M. Sung, R. Maboudian, *Langmuir* **13**, 3775-3780 (1997).

89. R. Younkin, K. K. Berggren, K. S. Johnson, M. Prentiss, D. C. Ralph *et al.*, *Applied Physics Letters* **71**, 1261-1263 (1997).

90. L. T. Cai, Y. X. Yao, J. P. Yang, D. W. Price, J. M. Tour, *Chemistry of Materials* **14**, 2905-2909 (2002).

91. J. M. Seminario, L. E. Cordova, P. A. Derosa, *Proceedings of the IEEE* **91**, 1958-1975 (2003).

92. J. Chen, J. Su, W. Wang, M. A. Reed, *Physica E-Low-Dimensional Systems & Nanostructures* **16**, 17-23 (2003).

93. F. R. F. Fan, J. P. Yang, L. T. Cai, D. W. Price, S. M. Dirk *et al.*, *Journal of the American Chemical Society* **124**, 5550-5560 (2002).

94. J. M. Tour, A. M. Rawlett, M. Kozaki, Y. X. Yao, R. C. Jagessar *et al.*, *Chemistry-A European Journal* **7**, 5118-5134 (2001).

95. Y. Karzazi, J. Cornil, J. L. Bredas, *Journal of the American Chemical Society* **123**, 10076-10084 (2001).

96. S. Lakshmi, S. K. Pati, *Physical Review B* **72**, 193410 (2005).

97. A. J. Read, R. J. Needs, K. J. Nash, L. T. Canham, P. D. J. Calcott *et al.*, *Physical Review Letters* **69**, 1232-1235 (1992).

98. C. Delerue, G. Allan, M. Lannoo, *Physical Review B* **48**, 11024-11036 (1993).

99. J. B. Xia, K. W. Cheah, *Physical Review B* **55**, 1596-1601 (1997).

100. J. B. Xia, K. W. Cheah, *Physical Review B* **55**, 15688-15693 (1997).

101. J. B. Xia, K. W. Cheah, *Journal of Physics: Condensed Matter* **9**, 9853-9862 (1997).

102. B. Delley, E. F. Steigmeier, *Applied Physics Letters* **67**, 2370-2372 (1995).

103. P. Avouris, I. W. Lyo, Y. Hasegawa, *Journal of Vacuum Science & Technology A: Vacuum Surfaces and Films* **11**, 1725-1732 (1993).

104. G. D. J. Smit, S. Rogge, T. M. Klapwijk, *Applied Physics Letters* **80**, 2568-2570 (2002).

105. W. Wang, T. Lee, M. Kamdar, M. A. Reed, M. P. Stewart *et al.*, *Superlattices and Microstructures* **33**, 217-226 (2003).

106. L. A. Curtiss, P. C. Redfern, K. Raghavachari, J. A. Pople, *Journal of Chemical Physics* **109**, 42-55 (1998).

107. G. de Oliveira, J. M. L. Martin, F. de Proft, P. Geerlings, *Physical Review A* **60**, 1034-1045 (1999).

108. V. N. Staroverov, G. E. Scuseria, J. M. Tao, J. P. Perdew, *Journal of Chemical Physics* **119**, 12129-12137 (2003).

109. J. P. Perdew, M. Levy, *Physical Review B* **56**, 16021-16028 (1997).

110. J. P. Perdew, R. G. Parr, M. Levy, J. L. Balduz, *Physical Review Letters* **49**, 1691-1694 (1982).

111. R. G. Parr, R. A. Donnelly, M. Levy, W. E. Palke, *Journal of Chemical Physics* **68**, 3801-3807 (1978).

112. O. A. Vydrov, G. E. Scuseria, *Journal of Chemical Physics* **122**, 184107 (2005).

113. J. L. Bahr, E. T. Mickelson, M. J. Bronikowski, R. E. Smalley, J. M. Tour, *Chemical Communications*, 193-194 (2001).

114. K. Kamaras, M. E. Itkis, H. Hu, B. Zhao, R. C. Haddon, *Science* **301**, 1501-1501 (2003).

115. S. Banerjee, S. S. Wong, *Journal of the American Chemical Society* **126**, 2073-2081 (2004).

116. R. S. Mulliken, *Journal of Chemical Physics* **23**, 2338-2342 (1955).

117. R. S. Mulliken, *Journal of Chemical Physics* **23**, 2343-2346 (1955).

118. R. S. Mulliken, *Journal of Chemical Physics* **23**, 1833-1840 (1955).

119. R. S. Mulliken, *Journal of Chemical Physics* **23**, 1841-1846 (1955).

120. G. D. J. Smit, M. G. Flokstra, S. Rogge, T. M. Klapwijk, *Microelectronic Engineering* **64**, 429-433 (2002).

121. G. D. J. Smit, S. Rogge, T. M. Klapwijk, *Applied Physics Letters* **81**, 3852-3854 (2002).

122. J. M. Seminario, J. M. Tour, *Molecular Electronics: Science and Technology* **852**, 68-94 (1998).

123. J. M. Seminario, L. M. Yan, *International Journal of Quantum Chemistry* **102**, 711-723 (2005).

APPENDIX I

```
Gold crystal: input file (*.d12) for Crystal 98
-----------------------------------------------
Gold LANL2DZ ECP
CRYSTAL
0 0 0
225
4.0782
1
279 0.0 0.0 0.0
END
279    6
INPUT
      19 5  6  4  5  0
   622.628784      -60.000000     -1
   136.284363     -555.529236      0
    33.154980     -168.001984      0
     9.989490      -63.039986      0
     3.048131       -4.251668      0
   194.737427        3.000000     -2
   351.532745       38.602089     -1
   122.327042      864.837097      0
    32.091461      374.993561      0
     5.245181      289.791016      0
     4.491622     -152.453278      0
   420.615875        2.000000     -2
   109.441780       73.888565     -1
    34.171429      326.672974      0
     5.987975      126.581459      0
   219.266617        3.000000     -2
   122.729782       55.679314     -1
    63.106339      449.198730      0
    18.368452      215.026917      0
     4.497284       64.084099      0
0   0 3     2.0   1.0
    2.809000     -1.202156
    1.595000      1.674158
    0.532700      0.352659
0   0 4     1.0   1.0
    2.809000      1.160848
    1.595000     -1.864285
    0.532700     -1.035623
    0.282600      1.306440
0   2 3     6.0   1.0
    3.684000     -0.280268
    1.666000      0.781840
    0.598900      0.480478
0   2 1     0.0   1.0
    0.683800     -0.095208
0   3 2     10.0   1.0
    1.287000      0.584427
    0.433500      0.529816
0   3 1     0.0   1.0
    0.139600      1.000000
99 0
```

```
END
DFT
EXCHANGE
BECKE
CORRELAT
PWGGA
BASIS
0
279 3
1 0 12 0.1 2000.
1 2 12 0.1 2000.
1 3 12 0.5 2000.
99 0
END
TOLINTEG
6 6 20 20 20
END
16 4 32
MAXCYCLE
60
FMIXING
70
TOLSCF
6 6
END
```

```
Gold crystal: input file (*.d3) for Crystal 98
-----------------------------------------------
EDFT
END
NEWK
10 10 24
1 0
ANBD
0 5 10
7 8  9 10 11
BAND
band structure
4 2 29 7 11 1 0
0 0 0 1 0 0
1 0 0 0 1 0
0 1 0 1 1 1
0 0 0 -1 0 0
DOSS
2 200 7 11 1 18 0
3 1 2 3 4 5 6
2 5 6
END
```

APPENDIX II

Silicon crystal: input file (*.d12) for Crystal 03

```
------------------------------------------------
SILICON BULK - BASIS SET 6-31*
CRYSTAL
0 0 0
227
5.42
1
14  .125  .125   .125
END
14 5
0 0 6 2. 1.
      0.1611590000E+05  0.1959480216E-02
      0.2425580000E+04  0.1492880164E-01
      0.5538670000E+03  0.7284780801E-01
      0.1563400000E+03  0.2461300271E+00
      0.5006830000E+02  0.4859140535E+00
      0.1701780000E+02  0.3250020358E+00
0 1 6 8. 1.
      0.2927180000E+03 -0.2780941415E-02  0.4438264521E-02
      0.6987310000E+02 -0.3571461817E-01  0.3266793328E-01
      0.2233630000E+02 -0.1149850585E+00  0.1347211372E+00
      0.8150390000E+01  0.9356344760E-01  0.3286783348E+00
      0.3134580000E+01  0.6030173068E+00  0.4496404580E+00
      0.1225430000E+01  0.4189592131E+00  0.2613722662E+00
0 1 3 4. 1.
      0.1727380000E+01 -0.2446310042E+00 -0.1779510605E-01
      0.5729220000E+00  0.4315737717E-02  0.2535390863E+00
      0.2221920000E+00  0.1098184508E+01  0.8006692724E+00
0 1 1 0. 1.
      0.7783690000E-01  0.1000000000E+01  0.1000000000E+01
0 3 1 0. 1.
      0.4500000000E+00  0.1000000000E+01
99 0
END
DFT
B3PW
END
END
8 4 8
FMIXING
30
LEVSHIFT
6 1
END
```

Silicon crystal: input file (*.d3) for Crystal 03

```
------------------------------------------------
NEWK
12 0 48
1 0
```

```
DOSS
3 400 -1 -36 1 18 0
-0.55124 0.36749
8 1 2 6 10 19 20 24 28
18 3 4 5 7 8 9 11 12 13 21 22 23 25 26 27 29 30 31
10 14 15 16 17 18 32 33 34 35 36
END
```

APPENDIX III

```
(4,4) CNT: input file (*.d12) for Crystal 03
-----------------------------------------
Carbon Nano Tube - POLYMER CNT   GROUP P 1
POLYMER
1
2.473115
16
6                   0.250012232         2.776716  -0.023251
6                   0.250011423         2.417442  1.368151
6                   0.250012636         0.023242  2.77671
6                   0.250011423         -1.368164 2.417451
6                   0.250012232         -2.776704 0.023245
6                   0.250011423         -2.417447 -1.368162
6                   0.250011423         -0.02325  -2.776698
6                   0.250011018         1.368156  -2.417435
6                   -0.25005954         1.979877  1.94655
6                   -0.250059945        0.741187  2.67556
6                   -0.250059945        -1.946562 1.979888
6                   -0.250059945        -2.675563 0.741193
6                   -0.250060349        -1.979892 -1.946566
6                   -0.250061158        -0.741198 -2.675567
6                   -0.250059945        1.946565  -1.979883
6                   -0.250060753        2.675578  -0.741197
ENDG
6 3
0 0 6 2.0 1.0
      0.3047524880E+04  0.1834737132E-02
      0.4573695180E+03  0.1403732281E-01
      0.1039486850E+03  0.6884262226E-01
      0.2921015530E+02  0.2321844432E+00
      0.9286662960E+01  0.4679413484E+00
      0.3163926960E+01  0.3623119853E+00
0 1 3 4.0 1.0
      0.7868272350E+01 -0.1193324198E+00  0.6899906659E-01
      0.1881288540E+01 -0.1608541517E+00  0.3164239610E+00
      0.5442492580E+00  0.1143456438E+01  0.7443082909E+00
0 1 1 0.0 1.0
      0.1687144782E+00  0.1000000000E+01  0.1000000000E+01
99 0
ENDBS
DFT
B3PW
END
SCFDIR
ENDM
9 9 9
ENDSCF



(4,4) CNT: input file (*.d3) for Crystal 03
-----------------------------------------
ADFT
```

```
END
NEWK
100 0 240
1 0
DOSS
2 400 -1 -144 1 24 0
-0.551235 0.367490
48 1      2         6
10        11        15
19        20        24
28        29        33
37        38        42
46        47        51
55        56        60
64        65        69
73        74        78
82        83        87
91        92        96
100       101       105
109       110       114
118       119       123
127       128       132
136       137       141
96 3      4         5         7         8         9
12        13        14        16        17        18
21        22        23        25        26        27
30        31        32        34        35        36
39        40        41        43        44        45
48        49        50        52        53        54
57        58        59        61        62        63
66        67        68        70        71        72
75        76        77        79        80        81
84        85        86        88        89        90
93        94        95        97        98        99
102       103       104       106       107       108
111       112       113       115       116       117
120       121       122       124       125       126
129       130       131       133       134       135
138       139       140       142       143       144
```

APPENDIX IV

```
Geometry of Molecule 9: Input file for Gaussian 03
--------------------------------------------------
%nproc=4
%mem=4Gb
%chk=nitro_small_sibulk_cnt44_2_without_h.chk
%rwf=nitro_small_sibulk_cnt44_2_without_h.rwf
#p rb3pw91/6-31g(d) iop(3/8=1)

Title Card Required
0 1
 Si                  0.00000000    0.00000000    0.00000000
 Si                  3.84783472    0.00000000    0.00000000
 Si                 -3.69362990    4.72512636    0.00000000
 Si                 -1.94366139    3.29981591    0.61822214
 Si                  5.78985268    3.18491964    0.77168291
 H                   7.02056374    3.98150536    0.50241075
 Si                  5.77976311    1.22492633   -0.51515553
 Si                  5.74756661    1.71101261   -2.80758744
 H                   7.02608992    2.35007551   -3.23122681
 Si                  3.76464733    3.54440119   -5.61397302
 H                   4.99106765    4.24035129   -6.10392095
 Si                  1.86543791    4.83666307   -6.10692620
 Si                  1.99782370    6.86755639   -4.91276648
 H                   3.27782889    7.47704941   -5.40624180
 Si                 -1.83678598    7.90278649    0.59805427
 Si                 -3.70898911    3.13396498   -3.45229807
 Si                 -1.66872292    6.52307285   -2.90363865
 Si                 -1.98372994    4.84937468   -6.27446392
 Si                 -0.07772860    3.59987785   -5.62617850
 Si                  2.07206390    6.42929092   -2.55362497
 Si                  2.09309868    8.36823194   -1.10585572
 H                   3.38407894    9.06529246   -1.41495274
 Si                  0.11505263    5.14329675   -2.16495407
 Si                  1.97469366    7.71002687    1.12424756
 Si                 -1.89971908    1.80579036   -2.79459478
 Si                 -0.06203358    6.54024983    1.35118129
 Si                 -1.90134103    1.26286320   -0.52582926
 Si                  0.00386011    4.54810595    0.13163052
 Si                  1.91531537    3.26726132    0.68487717
 Si                  1.92396822    1.25316708   -0.52375235
 Si                  3.77379047    6.33562998    1.72960830
 H                   5.04603615    7.11634854    1.70478720
 Si                  1.95349001    1.85518425   -2.79906908
 Si                  3.89188129    4.48801257    0.28053143
 Si                  0.01908597    3.08728790   -3.34540315
 Si                  3.97539141    5.09331645   -2.01629325
 Si                  3.90232537    3.09214337   -3.31294456
 C                   5.58224849    6.07671726   -2.36412183
 C                   6.53761636    5.68086818   -3.33274217
 C                   5.86011013    7.24951106   -1.62456504
 C                   7.70765495    6.42176831   -3.55426419
 H                   6.37478900    4.78692256   -3.92710433
 C                   7.02090313    7.99533348   -1.83233719
 H                   5.16485095    7.59178354   -0.86404742
```

H	8.42541349	6.09641600	-4.30214700
H	7.21006332	8.88971666	-1.24602194
C	7.96731835	7.59391999	-2.80214903
C	9.15038603	8.36783440	-2.98565687
C	10.14599892	9.08213072	-3.05845511
C	11.32850567	9.84868505	-3.23052867
C	11.69835749	10.95910913	-2.42836184
C	12.23560785	9.49504410	-4.26972217
C	12.88251362	11.67069334	-2.63419198
N	10.84335244	11.41702433	-1.32143047
C	13.41826068	10.19827375	-4.48594800
H	11.98209750	8.64852515	-4.89941768
C	13.76610878	11.30500425	-3.66387960
H	13.10760548	12.50643204	-1.98235522
O	9.76103980	10.79307464	-1.08710392
O	11.23223867	12.42704810	-0.64497935
H	14.09030039	9.90097287	-5.28514646
C	14.97897285	12.02962916	-3.85628561
C	16.02314480	12.65539733	-4.00760162
C	17.23546786	13.39788959	-4.16180978
C	17.54932006	14.43989223	-3.25664827
C	18.14983746	13.10796663	-5.20295507
C	18.73732326	15.15853602	-3.38813106
H	16.85720235	14.66891992	-2.45229375
C	19.33957535	13.83718128	-5.32962961
H	17.92239232	12.30935385	-5.90216826
C	19.64845716	14.86565193	-4.42160931
H	18.96428629	15.95003830	-2.67887824
H	20.03378974	13.59429569	-6.12769798
C	20.94434947	15.70458340	-4.52335655
C	21.67689458	15.67385343	-3.17927373
C	21.95792324	15.18539909	-5.57481836
C	20.59215949	17.13578566	-4.93636818
C	22.28163332	14.42779737	-2.79647431
C	22.08969657	16.82709468	-2.49918055
C	21.98821918	15.76093841	-6.85467257
C	23.02798170	14.35457390	-5.15335140
C	21.02846829	18.27329028	-4.22737146
C	20.19223607	17.34670261	-6.29950343
C	22.69342216	14.25643501	-1.41656223
C	22.98398168	13.70154253	-3.85441629
C	22.98281811	16.70859473	-1.36454069
C	21.95533563	18.11967101	-3.14097844
C	23.24820529	15.87760408	-7.53463067
C	20.89670629	16.61624363	-7.30938152
C	24.28720938	14.46410574	-5.81889474
C	20.90702483	19.57585628	-4.84922587
C	19.58341209	18.59327962	-6.67252955
C	23.32221027	12.99963350	-1.26470605
C	23.03473361	15.44063122	-0.66735931
C	24.03407403	12.77553033	-3.52078685
C	24.11052687	17.62325533	-1.29822583
C	23.06027403	19.00857562	-3.07306800
C	24.41935612	15.43081476	-6.86334571
C	23.36813377	16.85893044	-8.57652630
C	20.90452344	17.12253751	-8.64403069
C	25.47181010	13.96920008	-5.16239034
C	22.01979081	20.46380087	-4.77795937
C	19.93983815	19.76828459	-5.89115281
C	19.12841216	18.74523289	-8.04499768

C	23.89163238	12.35523719	-2.17709052
C	23.99582483	15.50498862	0.36749199
C	25.31737800	12.90617778	-4.19200919
C	25.30249374	17.27070332	-0.54801574
C	24.23996261	18.58443629	-2.35983238
C	23.19106524	20.02616309	-4.07344848
C	25.56546822	16.30635691	-6.83338128
C	24.49409308	17.73091359	-8.54184356
C	22.19859371	17.24811464	-9.32045013
C	19.79420116	17.97928588	-9.05966298
C	26.62004208	14.86011257	-5.11275663
C	22.14053367	21.50817905	-5.76318704
C	19.79761307	21.09874236	-6.46739951
C	18.57994353	20.03877469	-8.21721507
C	24.97618606	16.28570918	0.41001215
C	26.56556875	12.63050041	-3.60358333
C	26.57685256	17.39331371	-1.21464842
C	25.49728347	18.72504690	-3.00699851
C	24.45861568	20.16302587	-4.72680898
C	26.47641880	16.15291333	-5.73373678
C	25.44001352	17.57410297	-7.46546766
C	24.39719179	18.99620807	-9.21719367
C	22.36941721	18.19253314	-10.40301071
C	20.00514083	18.41177674	-10.38885180
C	27.60612104	14.71309490	-4.05617970
C	23.42310412	21.63075188	-6.44158134
C	20.92763739	21.98669156	-6.40368530
C	18.86990013	21.05029276	-7.53317723
C	27.55946556	13.39808429	-3.55437460
C	27.68032895	16.53627657	-1.01644232
C	26.58574814	17.88289684	-2.58214103
C	25.51789197	19.29444381	-4.32921748
C	24.46257623	20.71390668	-6.05608175
C	26.81333068	17.31326957	-4.97535016
C	25.77805441	18.74601297	-6.70495648
C	24.73519480	20.18397660	-8.44476211
C	23.49221852	19.09373993	-10.35121515
C	21.10818710	18.49510599	-10.98034899
C	27.95290523	15.89069016	-3.28916373
C	23.49114617	22.21968872	-7.76989901
C	21.26171367	22.95175088	-7.38186402
C	28.26591716	15.88311736	-1.91422850
C	27.27618363	17.13201713	-3.62088444
C	26.20356674	18.55964052	-5.35300021
C	25.13761873	19.97932565	-7.07571743
C	24.15942328	21.46817201	-8.80272145
C	23.48485619	20.42441262	-10.82770865
C	22.36442529	23.04731302	-7.97271147
C	23.77453333	21.44789004	-10.16264814
Si	0.39322555	9.89136478	-1.70730762
Si	-3.81635183	6.77287693	1.09564368
Si	-1.56484730	8.54922819	-1.63082583
Si	-3.57347555	5.24432206	-2.33385745
Si	0.21974029	8.14043464	-5.88846776
Si	-3.86198786	3.61159679	-5.71842467
Si	-1.69852674	6.92051645	-5.28586907

APPENDIX V

List of the molecules used in this work. The Gaussian 03 output files are located in the digital attachment. The calculations are performed using the B3PW91 method.

Molecule	Basis set	Description	Filename
Molecule 1		nitroOPE-acetyl	
Molecule 2		octyltrichlorosilane	
Molecule 3	LANL2DZ	Au_6-nitroOPE	nitro_6au.log
Molecule 4	6-31G	CNT-benzene-CNT	a8-benzene-8_6.log
Molecule 5	LANL2DZ	Au_6-nitroOPE-Si coplanar	nitro_small_sibulk_a6.log
Molecule 6	LANL2DZ	Au_6-nitroOPE-Si perpendicular	nitro_small_sibulk_a6_perp.log
Molecule 7	LANL2DZ	Au_6-nitroOPE-Si anion	nitro_small_sibulk_a6_q-1.log
Molecule 8	LANL2DZ	Au6-Si	nitro_small_sibulk_a6_tunnel_1.log
Molecule 9	6-31G(d)	CNT-nitroOPE-Si coplanar	nitro_small_sibulk_cnt44_2_without_h.log
Molecule 10	6-31G(d)	CNT-nitroOPE-Si perpendicular	nitro_small_sibulk_cnt44_2_without_h_perp.log
Molecule 11	6-31G(d)	CNT-nitroOPE-Si anion	nitro_small_sibulk_cnt44_2_without_h_q-1.log
Molecule 12	6-31G(d)	CNT-Si	nitro_small_sibulk_cnt44_tunnel_1.log
Molecule 13	LANL2DZ	nitroOPE	nitro.log
Molecule 14	6-31G(d) Method: PW91PW91	CNT-benzene	cntfull_benzene_13
Molecule 15	LANL2DZ	benzene-Si	benzene_sibulk.log
Molecule 16	LANL2DZ	nitroOPE-Si	nitro_sibulk.log
Molecule 17	LANL2DZ	Au_1-S-nitroOPE-S-Au_1 coplanar	au1_nitro_au1.log
Molecule 18	LANL2DZ	Au_1-S-nitroOPE-S-Au_1 perpendicular	au1_nitro_au1_perp.log
Molecule 19	LANL2DZ	Au_1-S-nitroOPE-S-Au_1 anion	au1_nitro_au1_q-1.log
Molecule 20	LANL2DZ	Au_6-nitroOPE-S-Au_1 coplanar	au_nitro_au6.log
Molecule 21	LANL2DZ	Au_6-nitroOPE-S-Au_1 perpendicular	au_nitro_au6_perp.log
Molecule 22	LANL2DZ	Au_6-nitroOPE-S-Au_1 anion	au_nitro_au6_q-1.log
Molecule 23	6-31G(d)	CNT-nitroOPE-CNT coplanar	cnt_nitro_cnt_rev1.log
Molecule 24	6-31G(d)	CNT-nitroOPE-CNT perpendicular	cnt_nitro_cnt_perp.log
Molecule 25	6-31G(d)	CNT-nitroOPE-CNT anion	cnt_nitro_cnt_q-1.log

VITA

Luis Alberto Agapito received his Bachelor of Science degree in mechatronics engineering from the Universidad Nacional de Ingeniería, Lima, Peru in 2000. He received his Master of Engineering degree in electrical engineering from the University of South Carolina in 2003 and his doctoral degree in May 2006 from Texas A&M University. His email address is luis.agapito@hotmail.com. He can be reached at the following address:

c/o Dr. Jorge M. Seminario
Department of Chemical Engineering
Texas A&M University
TAMU 3122
College Station, TX 77843-3122